University of Trás-os-Montes and Alto Douro

Titanium-45: development and optimization of the production process in low energy cyclotrons

PhD Thesis in Physical Sciences

PEDRO SILVA COSTA

Supervisors:
Prof. Doutor Marco Paulo Duarte Naia
Prof. Doutor Francisco José Cerqueira Alves

VILA REAL, 2016

University of Trás-os-Montes and Alto Douro

Titanium-45: development and optimization of the production process in low energy cyclotrons

PhD Thesis in Physical Sciences

PEDRO SILVA COSTA

Supervisors:
Prof. Doutor Marco Paulo Duarte Naia
Prof. Doutor Francisco José Cerqueira Alves

Jury:
Prof. Doutor José Boaventura Ribeiro da Cunha (President)
Prof. Doutor Luís Filipe dos Santos Garcia Peralta
Prof. Doutor Francisco José Cerqueira Alves
Prof. Doutor Armando da Assunção Soares
Prof. Doutor Norberto Jorge Alves Parente Gonçalves

VILA REAL, 2016

Obstacles can't stop you.

Problems can't stop you.

Most important of all, other people can't stop you.

Only you can stop you.

Jeffrey Gitomer

Agradecimentos / *Acknowledgments*

Porque este trabalho não seria possível sem a intervenção (direta ou indireta) de várias pessoas, não poderia deixar de lhes expressar o meu profundo agradecimento:

- Ao meu Orientador, **Prof. Doutor Marco Naia**; por me receber e aceitar como doutorando na UTAD, por ter encarado esse papel com a máxima dedicação e profissionalismo, por me ter mostrado o mundo da Física no seu estado puro e sem condicionar a minha própria visão pessoal, pelo desenho do meu plano de formação no Curso de Doutoramento, por todos os ensinamentos, por todos os momentos de discussão e reflexão, por todo o rigor, por toda a tranquilidade e por ter tornado este importante passo numa etapa incrivelmente proveitosa e agradável;
- Ao meu Co-Orientador, **Prof. Doutor Francisco Alves**, por me aceitar como doutorando no ICNAS, por me abrir as portas do "seu" ciclotrão para toda a componente experimental deste trabalho, por toda a diversão e jeito peculiar de encarar cada noite de trabalho ou cada momento de discussão técnico-científica, por ter sido um importante contributo para a implementação deste trabalho;
- Ao **Prof. Luís F. Metello**, meu "boss" na ESTSP.IPP e mentor deste trabalho; pelo desafio lançado, pela forma como encontrou sempre modo de financiar o material das experiências, pela insatisfação constante, pela exigência, pela pressão, mas também pela oportunidade de aprender, de crescer, de ser eu a implementar esta ideia que ele tinha em mente, pela sua rede de contactos que não hesitou em partilhar comigo, pelas viagens (nacionais e internacionais) para congressos e outros eventos científicos recheadas de discussão e aprendizagem, pela companhia nas noites de experiências, pela amizade e pelo incentivo;
- Ao **Doutor Sérgio do Carmo**, Físico do ICNAS; pelo apoio prático inestimável, por operar o ciclotrão, pelas horas a fio de medições de espectros com o detetor HPGe, pelos contributos positivos na discussão de resultados e pela acessibilidade e diversão;
- *For all international collaborations, namely **R.R. Johnson** (BEST), **W. Gelbart** (ASD) and **C. Artner** (IASON), that made possible experimental work with beneficial technical inputs;*
- Aos meus colegas de gabinete na ESTSP.IPP (**Diana**, **Domingos**, **Joana**, **Lídia**, **Mariana** e **Sara**); pela amizade e companheirismo, por demonstrarem que a opção de trabalhar em simultâneo com a realização de um doutoramento foi a mais louca, mas também a mais acertada, pelo ambiente de trabalho que sempre ajudou a transformar os piores momentos em momentos de diversão, por manterem sempre a "orquestra a tocar" e por estarem lá sempre que necessário – razão pela qual vários de vocês são já bons amigos;
- Aos vários Professores do **Departamento de Física** da UTAD; pela acessibilidade, pelos ensinamentos nas unidades curriculares do 1º Ano do Curso de Doutoramento, pelo apoio, pela exigência em todas as

apresentações de trabalhos e por também terem contribuído, ao seu jeito e como lhes foi possível, para a concretização deste trajeto;

- Aos meus **amigos**; por constantemente serem uma boa desculpa para atrasar o trabalho e me ir divertir, por incentivarem este trabalho e pela amizade que tanto ajuda nos momentos de maior tensão;
- A toda a minha **família**; por saber da importância deste passo, por se preocupar, por incentivar e desejar o maior sucesso para mim;
- Em especial, aos meus **pais**; por terem feito de mim aquilo que eu hoje sou, com as virtudes e defeitos que tenho, pela educação e valores que me transmitiram, por terem feito de mim uma pessoa feliz e grata, por saberem do peso deste trabalho para a minha vida e carreira, por estarem sempre lá independentemente do que a vida lhes possa ter trazido e dos rumos que possam ter tomado, por me amarem, por me darem o espaço e tempo necessário para me dedicar a este trabalho, por me mostrarem que seria sempre eu a beneficiar (ou sair prejudicado) por todas as minhas opções e atitudes… por tudo o que são;
- À (muito especial) **Joana**; por ter transformado este projeto num projeto comum e numa luta a dois, pelo amor, pela amizade, pelo constante incentivo, motivação e preocupação, por tolerar as minhas falhas e ausências, por ter ouvido pacientemente os assuntos que nada lhe interessavam, por ser corresponsável pela exequibilidade deste trabalho em vários aspetos que nunca esquecerei…por perceber que isto é apenas um início e por aceitar que este tipo de projetos venha a fazer parte das nossas vidas;

- …entre outros; porque todos aqueles que algum dia se cruzaram na minha vida são responsáveis pela pessoa e profissional em que me tornei e, para o bem ou para o mal, tiveram um determinado impacto neste trabalho;

Resta-me ainda agradecer de uma forma global a vida que eu tenho, os obstáculos e dificuldades que surgiram, os desafios e oportunidades aos quais estou grato, e tudo aquilo que me faz sonhar ou ambicionar mais e mais, e faz de mim aquilo que eu sou e que tento refletir em tudo o que faço.

OBRIGADO!

Termo de responsabilidade

Declara-se que o autor desta Tese participou activamente na concepção e na execução de todo o trabalho experimental que esteve na origem dos resultados aqui apresentados, bem como em todo o trabalho teórico prévio, interpretação e discussão dos dados obtidos. Por opção, os capítulos textuais da Tese serão apresentados com recurso à Língua Inglesa.

Preface

In my personal point of view, a Doctoral Thesis is a restrict synthesis of a long route of learning, personal and professional development, and scientific achievements. There is much more than a hundred of written pages! Between literature reviews, hundreds of papers read, presentation of oral communications and posters in conferences, preparation and submission of papers…a PhD is really a hard task, a long way, a long journey to find the (hopefully) positive end.

The Thesis that will be presented here is the reflex of four years of work, always in part-time dedication, but always with a deep motivation and enthusiasm. And, of course, it is the reflex of my own soul, of the way I see physical phenomena, Nuclear Medicine or even the world itself.

Just to introduce the birth of this work, following a series of fruitful conversations and discussions, and always considering my background, expectations, profile and interests, my institutional boss (Prof. Luís F. Metello, ESTSP.IPP) gave me a preliminary idea that until that date was only on his mind; the challenge of studying the viability of produce an unconventional radionuclide (Titanium-45) in low energy cyclotrons to be used in PET imaging. After some study and investigation, the challenge was accepted and this PhD project started to be conceptualized, designed and implemented. And the rest of this story is written in the scientific work called Thesis and that will be presented in the next pages.

I would also like to state that this Thesis has also a challenging message: Nuclear Physics research is a field that could be occupied by a non-physicist researcher; and I humbly hope that this Thesis could prove that with the quality desirable and required for this level.

Finally, it is also important to add that this Thesis, but also all the research project involved on it, is the study to find a solution with the application of theory already known from fundamental research and using methodologies and approaches that came from applied research to design science research methods, but passing also through experimental science, culminating in the viability study of an industry-tailored process.

Read, analyze, criticize…and enjoy!

This Thesis is my first formal contribution for a better society!

Pedro Costa

Publications List

The work performed under the scope of this Thesis resulted in the publication of the following scientific contributions:

Posters:

1. **P. Costa**, F. Alves, M. Duarte Naia, L.F. Metello. "New methods using low energy cyclotrons in radioisotope production for Nuclear Medicine", in E3 Forum - Education, Employment & Enterpreneurship Conference, Lisboa (2013);
2. **P. Costa**, L.F. Metello, F. Alves, M. Duarte Naia. "Application of Monte Carlo simulation codes to plan an activation experiment in Scandium-45 targets" in Annual Congress of the European Association of Nuclear Medicine, Goteborg (2014);
3. **P. Costa**, L.F. Metello, F. Alves, M. Duarte Naia. "The use of radiolabeled nanoparticles for biomedical imaging" in Low Dose PT, Lisboa (2015);
4. **P. Costa**, L.F. Metello, L. Cunha, R.R. Johnson, L. Mattei, W. Gelbart, J. Obermair, B. Dietl, R. Nauschnig, C. Artner, P. Lass, G. Currie, S. Carmo, F. Alves, M. Duarte Naia. "Cyclotron produced ^{45}Ti-Titanium: why & how…so Why Not?" in 5th Symposium on Medical Radionuclides, Brussels (2015);
5. **P. Costa**, L.F. Metello, L. Cunha, R.R. Johnson, L. Mattei, W. Gelbart, J. Obermair, B. Dietl, R. Nauschnig, C. Artner, P. Lass, G. Currie, S. Carmo, F. Alves, M. Duarte Naia. "Excitation function determination for ^{45}Ti production using ^{45}Sc(p,n) ^{45}Ti reaction using low energy cyclotrons" in Annual Congress of the European Association of Nuclear Medicine, Hamburg (2015)

Oral Communications:

1. **P. Costa,** M. Naia. "Gamma Spectroscopy: Code for Analysis and Simulation" in Física 2012, Aveiro (2012);
2. **P. Costa**, L. Cunha, R.R. Johnson, W. Gelbart, C. Artner, F. Alves, M. Duarte Naia, L.F. Metello. "Using Monte Carlo to approach ^{45}Ti direct production on low energy – medical – cyclotrons" in Cycleur 2014 – Cyclotron European Network Workshop, Ispra (2014);
3. **P. Costa**, L.F. Metello, L. Cunha, R.R. Johnson, W. Gelbart, J. Obermair, C. Artner, S. Carmo, F. Alves, M. Duarte Naia. "Experimental results on excitation functions for ^{45}Ti direct production on low energy – medical – cyclotrons" in 11th Cycleur – Cyclotron European Network Workshop, Monastir (2015);
4. **P. Costa**, L.F. Metello, L. Cunha, P. Lass, G. Currie, R.R. Johnson, W. Gelbart, J. Obermair, C. Artner, F. Alves, M. Duarte Naia. "^{45}Ti-Titanium: from cyclotron production to potential applications evaluation" in Low Dose PT, Lisboa (2015);

5. **P. Costa**, L. Cunha, L.F. Metello. “The role of the Nuclear Medicine Technologist in cyclotron related Research & Development” in Annual Congress of the European Association of Nuclear Medicine, Hamburg (2015);
6. **P. Costa**, M. Naia, F. Alves, L.F. Metello. “Development of ^{45}Ti for radiopharmaceutical purposes: results obtained and future perspectives” in 12th Cycleur – Cyclotron Cyclotron European Network Workshop – and 2nd Bern Cyclotron Symposium, Bern (2016);

Published abstracts:

1. **P. Costa,** L.F. Metello, F. Alves, M. Duarte Naia. PET imaging using Titanium-45: Could it be useful? Nuclear Medicine and Biology. 2014; 41(7). DOI: 10.1016/j.nucmedbio.2014.05.129

Peer-review journal articles:

1. **P. Costa**, L.F. Metello, F. Alves, M. Duarte Naia. *Nanoparticle-based radiopharmaceuticals: Status quo and future developments*.
   Under submission in: Molecular Diagnosis and Therapy (Impact Factor 2014: **2.891**)
2. **P. Costa**, L.F. Metello, F. Alves, M. Duarte Naia. *Study of ^{45}Ti production by the experimental determination of the excitation function of ^{45}Sc(p,n)^{45}Ti nuclear reaction*.
   Under submission in: Applied Radiation and Isotopes (Impact Factor 2014: **1.231**)

Abstract

Introduction: Modern practice of Medicine include the use of technological innovations such as Medical Imaging. *In vivo* imaging techniques can be used to evaluate biological structures and functions non-invasively in almost all living subjects.

In this Thesis it will be highlighted Nuclear Medicine. As a simple definition, Nuclear Medicine is a medical imaging modality based on the measurement of an internal source from an internal tracer, reason why it uses radiolabeled compounds to study *in vivo* physiologic processes. So, Nuclear Medicine relies on the supply of radionuclides.

In the specific context of Positron Emission Tomography (PET) imaging, positron emitters are used to label several different compounds, allowing the study of almost all the major biological systems. Although there are several radionuclides to be potentially applied in PET imaging, routine clinical applications are still based on a small group constituted by ^{18}F, ^{11}C, ^{13}N and, more recently, ^{68}Ga. However, recent literature indicates that this trend is changing. Among others, ^{45}Ti is being proposed as a potential candidate for PET imaging, since it presents some interesting properties: abundant positron emission, reduced positron energy, physical half-life of 3.09h, and relevant chemical properties, that enable radiolabelling with bifunctional chelates, ligands or even to radiolabel titanium dioxide nanoparticles. Given this, several issues should be solved before the real possibility to implement ^{45}Ti clinical applications.

Aim: Considering that Radionuclide production is the first crucial technical step involved in PET, and that production of ^{45}Ti is yet very poorly explored in literature, this Project was designed and implemented with the aim to study the viability of the production of ^{45}Ti in low energy cyclotrons, expecting the characterization of the excitation functions of the appropriate nuclear reaction, yield determination and development of a critical analysis to select the best methodology.

Materials and Methods: To evaluate nuclear reactions activation studies should be implemented. Nevertheless, the execution of nuclear activation studies deserve special attention and a careful integration of all the available information already collected. In this sense, the first step of this activation experiment was the adequate planning using Monte Carlo simulation codes in the way to obtain several results that were totally integrated in the design of experimental studies.

Still before the experimental activation study, some preliminary experimental studies with gamma-spectroscopy were performed with calibrated radionuclide sources as demonstration of the ability of the technique to illustrate physical phenomena such as radioactive decay and radiation interaction with matter, and in the way to refine the analysis of the main experiment.

Then, the stacked foil technique was implemented in a 18 MeV cyclotron to study the $^{45}Sc(p,n)^{45}Ti$ nuclear reaction and its feasibility to effectively produce ^{45}Ti. Activation was measured using HPGe gamma-spectroscopy.

Theoretical insight about the potential applications of ^{45}Ti for PET imaging were also reviewed, analyzed, proposed and discussed.

Results: According to TALYS code, and also due to other practical considerations, $^{45}Sc(p,n)^{45}Ti$ nuclear reaction was selected as the one with much more potential for industrial implementation in the way to obtain significant quantities of ^{45}Ti. SRIM code simulations were used to understand the beam energy degradation along the stacked foil designed for the activation study, while SSSM sub-routine was used to study the implantation of the beam in the successive targets.

Results on the main excitation function under study were collected, with the addition of information regarding concurrent reactions leading to ^{44m}Sc, ^{44}Sc and ^{44}Ti. Experimental results showed that $^{45}Sc(p,n)^{45}Ti$ nuclear reaction seems to be feasible in low energy cyclotrons, with cross-section values presenting a peak for proton beam energies in the range between 10 and 14 MeV, while energies higher than 17 MeV should be avoided due to the increased production of contaminants such as ^{44}Ti, ^{44}Sc and ^{44m}Sc. Thick target yield for a saturation condition was experimentally determined as 433.64 $MBq.\mu A^{-1}sat$.

Theoretical evidences collected demonstrate that ^{45}Ti could provide good PET image quality, with some preclinical applications already tested in studies related to a new class of anticancer drugs based on titanium complexes. Other possible applications already cited include ^{45}Ti-ligands for theranostics and personalized medicine. An innovative proposal on the use of ^{45}Ti to radiolabel of titanium dioxide nanoparticles will also be presented and discussed.

Conclusion: Thus, there is the possibility to effectively obtain significant quantities of ^{45}Ti allowing its possible commercial and industrial production, distribution and use. Given this, ^{45}Ti could then provide good PET images and be used for labeling of different compounds already tested or to be incorporated in the development of nanoparticle-based radiopharmaceuticals.

Keywords: Cyclotron; Nuclear Medicine; PET; Radionuclide production; ^{45}Ti;

Resumo

Introdução: A Medicina praticada atualmente inclui o uso de inovações tecnológicas, tais como a Imagiologia Médica. As técnicas de imagiologia *in vivo* permitem avaliar estruturas e funções de forma não-invasiva, em quase todos os sistemas biológicos. O tema deste trabalho está centrado na Medicina Nuclear, que é uma modalidade de imagiologia médica com base na medição de uma fonte utilizando um marcador interno. Este método utiliza compostos marcados radioactivamente para estudar processos fisiológicos *in vivo*, pelo que a Medicina Nuclear está baseada no fornecimento de radionuclídeos.

No contexto específico da imagiologia por Tomografia de Emissão de Positrões (PET), os emissores de positrões são utilizados para radiomarcar vários compostos diferentes que permitem o estudo de praticamente todos os principais sistemas biológicos. Embora existam vários radionuclídeos para ser potencialmente aplicados em imagens de PET, as aplicações clínicas de rotina utilizam apenas um pequeno grupo de nuclídeos, constituído por ^{18}F, ^{11}C, ^{13}N e, mais recentemente, o ^{68}Ga. No entanto, a literatura recente indica que esta tendência está a mudar. Entre outros, ^{45}Ti tem sido proposto como um candidato potencial para geração de imagens PET, uma vez que apresenta algumas propriedades interessantes: emissão eficiente de positrões, reduzida energia dos positrões, semi-vida física de 3,09 h, bem como as suas propriedades químicas relevantes, que permitem a marcação radioativa com quelatos bifuncionais, ligandos diversos ou mesmo para marcar radioactivamente nanopartículas de dióxido de titânio Porém, várias questões devem ser resolvidas antes da real possibilidade de implementar aplicações clínicas de ^{45}Ti.

Objetivo: A produção do radionuclídeo é o primeiro passo técnico fundamental envolvido em PET, contudo a produção de ^{45}Ti é ainda muito pouco explorada na literatura. O projeto relatado neste trabalho foi delineado e implementado de forma a estudar a viabilidade da produção de ^{45}Ti em ciclotrões de baixa energia. Com este objetivo principal desenvolveu-se um programa de pesquisa completo para obter uma caracterização completa das funções de excitação da reação nuclear mais apropriada, determinação dos respetivos rendimentos e desenvolvimento de uma análise crítica para selecionar a metodologia mais apropriada.

Material e Métodos: Para avaliar as reações nucleares foram implementados estudos de ativação nuclear. No entanto, a execução desses estudos merece atenção especial e uma integração cuidadosa de toda a informação disponível já recolhida e publicada. Neste sentido, o primeiro passo desta experiência de ativação foi o planeamento adequado utilizando códigos de simulação Monte Carlo para prever resultados e selecionar os cenários mais prováveis. Os dados calculados foram totalmente integrados na conceção dos estudos experimentais. Ainda antes do estudo experimental de ativação, foram realizados ensaios experimentais preliminares com espectroscopia-gama com fontes calibradas de radionuclídeos, para avaliar a capacidade da técnica para ilustrar fenómenos físicos, tais como o decaimento radioativo e a interação de radiação com a matéria, e refinar a análise da experiência principal.

Finalmente, utilizou-se a técnica da pilha de lâminas num ciclotrão de 18 MeV para estudar a reação nuclear $^{45}Sc(p,n)^{45}Ti$ e a sua viabilidade para produzir efetivamente ^{45}Ti. A ativação foi medida utilizando espectroscopia-gama com recurso a um detetor HPGe.

Resultados: De acordo com o código TALYS, e também devido a outras considerações práticas, a reação nuclear $^{45}Sc(p, n)^{45}Ti$ foi selecionada como aquela com mais potencial para obter quantidades significativas de ^{45}Ti para aplicação industrial.

O cálculo com os códigos SRIM permitiu compreender a degradação da energia do feixe ao longo da pilha de lâminas concebida para o estudo da ativação induzida, enquanto que a sub-rotina SSSM foi usada para estudar a implantação do feixe do ciclotrão nos alvos sucessivos na pilha.

Obtiveram-se os dados relativos à função de excitação principal, bem como informações adicionais sobre reações concorrentes que levam à produção de ^{44m}Sc, ^{44}Sc e ^{44}Ti. Os resultados experimentais mostraram que a reação nuclear $^{45}Sc(p,n)^{45}Ti$ parece ser exequível em ciclotrões de baixa energia, com valores de secção eficaz que apresentam um pico para energias do feixe de protões compreendidas entre os 10 e os 14 MeV, enquanto que as energias superiores a 17 MeV devem ser evitadas, devido ao aumento da produção de contaminantes como o ^{44}Ti, o ^{44}Sc e o ^{44m}Sc. O rendimento de alvo espesso para uma condição de saturação foi determinado experimentalmente como 433,64 $MBq.\mu A^{-1}sat$.

As evidências teóricas recolhidas demonstram que o ^{45}Ti pode proporcionar uma boa qualidade de imagem PET, com algumas aplicações pré-clínicas já testadas em estudos relacionados com uma nova classe de fármacos anticancerígenos à base de complexos de titânio. Outras possíveis aplicações do ^{45}Ti já citadas incluem a radiomarcação de ligandos para teragnóstico e medicina personalizada. Apresenta-se também uma proposta inovadora de uso de ^{45}Ti para a marcação radioativa de nanopartículas de dióxido de titânio.

Conclusão: Existe a possibilidade de obter de forma eficaz quantidades significativas de ^{45}Ti permitindo a sua possível produção comercial, distribuição industrial e utilização clínica. Como o ^{45}Ti tem potencial de proporcionar boas imagens PET, e ser utilizado para a radiomarcação de diferentes compostos, deve ser testado de forma a ser incorporado no desenvolvimento de radiofármacos para imagiologia PET ou na marcação de nanopartículas para estudos aplicados de farmacologia e diferentes aplicações biomédicas.

Palavras-chave: Ciclotrão; Medicina nuclear; PET; Produção de radionuclídeos; ^{45}Ti;

Index

Figures index

Chapter 1

Chapter 2

Chapter 3

Chapter 4

Chapter 5

Tables index

Abbreviations, Acronyms and Symbols List

A – number of mass

Am – Amaricium

Ba – Barium

C – Carbon

Co – Cobalt

Cs – Cesium

CT – Computed Tomography

Cu – Copper

Da – Dalton

e^- - electron

E – energy

EC – electron capture

EOB – end of bombardment

Eu – Europium

eV – electron-volt

F – Fluorine

FDA – Food and Drugs Administration

Ga – Gallium

GSA – Gamma Spectra Analyzer

GUI – Graphical User Interface

h - hour

HPGe – High purity germanium

I – Iodine

IAEA - International Atomic Energy Agency

ICNAS – Instituto das Ciências Nucleares Aplicadas à Saúde

In – Indium

IT – isomeric transition

K – Potassium

keV – kiloelectron-volt

LET – Linear Energy Transfer

MeV – Megaelectron-volt

MR – Magnetic Resonance

n - neutron

N – Nitrogen

Na – Sodium

NaI – Sodium iodide

NaI(Tl) – Sodium iodide doped with Tallium

NM – Nuclear Medicine

O – Oxygen

p - proton

Pb – Lead

PET – Positron Emission Tomography

Ra – Radium

Rb – Rubidium

Re – Renium

RF - radiofrequency

SATP – Standard Ambient Temperature and Pressure

Sc - Scandium

Se – Selenium

Sm – Samarium

SPECT – Single Photon Emission Computed Tomography

SRIM – Stopping and Range of Ions in Matter

SSSM – SRIM Supporting Software Modules

Tc – Technetium

TENDL – Talys Evaluated Nuclear Data Library

Ti – Titanium

TiO_2 – titanium dioxide

Tl – Tallium

TRIM – Transport and Range of Ions in Matter

US – Ultrasonography

WHO – World Health Organization

Y – Yttrium

Z – atomic number

Zn – Zinc

α – alpha particle

β^- - electron

β^+ - positron

μ – linear attenuation coefficient

1. Introduction

In modern practice of Medicine the use and incorporation of technological developments into the clinical routine is becoming more and more common. In such an environment, one can specify the case of Medical Physics methods and technologies. In fact, it is very difficult to define the range and scope of Medical Physics, but for the purpose of this work it is sufficient to refer that it includes the use of radiation for diagnostic or therapeutic purposes, including specifically the field of Medical Imaging.

The application of imaging modalities and technologies has improved the quality of medical care and procedures available in nowadays' practice of medicine. With the implementation of the current paradigms of Evidence Based Medicine and Science Based Medicine, medical imaging is occupying a primary position in clinical decision algorithms.

Noninvasive imaging modalities could allow accurate diagnosis, increase the precision in treatment choice and planning and give opportunity to follow the evolution of patients' clinical status [1].

Medical or biomedical imaging modalities are actually the main pillars of medical care with many advantages including real time monitoring, accessibility without tissue destruction, minimal or no invasiveness. These modalities could also act over wide ranges of time and size scales involved in biological and pathological processes [2].

In vivo imaging techniques can be used to evaluate biological structures and functions non-invasively in almost all living subjects. Multiple imaging techniques are available, including X-ray imaging, Computerized Tomography (CT), Magnetic Resonance (MR) imaging, Ultrasonography (US), Optical Imaging using fluorescent molecules and Nuclear Medicine (NM) using radioisotopes (planar imaging, Single Photon Emission Computed Tomography - SPECT - and Positron Emission Tomography - PET) [3].

Generally, imaging modalities can be divided according to different classifications; one option could be based on two main groups: those that primarily provide structural information (for example, CT or MR) and those that primarily provide functional and molecular information (for example, SPECT and PET) [4].

Another kind of classification of medical imaging modalities could be observed in Figure 1.1, showing the division based on the source of the measured signal and on its physical basis. Different imaging modalities or techniques are based on the detection of signals from different sources meaning different biological properties, as it is the example of CT and MRI where a contrast is produced by detecting differences in tissue density and water content, respectively, or in radionuclide imaging where contrast is conferred by detection of a clearly identified molecule labeled with a radioactive isotope [4].

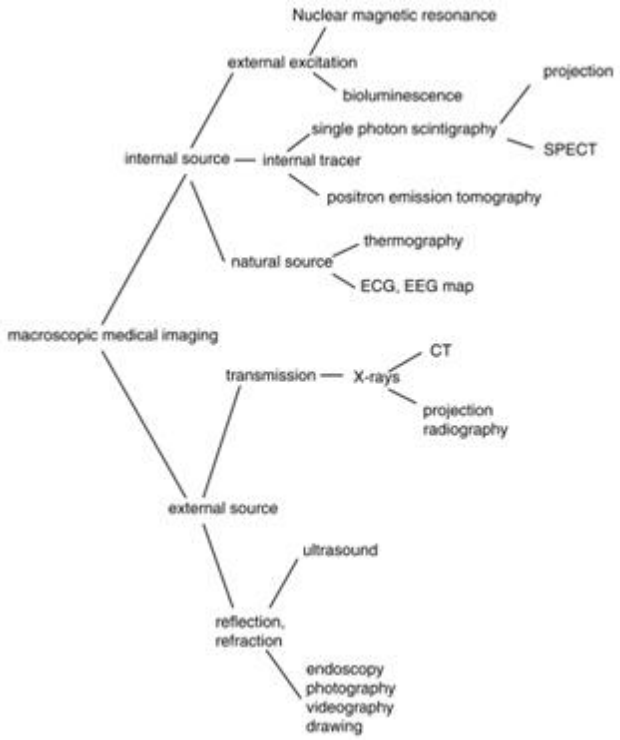

Figure 1.1 - Spectrum of macroscopic medical imaging modalities.

Source: H. Zaidi and B. H. Hasegawa, "Overview of Nuclear Medical Imaging: Physics and Instrumentation," in *Quantitative Analysis in Nuclear Medicine Imaging*, H. Zaidi, Ed., ed: Springer, 2006, pp. 1-35

This thesis will focus especially on Nuclear Medicine, more specifically in the PET field. The next topics will be dedicated to the definition and exploitation of Nuclear Medicine and the classification and description of the most important medically useful radionuclides.

1.1 Nuclear Medicine basics

Nuclear Medicine is an independent medical specialty defined by World Health Organization (WHO) since 1972, that "encompasses applications of radioactive materials in diagnosis, treatment or in medical research, with the exception of the use of sealed radiation sources in radiotherapy" [5].

Following the classification and differentiation present in Figure 1.1, Nuclear Medicine comprehends the medical imaging modality based on the measurement of an internal source from an internal tracer. It is considered to be a part of functional imaging field that is more uncommon in clinical practice than morphological imaging, even considering that it is gaining importance and frequency of application. This kind of methodology allows to access very important data, so increasing the efficiency of clinical diagnosis, essentially because of sooner detection of pathological processes. In fact almost all diseases start with functional/biochemical changes prior the morphological expression.

Nowadays it is quite common to present Nuclear Medicine imaging at the leading edge of Molecular Imaging, even considering that it is a hard task to define the real range of the Molecular Imaging field. Nevertheless, Nuclear Medicine is for sure one of the main parts of it, as it allows the *in vivo* measurement and follow-up of biological processes while enables the determination of different changes in cellular or molecular physiology [6].

This medical specialty implies a multidisciplinary environment, since its appearing, either as fundamental knowledge or as application to the specific context. This characteristic can be illustrated through the analysis of primary inputs such as: discovery of radioactivity (Henri Becquerel, 1896), definition of radioactivity (Marie Curie, 1897), the principle of radioactive tracer (George de Hevesy, 1924); followed by the application of these and other principles, for instance with the invention of the cyclotron (Ernest Lawrence, 1930), the gamma camera (Anger Hall, 1958) or upon obtaining the first image of cerebral neurotransmission (Henry Wagner, 1983) [7]. In summary, this field of science conjugates the knowledge and the experience from different scientific fields leading to the development of solid and valid solutions and methodologies (Figure 1.2).

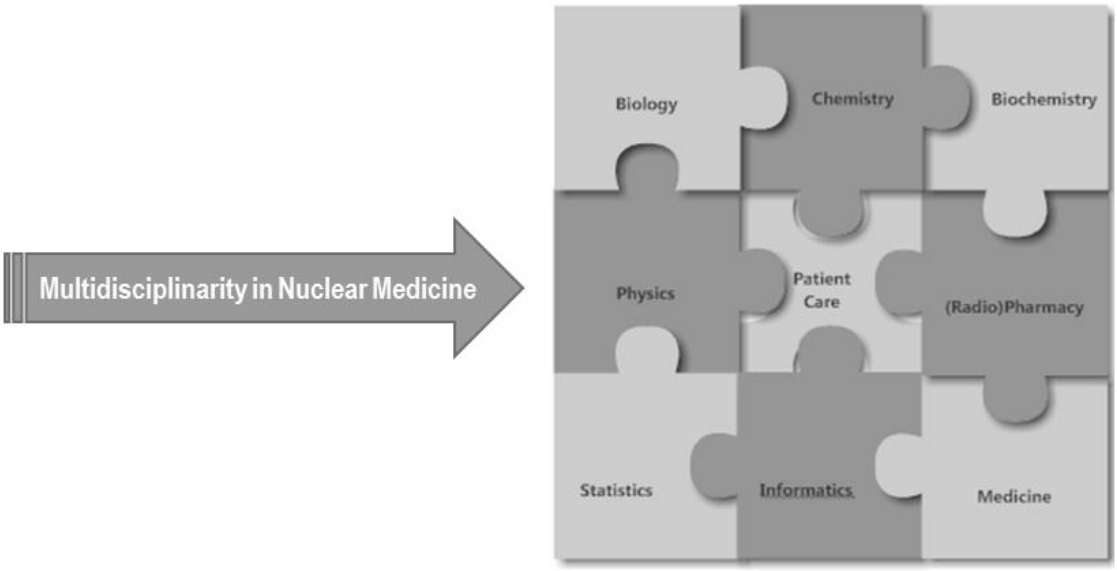

Figure 1.2 - Schematic representation of multidisciplinarity in Nuclear Medicine.

From Figure 1.2 it is very clear the need for a continuous and complementary interaction between many different scientific fields in the Nuclear Medicine practice and application.

Moreover, Nuclear Medicine presents a tendency of growth over the past years. For instance, in the United States the number of procedures per year grown from 14 to 20 million between 1999 and 2005 [8]. Another study (Dose DATAMED II), designed to collect available data on the patient doses from the radiodiagnostic procedures (X-ray and Nuclear Medicine) in the European Union, shown that the frequency of Nuclear Medicine procedures over European Countries varies from 527 (Romania) to 35468 (Luxembourg) per year per million of inhabitants [9]. Together with other conclusions of that study, this data illustrate the high variability in frequency of examinations

between countries, but also identify a trend to homogenization with the increase of the annual number of procedures in several countries (even in the developing countries).

This situation of continuous and sustainable growth is related with clinical importance of the use of radiotracers that allows exceptional target specificity at the molecular level that cannot be accomplished with any other imaging technique [10]. Another advantage of radionuclide imaging is the ability to perform real time imaging studies, in order to increase understanding of physiological mechanisms underlying pathological processes or revealing the effects of drug administration [11].

Diagnostic Nuclear Medicine contributes to the clinical care, with all the advantages mentioned before, using radiopharmaceuticals (that combine a radionuclide with a specific molecule/probe), being possible to find specific radiopharmaceuticals for each organ, tissue or process. In overview, diagnostic Nuclear Medicine is playing an important clinical role in Oncology, Cardiology and Neurology, but also in Nephrology and investigations related with Infection or Inflammation processes, while the therapeutic branch of Nuclear Medicine is mainly concentrated in the Oncology field [12].

It is also known that Nuclear Medicine relies on the application of photons from the radioactive decay scheme of several elements, that can be detected from outside a patient or a simple organ or tissue sample [13]. On other hand, the possible usefulness of other decay particles for therapeutic purposes should also be considered.

Considering that Nuclear Medicine rely on the use of radiopharmaceuticals it is very important to state a clear definition of these compounds. Radiopharmaceuticals are substances that result from the combination of a radionuclide and a molecular probe. The first is responsible for the signal to be read (or the energy to destroy the cells in therapeutic applications) after radioactive decay, and the second is the biological vector that guides the radionuclide during its biological distribution. Indeed, there are many possible combinations using a number of radionuclides and several molecules that have the ability to target cells, tissues or biochemical processes, demonstrating, and quite often quantifying, their respective metabolic/catabolic properties, creating real time information without interfering in the processes under study.

1.1.1. Nuclear (in)stability

Considering that radiopharmaceuticals are constituted by useful radionuclides, thus resulting in the dependence of Nuclear Medicine on radionuclides, it is important to point out physical basis inherent to the instability of nuclides.

To understand and discuss the concept of nuclear stability, it is important to realize that atomic nuclei are quantum bound states of particles called nucleons (classified as hadrons - aggregates of quarks) of which there are two types; the positively charged (proton) and the uncharged (neutron).

One of the major aims of Nuclear and Particle Physics is to understand the properties of atomic nuclei mainly in terms of the interaction between pairs of nucleons. However, actually, with the onset of Quantum Chromodynamics, it became clear that the interaction between pairs of nucleons is not fundamental. According to this complex theory the strong nuclear force determines the interaction between quarks, and not exactly between aggregates of quarks

(such as nucleons) directly [14]. This consideration changes the paradigm of analysis from a two-body problem (nucleon-nucleon) to a six-body problem (three quarks for each nucleon). Even so, in the simplest approach towards a nuclear structure problem, it is common to assume nucleons to be elementary particles that interact by the strong nuclear force. The next theoretical background provided here will follow this simpler approach.

Only hadrons (including nucleons) can interact via the strong interaction, being scattered from other hadrons, producing changes in their motion and/or producing other particles, via this mechanism of interaction [15].

This strong interaction is charge independent (it is the same for neutrons as for protons), spin dependent and of short range (in the order of 10^{-15} m). Strong nuclear force is sufficiently strong to bind low energy hadrons together, and could be divided in three components: i) short-range; ii) intermediate/medium-range; and iii) long-range. Figure 1.3 illustrates the total nucleon-nucleon force according to the range of interaction.

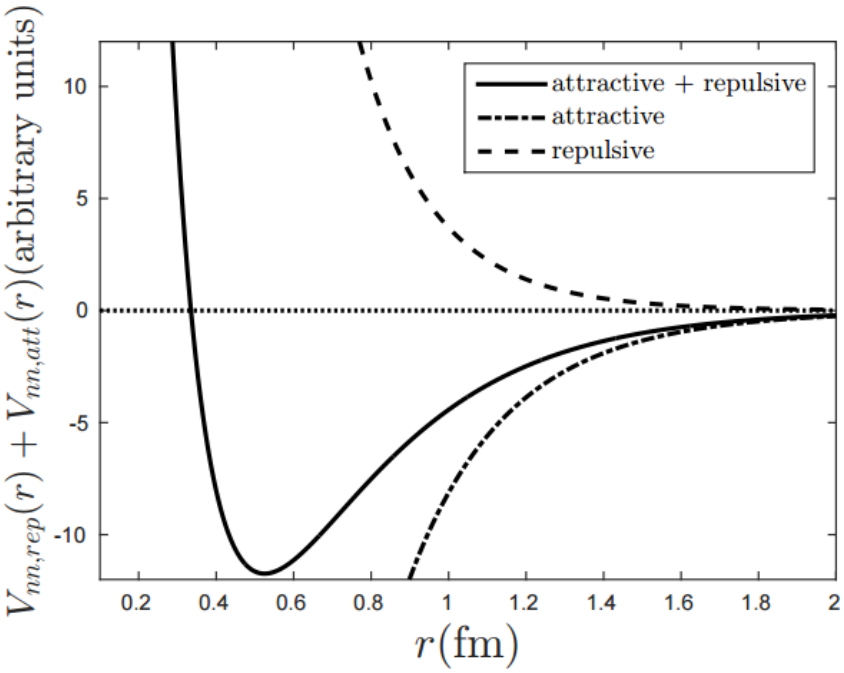

Figure 1.3 – Total nucleon-nucleon force.

Source: M. Naghdi, "Nucleon-Nucleon Interaction: A Typical/Concise Review," *Phys. Part. Nucl.,* vol. 5, 2014.

Thus, strong force is responsible, for example, for the binding of neutrons and protons in the nucleus, and for the nuclei shape [16, 17]. Therefore, it is necessary to provide energy to separate its components. Inversely, a certain amount of energy is released during the formation of the stable structures from its components. Binding energy of the nucleus $B(A,Z)$ is deducted from the energy difference between the nucleus and its stable free components [Z protons and N (=A-Z) neutrons]. From the relativistic conservation of mass-energy, the total mass of the stable nucleus must be inferior than the sum of the masses of its components ($M_{nucleus} < \Sigma$ mi) and this is verified in this situation [18, 19].

Binding energy per nucleon is an important parameter that allows the understanding of stability in different nuclides. In stable isotopes binding energy per nucleon is comprehended between 7 and 9 MeV, and this binding energy

between nuclei components depends on several factors. Overall binding energy is proportional to the number of nucleons (number of mass - *A*).

The binding energy per nucleon as a function of the number of mass is shown in Figure 1.4. As it can be observed, binding energy increases with the mass number in light nuclei until reaching a maximum at mass number of around 55-60 (in the iron-nickel region), with the nuclei ^{56}Fe normally indicated as the one that has greater binding energy per nucleon. Beyond, it starts to decrease slowly in function of the rise of mass number. Larger binding energy and lower mass mean more stable nuclei. Of course, the more nucleons mean the greater the total binding energy. The combination of this trend show us that energy can be released by the fusion of light nuclei into heavier ones or by the fission of heavy nuclei into lighter ones [19].

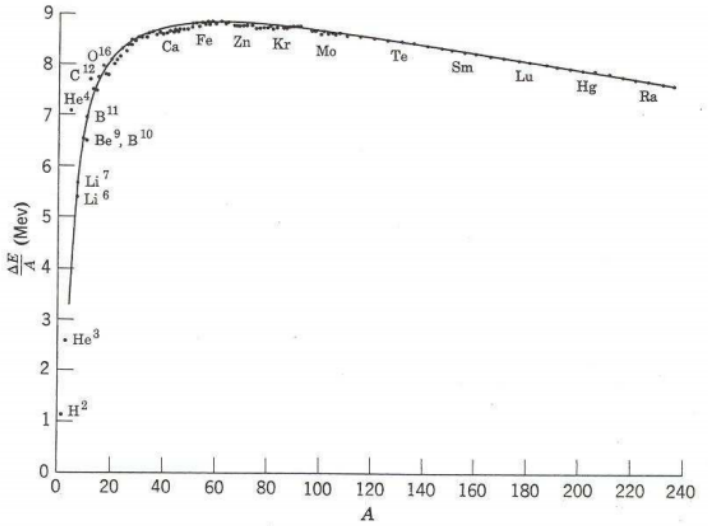

Figure 1.4 - Binding energy per nucleon versus the mass number of the isotope.

Source: Contemporary Physics Education Project, *Nuclear Science - A Guide to Nuclear Science Wall Chart*, Third ed.: Science Kit, 2003.

However, other corrections should be considered in the determination of the binding energy per nucleon, including the contribution of the electrostatic repulsion between protons, which in turn is dependent on the square of its charge (Z^2), leading to the importance of the relationship between *A* and Z^2 in the study of nuclear stability [18-20]. These two considerations (dependence on A and on Z^2) are mainly based on the liquid drop model for the nuclear structure.

On a first approximation, the later factor mentioned, Coulomb contribution to the binding energy, seems to indicate that it would be favorable to have less protons than neutrons in a nucleus. However, this is not the case and it is important to use some considerations from other nuclear structure model (shell model) to explain the fact that it is common to have roughly the same number of neutrons and protons in stable nuclei. The notion underlying this phenomenon is called symmetry and takes into account quantum mechanics in nuclei (quantum states of nucleons) [19]. Since isotopes have different mass numbers they will possess different levels of binding energy, which leads

to the appearance of isotopes of the same element with greater or lesser stability. A way to assess the stability of a nuclide is to evaluate the ratio of the number of neutrons and protons (*N*/*Z*) – Figure 1.5.

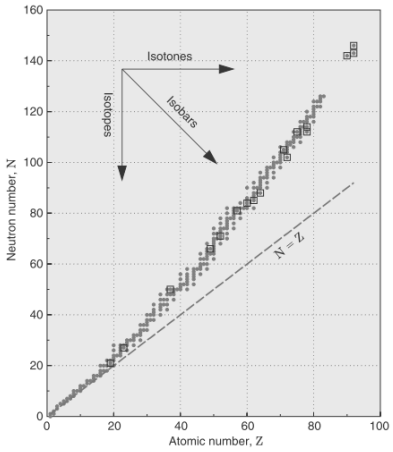

Figure 1.5 - Neutron (N) *vs.* Atomic (A) number in nuclides found in nature.

Source: S. R. Cherry, *et al.*, *Physics in Nuclear Medicine*, Fourth ed.: Saunders, 2012.

Indeed, the analysis of this *N*/*Z* ratio will also give an important data to predict the type of nuclear decay of each radionuclide, as it will be explained later.

Finally, the last factor contributing to the binding energy, and consequently to nuclear stability, is the physical evidence that nucleons tend to pair off. This means that binding energy is greater in nuclei where all the neutrons and protons are paired-off. Inversely, an odd-odd nucleus (odd number of protons and neutrons) tend to present a lower binding energy [18, 19].

1.1.2. Radioactive decay

Actually more than 2700 isotopes from elements of the Periodic Table are known. All the unstable nucleus tend to transform themselves into more stable ones, through one of several allowed processes: division into smaller fragments, particle emissions and/or emission of energy in the form of electromagnetic waves [21]. This is what is meant by radioactive decay and nuclides undergoing such transformations are called radionuclides.

The most common decay processes are based on the spontaneous emission of photons (gamma or X-rays) or particles (α, β^- or β^+). A possible method of division and classification is based on the fundamental force underlying to the decay process, i.e.: strong nuclear force or weak nuclear force. Other interactions due to some quantum nuclear structure rearrangements could also be added to this division.

There are radionuclides that decay to a nuclear state with increased energy compared to the ground state (excited state) with relatively long physical half-life. Radionuclides could have these excited states with duration longer than the nanosecond scale (meaning 100 to 1000 times longer than the other excited states) being designated by

metastable states [22, 23]. In these cases, the radioactive decay occurs by releasing the excess of energy by emitting gamma photons, in a process called isomeric transition.

Another possibility of decay in excited states is the internal conversion, namely the release of energy by a gamma photon that is absorbed internally by an orbital electron (typically from the layers K or L). By absorbing this energy, the electron is ejected from the electron cloud and remains with the difference between the photon energy and the binding energy as kinetic energy. Subsequently, occurs the occupation of the gap created by the electron in the cloud by an electron from an higher orbital and the consequent release of energy in the form of characteristic X-rays or Auger electrons [22].

Together, isomeric transition and internal conversion are examples of radiative processes, involving fundamental electromagnetic interactions, and resulting in the conservation of atomic and mass number [19].

In what concerns to strong force mediated decays, an alpha (α) particle could be emitted from the nucleus, in a process relatively common in very heavy elements.

Generally, individual nucleons cannot escape from the nucleus. However, a bound group of nucleons can sometimes escape because its binding energy increases the total energy available for the process. The most significant demonstration of this possibility is α-decay process. This aggregate of nucleons is very strongly bound and has this ability to escape from the nucleus. The potential energy of an α-particle is dependent on its distance from the center of the nucleus (due to the strong nuclear interaction) [18].

Alpha particles are helium nuclei (A = 4 ; Z = 2), and have the ability to deposit large amounts of energy (4 ∼ 8 MeV) within a very short range travelled in matter, due to their charge and mass - reason why they own high Linear Energy Transfer (LET). Equation

$$ {}^{A}_{Z}\mathrm{X} \rightarrow \alpha + {}^{A-4}_{Z-2}\mathrm{Y} + energy, \qquad \textbf{Eq. 1.1} $$

represents this decay in which the resulting nucleus will have a decrease in the atomic number (Z - 2) and in the mass number (A - 4).

One of the many facets of the weak interaction is the Beta-decay (β decay). Being slower by several orders of magnitude than electromagnetic and strong interactions, these weak processes cannot be observed if there are these competing interactions [24]. Weak interactions transform protons in neutrons or vice versa, changing as well the number of charged leptons (positive or negative electrons) and number of neutrinos [19].

β-decay processes include β-minus decay (β^-), β-plus decay (β^+) and electron capture. These processes occurs always in a strict dependence on the existence of isobars with smaller masses [18].

Given this, β^- emission is energetically possible whenever the mass of the daughter atom is smaller than its isobaric neighbor in Z. In such cases, β^- particles (negatively charged and very high speed electrons) are emitted simultaneously with an anti-neutrino, while a neutron is converted into a proton, resulting in a nucleus with an increase in the atomic number and maintenance of mass number according to

$$ {}^{A}_{Z}\mathrm{X} \rightarrow \beta^{-} + {}^{A}_{Z+1}\mathrm{Y} + \bar{\upsilon} + energy. $$ **Eq. 1.2**

β^- particles are normally emitted from isobars that have an excess number of neutrons. The emitted β^- particles present a continuous kinetic energy spectrum, ranging from 0 to the energy endpoint (E_{max}) - correspondent to each radionuclide, with an average energy of β^- emitted particles that is often approximately equal to 1/3 $E_{máx}$ (Figure 1.6). The cited energy spectrum applies also to β^+ (positrons) - to be described in detail in an appropriate topic.

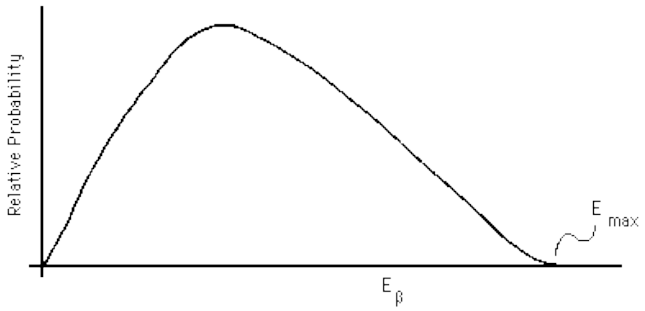

Figure 1.6 - Beta decay energy spectrum.

Source: S. R. Cherry, *et al.*, *Physics in Nuclear Medicine*, Fourth ed.: Saunders, 2012.

In isobars that have an "excess" of protons, stability could be found by emitting a positron (positive electron). In this decay a proton is transformed in a neutron with the release of an antimatter particle named positron (or beta plus particle - β^+) and a neutrino:

$$ \mathrm{p}^{+} \rightarrow \mathrm{n} + \mathrm{e}^{+} + \upsilon + energy. $$ **Eq. 1.3**

This decay results in a nucleus with a decrease of one unit in the atomic number and maintenance of the mass number, as it is represented in equation

$$ {}^{A}_{Z}\mathrm{X} \rightarrow {}^{A}_{Z-1}\mathrm{Y} + {}^{0}_{+1}\mathrm{e}^{+} + \upsilon + energy. $$ **Eq. 1.4**

If the nuclear masses of neighboring isobars in Z differ by less than the electron mass, stability could be reached by capturing an orbital electron that combines with a proton to obtain a neutron - <u>electron capture</u> decay. In this case, the resulting nuclide is an isotope of a different element, maintaining the mass number as it could be concluded by the decay equation

$$ {}^{A}\mathrm{X}_{Z} + \mathrm{e}^{-} \rightarrow {}^{A}\mathrm{Y}_{Z-1} + \upsilon + energy. $$ **Eq. 1.5**

The layer of the electron which is captured is filled by another electron, which in turn is more energetic and leads to the release of X-rays.

Except for a small difference in the energies involved, electron capture process has the same selection rules applied to β^+ decay and is usually in competition with it. The probability of electron capture increases with Z^3, due to the increased strength of the nuclear Coulomb field and decreased radii of electronic orbits [23].

1.1.3. Positron and positronium physics

Due to the main theme of this work, positron should be covered with a special attention and a detailed description here.

Back to its discovery, on 2nd of August of 1932 the scientist Carl D. Anderson was photographing cosmic-rays track using a Wilson chamber (based on a magnetic field of 1.5 T) and registered an interesting finding (Figure 1.7) [25]. At that time, properties of the discovered particle were carefully described although some limitations of the experiment: "*(…) It is possible with the present experimental data only to assign rather wide limits to the magnitude of the charge and mass of particle (…) It is concluded, therefore, that the magnitude of the charge of the positive electron which we shall henceforth contract to positron is very probably equal to that of a free negative electron (…) The magnitude of the proper mass cannot as yet be given further than to fix an upper limit to it about twenty times that of the electron mass*" *[25]*.

In fact, this insights were true and the photo presented below is yet known as the first photo of a positron path. Moreover, in Anderson's paper it was already suggested that positrons must be secondary particles, ejected from unstable atomic nucleus [25].

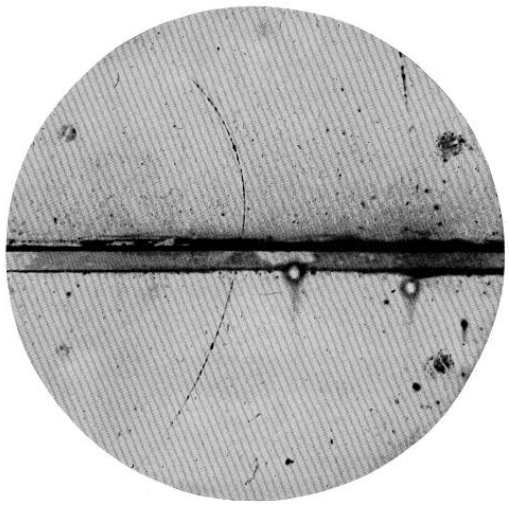

Figure 1.7 - First known photo of the path of a positron.

Source - C. D. Anderson, "The Positive Electron," *Physical Review,* vol. 43, pp. 491-499, 1933.

In physical terms, positron has the same quantity of charge as the electron, 1.6×10^{-19} C, but positively charged, the very same rest mass of an electron, 9.10×10^{-31} kg, and an intrinsic spin of ½ , being thus a fermion.
In matter it eventually annihilates with an electron after a short lifetime, even considering that current theories of particle physics emphasize that, in vacuum, positron is a stable particle [26]. The time frame from positron emission until the formation of positron-electron pair is inversely proportional to the local electron density. Its interaction with electrons in soft matter can result in the formation of positronium that is an unstable electron-positron bonded state. The positronium atom can be formed when the energy of the incident positron exceeds the difference between the ionization energy of the target atom and the binding energy [26]. However the probability of occurrence in condensed matter is very reduced, mainly due to the inexistence of free space in matter to its formation.
Positronium is electrically neutral, and its centre of mass is midway between the constituent electron and positron. When the positron-electron pair is in a singlet spin state it could totally annihilate with the consequent emission of two gamma-photons. The triplet spin state annihilates with the emission of three photons, having very reduced rates of occurrence, cause of pickoff [27]. Due to the long lifetime of triple state it become more probable that the positron annihilates with another electron via two photons.
In normal circumstances, the positron remains free in space and its annihilation with the electrons of matter result in two photons of around 511 keV - called annihilation photons [22]. This physical process is the basis of the signal measured in Positron Emission Tomography (PET) used in Nuclear Medicine – with special interest for the process reported in this work.

1.1.4. Nuclear Medicine procedures

As it was already focused, the information obtained in Nuclear Medicine depends on the detection of radioactive emissions from compounds known as radiopharmaceuticals, which are the combination of a drug with a pre-determined biological distribution with a radioactive isotope that decays to provide the signal for detection.
In this sense, the selection of the radionuclide (source) must guarantee that its decay mode is adapted to the desired purpose. Generally, for diagnostic purposes, it uses primarily two types of sources; gamma radiation emitting sources (radioactive isotopes that decay by isomeric transition or electron capture - that will not be highlighted here) for Conventional Nuclear Medicine or beta plus emitting sources for Positron Emission Tomography - that will be discussed along this work. On the other hand, Nuclear Medicine includes also some therapeutic procedures, where the main goal of the radionuclide is to destroy specific cells or tissues. Figure 1.8 illustrates the relation between the type of procedure and the nuclear decay mode of the radionuclide.

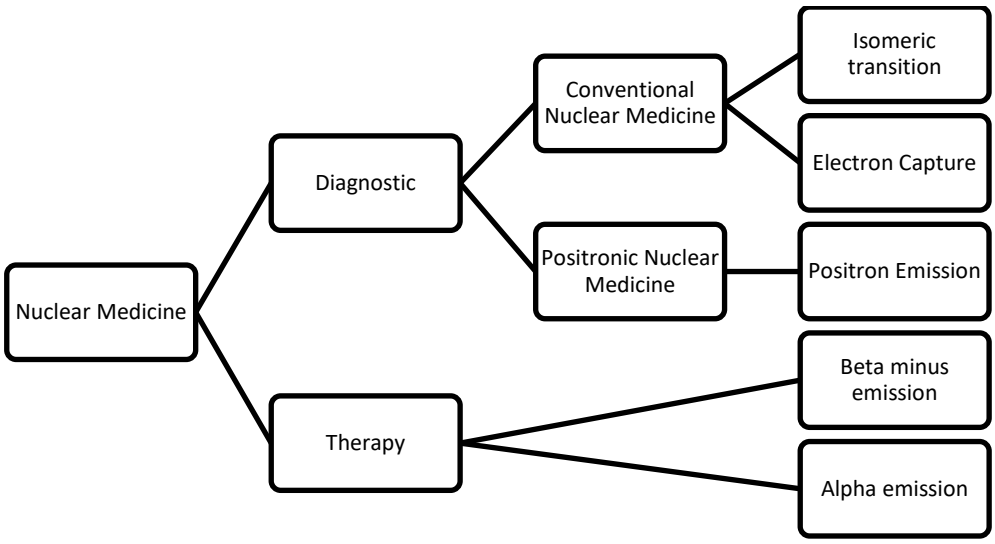

Figure 1.8 - Relationship between Nuclear Medicine procedures and the decay mode of applied radionuclides.

1.2 Radionuclides in Nuclear Medicine

In the sequence of Figure 1.8, a selected radionuclide will have an application to a specific kind of procedure mainly based on its physical properties – mainly centered on radioactive decay. This sub-chapter is divided in two different sections; the first will explore the most common radionuclides in the Nuclear Medicine environment; and the second will describe some of the radionuclides that constitute the most modern tendencies in the field.

1.2.1 Common radionuclides in Nuclear Medicine

In this context it is important to refer the most applied radionuclides in Nuclear Medicine and to characterize them in what regards to physical properties (decay mode and half-life) - Table 1.1.

There are several different reasons that increase (or decrease) the success of the application of a certain radionuclide. Considerations such as the physicochemical properties, availability, cost and easiness of use are some of the most relevant.

For instance, in classical literature, the most common clinical PET imaging practice relies only in four radionuclides, namely carbon-11 (^{11}C), nitrogen-13 (^{13}N), oxygen-15 (^{15}O) and fluorine-18 (^{18}F). All of them are characterized by relatively short periods of physical half-life [28]. The commercially available radiopharmaceuticals are almost invariably associated with ^{18}F, due to the technical constraints involved in the production and commercial distribution of the other short-lived nuclides. It must be cited againg and highlighted the importance of radiopharmaceuticals labeled with ^{18}F, mainly because of its physical properties; a period of half-life that allows local (*in situ*) production and short-medium scale distribution, and a β^+ energy that lead to good image quality [29].

From now on, topics under discussion will only focus aspects related with PET.

Table 1.1 - Physical properties of the radionuclides most commonly applied in Nuclear Medicine.

Radionuclide	Physical half-life	Decay mode	Application
^{11}C	20.4 min	β^+	PET
^{13}N	10.0 min	β^+	PET
^{15}O	2.07 min	β^+	PET
^{18}F	109.80 min	β^+	PET
^{67}Ga	3.26 d	EC (X-rays)	Conventional
^{68}Ga	68.30 min	β^+	PET
^{82}Rb	1.30 min	β^+	PET
^{90}Y	64.00 h	β^-	Therapy
^{99m}Tc	6.02 h	IT (γ rays)	Conventional
^{111}In	2.80 d	EC (X-rays)	Conventional
^{123}I	13.20 h	EC (X-rays)	Conventional
^{131}I	8.02 d	β^-	Conventional/Therapy
^{153}Sm	64.28 h	β^-	Therapy
^{186}Re	3.71 d	β^- / EC (X-rays)	Therapy
^{201}Tl	3.04 d	EC (X-rays)	Conventional
^{223}Ra	11.40 d	α	Therapy

EC - electron capture; *IT* - isomeric transition; *PET* - positron emission tomography

Looking at the national reality in Portugal, according to a report from one of the most important regulatory bodies in the Health sector in Portugal (*Entidade Reguladora da Saúde*), it is possible to illustrate the clear lead role of ^{18}F in the labeling of radiopharmaceuticals used. The ^{18}F is the selected marker in 98.8% of the total examinations performed, while the rest was due to ^{68}Ga labeled radiopharmaceuticals [30]. This fact emphasizes that the past role of ^{13}N and ^{15}O explicit in literature is not really translated into the clinical practice (at least in Portugal, according to this report). Other important aspect is the promising and growing role of ^{68}Ga-labeled radiopharmaceuticals.

1.2.2 Unconventional radionuclides in Positron Emission Tomography

Since the late 80s, PET technology has basically used only the already cited four radionuclides. However, in recent times, and as a way to increase the range of application of technology as well as diversify labeled compounds, it is being expanding the field of development related with the production processes, radiolabeling, and application of different radionuclides (named unconventional radionuclides). In this sub-chapter, the term unconventional radionuclides will be applied to name all PET radionuclides that do not be usually cited in the most classic literature on the field, even considering different levels of actual development in their production or application.

Examples that could be enumerated include radionuclides like: Titanium-45 (^{45}Ti), Cobalt-55 (^{55}Co), Copper-60/61/62/64 ($^{60/61/62/64}$Cu), Zinc-62 (^{62}Zn), Selenium-75 (^{75}Se), Gallium-68 (^{68}Ga), Rubidium-82 (^{82}Rb), Yttrium-86 (^{86}Y), Technetium-94 (^{94}Tc) and Iodine-124 (^{124}I) [31, 32].

One of the first demonstrations of this trend was the application of ^{82}Rb in human experiments [33], being actually available for clinical application. Actual reports indicate also that ^{68}Ga is passing from an "unconventional" radionuclide to one of the most applied and studied radionuclides for PET. The recent approval by the Food and Drugs Administration (FDA) of the first ^{68}Ga-radiopharmaceutical (^{68}Ga-DOTATATE) for clinical use is the major demonstration of this consideration [34].

A careful analysis of the short list of radionuclides shown on Table 1.2 illustrates that there has been some tendency to invest in the study of radioactive elements with higher periods of physical half-life of decay and chemical characteristics associated with the behavior of metals. Apparently, it seems to exist the need to study more than those cellular and molecular processes studied by most organic compounds (using biomolecules labeled with carbon and fluorine, for example). Some of the named unconventional radionuclides allow the study of processes with slow kinetics, while still allowing the production and large scale distribution of these compounds. Given the usefulness of these radionuclides, some ligands have been developed called bifunctional chelates, whose establish covalent bonds between the radionuclide metal and a reactive functional group which allows attachment to a vector that confers determined biodistribution - a radiochemistry strategy very interesting to label macromolecules.

Table 1.2 – Physical half-life of some of the unconventional radionuclides with most potential in PET imaging.

Radionuclide	Physical half-life
^{45}Ti	3.09 h
^{55}Co	18.2 h
^{64}Cu	12.7 h
^{62}Zn	9.2 h
^{75}Se	119.8 d
^{68}Ga	67.7 min
^{82}Rb	1.3 min
^{86}Y	14.7 h
^{94}Tc	4.9 h
^{124}I	4.2 d

Just to present an idea of the overall size of this market, the global radionuclide market was valued at almost 5000 million of dollars in 2012, with medical radionuclides accounting for about 80% of this, and is poised to increase significantly and reach about 8000 million by 2017. In regional terms, North America is the dominant market for

diagnostic radionuclides with close to half of the market share, while Europe represents about 20% of the economic transitions [35].

This trend could be attributed to the increased installation of PET and SPECT scanners, to the increase in the number of available cyclotrons (increasing availability of radionuclides/radiopharmaceuticals), and, finally, to the adoption of new modalities of diagnostic and radionuclide therapy. New radiopharmaceuticals, based on radionuclides rather than ^{18}F and ^{11}C, is one of the most expanding field.

1.3 The potential interest of Titanium-45

Following this trend, it was decided that one of the most interesting cases of unconventional radionuclides is ^{45}Ti.

Titanium is the element of the periodic table with atomic number 22, belonging to the group of transition metals. It has low density and oxidizes immediately upon exposure to air, possessing also a relatively high melting point of about 1650 °C. Twenty five titanium isotopes are known, from mass number of 39 until 63; including 5 stable, 7 proton-rich and 13 neutron-rich isotopes [36].

Motivations of the choice of ^{45}Ti relate to the physical characteristics of the radionuclide, with (i) the period of physical half-life of 3.09 hours, which allows its distribution within a range even broader than radiopharmaceuticals based on ^{18}F; (ii) its decay predominantly by positron emission (85%); and (iii) the maximum positron energy of 1040 keV and an average energy of 439 keV per positron, that put it at parity with radionuclides such as ^{11}C, or even in an advantageous positions when compared to ^{68}Ga, in terms of expected spatial resolution of images obtained [37].

The implications of these features in the resolution of obtained images has been already tested on phantoms and considered very advantageous in the context of small animal imaging (Preclinical imaging - where the spatial resolution is even more demanding) [38].

On the other hand, the potential applications of compounds labeled with ^{45}TI are also a major factor in this choice and investment in a project devoted to this subject. As an example, it can be highlighted the fact that there are some cytostatic agents based on titanium that are on development, so knowledge of its biodistribution in the human body and mechanisms of accumulation in tumor tissue are subjects of active research [38, 39].

Finally, it is also very important to add that it is very strong the growth in the area of Nanotechnology and Nanomedicine. Between nanoparticles used as drug delivery systems, titanium dioxide (TiO_2) nanoparticles have been suggested as one of the most interesting options. This nanoparticles can penetrate in biological cells (in a manner that is not yet correctly understood), allowing medical applications that could include cancer treatment due to its oxidizing and reducing power. However, if we concentrate in diagnostic purposes instead of treatment, it is possible to use TiO_2 nanoparticles to localize these processes, since it is known that they are internalized in malignant cells [40-42]. In this context, it is also possible to hypothesize that ^{45}Ti-radiolabelled TiO_2 nanoparticles could be interesting as an imaging tool.

However, to our knowledge, just one or two groups are currently working on the development of production strategies to obtain this radionuclide, all of them using low energy cyclotrons.

1.4 Aim and outline of the Thesis

Based on the physical and chemical properties mentioned above as well as its possible applications, both in terms of scientific research (in areas such as Pharmaceutical Sciences or Pre-clinical imaging) or at the clinical level (PET imaging with various radioligands), attention should be devoted to a research project that aims to study and develop aspects inherent to ^{45}Ti use in PET.

Before continuing, it is important to think a little bit in the technical steps needed to execute a PET examination that could be resumed in: radionuclide production, preparation of radiopharmaceutical and its respective quality control, radiopharmaceutical administration, image acquisition and its processing and interpretation - Figure 1.9.

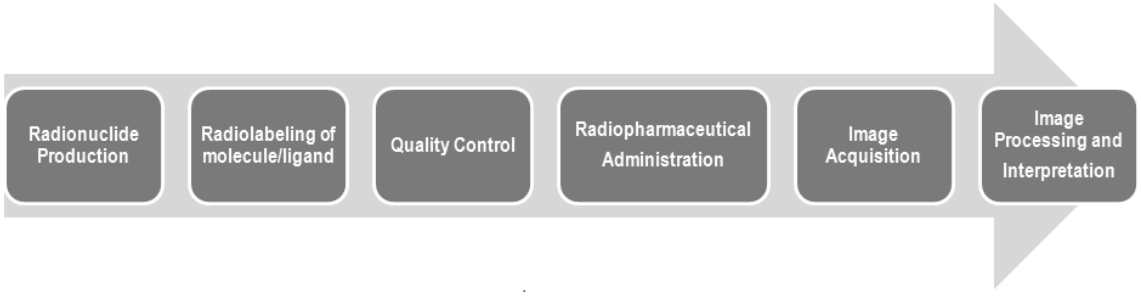

Figure 1.9 - Technical steps inherent to a PET examination.

Radionuclide production is the first crucial technical step involved in PET. Appling this idea to the example and specific context mentioned in this thesis, the production of ^{45}Ti is yet very poorly explored in literature. There is a lacking of dedicated and detailed studies, especially with regard to the construction of solutions and protocols allowing an industrial and systematic application - essential for widespread application of this radioisotope. This research was designed to fight against this lack of evidence found in literature.

To satisfy the global aim presented, this investigation project was designed with the following major objective:

- ✓ Study the viability of the production of Titanium-45 in low energy cyclotrons, expecting to characterize the excitation functions of the possible nuclear reactions, determine yield of the production and to develop a critical analysis to select the best methodology;

On the other hand, this Thesis possess the following specific objectives:

- ✓ Study and apply optimized methodologies to plan an activation experiment, using Monte Carlo simulation codes;

- ✓ Study and optimize technical procedures involved in an activation experiment;
- ✓ Apply data obtained in the major objective to conceptualize the optimization of all the production process (energy, current and time of irradiation, design and construction of the target, *etc*…) as a way to develop an efficient methodology to a widespread application in radionuclide production centers;
- ✓ Explore potential biomedical applications of Titanium-45, supporting the need to optimize its production;

In this sense, the Thesis begins with this chapter (**Chapter 1**), with the aim to introduce some transversal concepts related with Nuclear Medicine field and its physical basis, acting as the fundamental theoretical background of this work.

Continuing on the theoretical side, **Chapter 2** will be devoted to introduce the physical basis of radionuclide production and, more specifically, induction of nuclear reactions and cyclotron physics and operation.

Chapter 3 illustrates the usefulness of Monte Carlo simulation codes as a way to plan an activation experiment. While **Chapter 4** shows the theoretical background underlying Gamma Spectroscopy and its analysis.

Main experiments developed under the scope of this Thesis are described, analyzed and discussed in **Chapter 5**. Following that, **Chapter 6** presents the exploitation of the potential applications of ^{45}Ti for biomedical imaging, including a systematic review about nanoparticle-based radiopharmaceuticals, and other possible direct applications of the radionuclide considered.

Finally, **Chapter 7** is based on the general discussion of all the aspects involved in this Thesis and presents its final remarks and conclusions.

2. Production of Radionuclides for Nuclear Medicine

According to the widely accepted theory of the "big bang", all matter in the universe had its origin in a cosmic event that released an enormous amount of energy about 13.6 billion years ago. Scientific community believes that particles such as protons and neutrons, which form the building blocks of nuclei, were condensed as free particles during the first seconds after this explosion. In a resumed way, with the increase of temperature these particles undergone in a series of combinations culminating in all the elements in the periodic table that are known today. With years passing, the unstable combinations of particles undergone in transformation (radioactive decay) and several elements became more stable (and, of course, non-radioactive). However, even billions of years passed from the explosion, some natural radioactive elements with very long half-lives remain, such as ^{40}K, ^{204}Pb, ^{232}Th and the naturally occurring isotopes of uranium [43].

With the continuous growth of need of radionuclides for many different applications (that include, for instance, the case of medical imaging treated in this research), nature could not act as the supplier for these substances. It should be introduced the concept of induced radioactivity or, in other words, the need to artificially produce radionuclides. In fact, radionuclide production is the main area under study in the context of this work and it is pointed in the literature as one of the greatest contributions of Medical Physics to the field of Nuclear Medicine [44].

2.1 Introduction to radionuclide production

After the discovery of natural radioactivity by Becquerel, in 1896, several experiments were undertaken in this field of science. In 1924, Chadwick and Rutherford showed that protons are emitted when boron is irradiated by natural alpha particles. Some years later, in 1934, the couple I. Curie and F. Joliot was studying the results from an irradiation of boron and aluminum targets with alpha particles obtained from polonium and observed positron emission. The observed positrons were emitted from the targets, even after the removal of the alpha particle source [45]. This last experiment was the first unequivocal demonstration of artificial radioactivity.

Around the same time, the invention of the cyclotron, and discoveries of neutron and deuteron by various scientists of the field contributed to the artificial production of many more radionuclides.

In fact, the development of nuclear technology is one of the most significant achievements of the twentieth century. Nuclear technology is currently being used in very different fields and aspects of daily life, from applications in health and medicine, to manufacturing and construction, to powering common household items, and to producing electricity for some of the worldwide needs.

The production of radioisotopes can be considered an alchemy of modern times, where some elements are artificially transformed in others.

With the actual state of the art, the most relevant methods of radionuclide production include nuclear reactors or charged particle accelerators such as cyclotrons and linear accelerators. At the present moment, more than 2700 radionuclides have been produced artificially in cyclotrons, nuclear reactors and in linear accelerators [46]. Few

examples could also be obtained in radionuclide generators using a decay based approach. Table 2.1 describes the main production methods for the most common radionuclides used in Nuclear Medicine (NM) daily clinical practice.

Table 2.1 – Main production methods for the most common radionuclides in Nuclear Medicine.

Radionuclide	Main production method
^{11}C	Cyclotron
^{13}N	Cyclotron
^{15}O	Cyclotron
^{18}F	Cyclotron
^{67}Ga	Cyclotron
^{68}Ga	Generator or Cyclotron
^{90}Y	Nuclear Reactor
^{99}Mo	Nuclear Reactor
^{99m}Tc	Generator
^{111}In	Cyclotron
^{131}I	Nuclear Reactor

From Table 2.1 it is possible to extract the idea that different artificial methods to obtain radionuclides are being used and that most of the PET nuclides are produced via cyclotron irradiation (compatible with their status of "proton rich" radionuclides), while some "neutron rich" nuclides are produced in nuclear reactors. Another different but interesting example is the case of the widely known ^{99m}Tc, the most applied radionuclide in conventional NM, that is currently mainly obtained by a generator system that is based on the decay of ^{99}Mo produced in nuclear reactors.
In a general overview, for instance when mentioning Nuclear Reactor production of radionuclides, one can say from the history that the first installation build for this application used natural uranium as fuel and graphite blocks as moderators and was built in Oak Ridge in the United States of America, operating since 1943 until 1963. Nowadays, according to the database of the International Atomic Energy Agency (IAEA) [47], there are more than 275 research reactors operating, from whose around 73 are useful for radionuclide production.
On the other hand, also according to a database of the IAEA [48], in the end of 2005 there were 262 cyclotrons operating in the 39 member states of the agency, however at that date it was believed that around 350 cyclotrons were operating in the whole world. Considering its interest to the subject of this investigation project cyclotrons will be deeply covered in sub-chapter 2.3.
Excluding generator production, independently of the specific methods that could be chosen, radionuclide production rely on the induction on nuclear reactions in specific targets. To better understand and discuss the aim

of this research, the next sub-chapter of this Thesis will be dedicated to the exploration of the physics involved in nuclear reactions.

2.2 Nuclear reactions physics

Nuclear reactions generate energy spontaneously in stars, are used to generate energy in nuclear reactors, and contributed to the existence of all the elements in the universe. The generic concept of nuclear reactions denote reactions between nuclei, and between nuclei and other kinds of particles or certain types of electromagnetic radiation such as photons. In nuclear reactions two nuclei, a nucleus and a particle or a nucleus and a photon, come together in such a close contact that there is an interaction mediated by the strong nuclear force, with the consequent alteration of the energy, composition and/or structure of the atomic nucleus. This process happens, for instance, when a target is bombarded by particles coming from a nuclear reactor, an accelerator or from a radioactive substance [49, 50].

In nuclear physics it is common to classify nuclear reactions in detail [18]. Here it will be used the simpler approach of nuclear reaction classification, based only on the identification of the target, the projectiles and the products, and, when appropriate, additional data will be provided.

Using the example of the first known artificially induced nuclear reaction, notation of these reactions could be illustrated according to the equation

$$\alpha + {}^{14}_{7}\mathrm{N} \rightarrow {}^{17}_{8}\mathrm{O} + \mathrm{p}\,, \qquad \textbf{Eq.2.1}$$

in which an alpha particle was the projectile bombarding a nitrogen-14 target, resulting in the production of oxygen-17 and the release of a proton from the target.

A simplest representation of this reaction could be the equation

$${}^{14}_{7}\mathrm{N}(\alpha, \mathrm{p}){}^{17}_{8}\mathrm{O}\,. \qquad \textbf{Eq.2.2}$$

Basic processes involved in nuclear reactions are restricted by conservation laws that should be mentioned. In this context, it will be presented a series of six conservation laws that are applied to nuclear reactions, such as: i) Baryonic number; ii) Electric charge; iii) Energy and linear momentum; iv) Total angular momentum; v) Parity; and iv) Isospin [49].

Baryonic number conservation relates to the initial particles (targets) and final particles (products) involved in a nuclear reaction, and it gains importance when it is desired to predict nuclear reactions output results. Experimental evidences indicate that there are no processes in which nucleons are created or destroyed without the creation or annihilation of corresponding particles. That is, the sum of the baryonic number of all incoming particles is the very

same as the sum of the baryonic number of all products. Below the threshold for the production of mesons (~140 MeV), no process related to nuclear force is capable to transform a proton into a neutron and vice-versa, resulting in a separated analysis of proton and neutron conservation, which should show up with same amounts in both sides of a nuclear reaction equation [49, 51].

The second conservation law, conservation of charge, is also very important. In the analysis of nuclear reactions this principle is commonly verified by the sum of the number of protons, which should be identical at both sides of the reaction [49].

Energy and linear momentum conservation is also verified. Theory and experimental evidence show that angles and velocities of particles involved in nuclear reactions are related and dependent of the input parameters before the beginning of the reaction [49].

For the purpose here intended, conservation of total momentum, parity and isospin will not be fully covered and explored.

In this sense, nuclear reactions can occur due to distinct mechanisms and could be simply divided in two main groups: i) direct reactions; ii) compound nucleus reactions (absorption reactions). The direct reactions involve short duration interactions between the projectiles and the targets with possible exchange of energy or particles between them. The other possible mechanism involves the fusion of the projectile with the target with the consequent formation of a highly excited compound nucleus. The decay of the compound nucleus leads to the final products of the reaction [49, 52].

Direct reactions are defined as the ones where the incident particle interacts in a time comparable to the time taken to transit the nucleus (around 10^{-22} seconds) and are more likely to occur when the incident particle has an energy corresponding to a *de Broglie* wavelength closer to the size of a nucleon rather than that of the overall nucleus. In general, the collisions are largely peripheral, with only a relatively small fraction of the total energy transferred to the target atom [18].

To explain in detail the physical mechanisms involved in direct reactions it is important to separate two different types of interactions among this class: elastic scattering and inelastic scattering.

Elastic scattering reactions are defined as those where the initial and final particles are identical. A typical equation of an elastic scattering nuclear reaction could be

$$a + A \rightarrow a + A. \qquad \textbf{Eq.2.3}$$

For example, a reaction could be initiated by proton(s) as projectile(s) and the target nucleus could remain the same and the proton(s) itself could sometimes emerge, be deflected in a specific angle but having the same energy in the center-of-mass system, constituting a clear example of an elastic scattering nuclear reaction [53].

In opposition, inelastic scattering reactions could be defined as the situations where the final particles are the same physical species, but at least one is in an excited state [18]. This situation is shown in the following equation

Eq.2.4

$$a + A \rightarrow a + A^*.$$

Using the same analogy used above, and considering a proton-induced reaction, in these situations the proton will excite the target nucleus from its ground to some higher-energy state, thus losing some energy and at the same time being deflected in a specific angle [53].

The other important class of nuclear interactions is where the projectile becomes loosely bound in the nucleus (absorbed) and shares its energy with all the nuclear constituents, i.e., compound nucleus reactions. Statistical equilibrium of the system is dependent of many factors such as nuclear species involved, type of projectile and its energy. Independently of those factors, the reaction time frame will always be much longer than the transit time, taking around 10^{-18} seconds. The compound nucleus is thus in an excited state and is inherently unstable, leading to the eventual occurrence of the emission of particles or de-excitation by "decay" with gamma rays [18].

In fact, compound nucleus reactions are those in which the incident particle interacts successively with a number of nucleons until most of its energy has been shared among many nucleons. In this situations, the incident particle initiates a cascade of collisions, where the products of these collisions, including the incident particle, will continue in their course, leading to new collisions and new changes of energy, resulting in a compound nucleus that has too much energy to be stable. However, because the energy of the projectile is now shared among many nucleons, it will survive for a relatively long time compared with the duration of a direct reaction [49, 53].

This particular type of reactions is normally characterized by the energy of the compound nucleus, because there is a large number of collisions and a totally random distribution of the amount of energy shared with the nucleons, resulting in a compound nucleus that is independent of the particular way in which it was formed, leading to a decomposition ("decay") that can take place by different pathways, usually called exit channels [49]. Following the notation used before, a typical compound nucleus reaction involving the formation of two final products could be represented as

Eq.2.5

$$a + A \rightarrow C^* \rightarrow B + b.$$

Considering the nature of the processes involved, the majority of reactions induced to radionuclide production are from the compound nucleus class.

Even considering that the most applied classifications of nuclear reactions only include this division in these extreme situations, there are lots of other specific types of nuclear reactions and intermediate classes somewhere between direct and compound nucleus reactions that will not be fully covered here. Table 2.2 presents a list of some of the most common nuclear reaction types.

Table 2.2 – Overview of the most common nuclear reaction types.

Type of nuclear reaction	Classification	Main features
Elastic scattering	Direct reaction	Projectile and target stay in the ground state
Inelastic scattering	Direct reaction	Projectile or target left in an excited state
Fragmentation	Direct reaction	Three or more nucleons/nuclei as reaction products
Fusion	Compound nucleus	At least two nuclei summed and left together as a reaction product
Fusion-evaporation	Compound nucleus	Fusion followed by particle evaporation and/or gamma emission
Fusion-fission	Compound nucleus	Fusion followed by fission of nuclei

The conservation laws already cited apply to nuclear reactions. Concerning nuclear reaction energetics, it is very important to begin by the notion of the conservation of total energy. For instance, for a reaction illustrated by X*(a,b)*Y it can be computed as

$$m_a c^2 + m_X c^2 + T_a + T_X = m_b c^2 + m_Y c^2 + T_b + T_Y , \qquad \textbf{Eq.2.6}$$

or

$$Q + T_a + T_X = T_b + T_Y , \qquad \textbf{Eq.2.7}$$

where

$$Q = [m_a + m_x - (m_b + m_y)]c^2 . \qquad \textbf{Eq.2.8}$$

Using Eq.2.8, it is possible to obtain Q that is an important parameter in the analysis of the reaction energetics. Q is the reaction Q-value. When $Q > 0$, the reaction is exothermic (or exoergic), meaning that energy is released by the transformation occurred. When $Q < 0$, the reaction is endothermic (or endoergic), meaning that energy is required for the reaction to occur [54].

Maintaining the attention on reaction energetics, another important aspect is related with the threshold energies, i.e., the minimum energy necessary for the reaction to occur. When $Q > 0$ (exoergic), a reaction could begin spontaneously. For reactions with $Q < 0$ (endoergic) the incident projectile must supply a certain minimum amount of energy that is termed the total reaction threshold energy. There are two components of the reaction threshold energy that could be separated as kinetic threshold energy and Coulomb barrier threshold [55, 56].

The kinetic threshold energy component is independent of the incident particle charge, thus it exists for all projectiles (charged or neutral). The amount of energy required to induce a nuclear reaction is slightly greater than

the Q- value. Apart from energy, momentum must also be conserved in any nuclear reaction, leading to a fraction of the incident particle retained by the products, implying that only a residual fraction is available for the reaction [55].

The other threshold energy component is dependent on the incident particle charge. If the incident projectile is a neutron or a gamma photon, it can reach the nucleus of the target without any kind of repulsion. In this situation the minimum energy needed to induce the respective nuclear reaction is specified only by the kinetic threshold energy. However, if the incident projectile is a positively charged particle (a proton, for example) the situation is different and, as it approaches the target nucleus, Coulombic nuclear forces repel the projectile. In extreme situations, if the projectile does not have sufficient momentum, it could even be unable to reach the target nucleus. As it was already said, nuclear forces can only cause the two particles to interact and produce a nuclear reaction only if the projectile is able to reach the surface of the target nucleus [55]. This is the main reason why equipments dedicated to nuclear reactions induction are manly based on particle accelerators – giving to the desired particles the energy necessary to overcome the threshold energies for specific nuclear reactions.

To finalize the discussion on nuclear reactions physics it is crucial to pay some attention to the probability of occurrence of each nuclear reaction. This lead us to the concept of cross section that could be defined as the probability of a given nuclear reaction to happen and could be expressed as a surface [43]. More specifically, cross-section designates the physical quantity that characterizes the probability of induction of a given nuclear reaction by projectile current density unit. In this context, when a beam of particles is incident on a target in the form of a thin foil, not every particle interacts with a target nucleus via a particular reaction channel, and the probability that an interaction will occur in a certain channel depends on the ratio of the "effective" area of the target nucleus to the area of the foil [57]. On other hand, cross-section, being typical for a given reaction, depends significantly on the projectile energy when interacting with the target. Thus, the discussion on the concept of cross-section should always assume an infinitesimal thin target, an incident beam of particles parallel to the target, monoenergetic and constituted by particles with reduced dimensions when compared to the target nuclei.

In a first observation, cross section data could mean that the probability of a given reaction to occur is approximately stable and equal to the geometrical cross section (πR^2), around 10^{-28} m^2 or 10^{-24} cm^2, when considering R the nucleus radius as $6x10^{-15}$ m^2 [52]. However, this geometrical consideration does not consider the finite size of the incident particle and nor the range of interaction forces that are in effect between the incident particle and the target nucleus [56].

As an exemplificative situation, it is possible to imagine a parallel and monoenergetic beam of projectiles with a flux φ_0 (expressed in particles/sec) that is bombarded upon a target, resulting in the attenuation of the beam by reactions in the target in a manner such that the transmitted flux is φ. Following this example, it emerges the question about how many particles induced the given nuclear reaction in the target, i.e., what fraction of the incident beam of particles induced the nuclear reaction under study [58]. This is a physical problem that could be solved with activation equations and by the application of the concept of cross-section.

Thus, considering the bombardment of a target with N_v atoms per m^3, the change in the flux may be infinitesimal as the particles pass through a thin section of the target, with thickness *dx*. The overall loss of beam flux depends on the number of target atoms per unit area ($N_v dx$), the flux (φ) and the reaction cross-section (σ) [52]. In analytical terms,

$$-d\varphi = \varphi \sigma N_v dx \qquad \textbf{Eq.2.9}$$

represents the attenuation of beam flux, where the negative sign means that the flux is always reduced when passing the target. Since radionuclides are produced in reactors or particle accelerators by the induction of nuclear reactions, neutron and charged particle induced reaction cross-section data is required for the study and optimization of radionuclide production [59]. In such a context, the determination of the cross-section of a particular reaction in an activation experiment could be simplified as

$$R_i = Inx\sigma_i\,, \qquad \textbf{Eq.2.10}$$

where R_i is the number of reactions of type *i* per unit time, *I* is the intensity of incident beam in particles per unit time, *n* is the number of target nuclei per cubic centimeter of target, *x* is the target thickness in centimeters and σ_i is the cross-section for the reaction *i* in square centimeters [60]. Note that the target thickness must be sufficiently reduced (infinitesimal) to avoid beam energy loss, avoiding the need to consider another value of cross-section - related with the intrinsic energy dependence of the cross-section value.

Different nuclear reactions have usefulness in the context of radionuclide production, but one can highlight neutron and proton induced ones. In this sense, these reactions could be induced using several different approaches. Even though, most of them are induced using only two main approaches: nuclear reactors and charged particles accelerators (mainly cyclotrons).

Assuming that the induction of a nuclear reaction is a critical step for radionuclide artificial production, and taking in mind the specific context here presented, induction of reactions using protons as projectiles deserve a special attention, reason why the next sub-chapter will be devoted to cyclotron physics and operation.

2.3 Cyclotron principles

In the beginning of the XX century, research in the nuclear physics field was centered in the definition and validation of a model for the atomic structure, the discovery of electromagnetic radiation and the understanding of its interaction with matter, between other fundamental discoveries such as many of the elementary atomic particles.

According to the history, in the Spring of 1929, a nuclear physicist named Ernest Lawrence was studying at the library of the University of Berkeley in California (United States of America) and read an article about multiple acceleration of positive ions, allowing to double the energy of a projectile by switching from positive to negative potential in order to push ions and then to pull them, and started to think about the possibility to develop a particle

accelerator able to reach 1 MeV energies using circular paths instead of long linear paths used in linear accelerators [61].

Lawrence started to build an equipment that later was named cyclotron, and the first demonstration of its capacity was published in 1931, when Lawrence stated that he was able to develop "*a method for the production of high speed protons without the use of high voltages*", capable of accelerating protons up to 80000 electron-volts [62]. Some months later, Lawrence and his laboratory fellow Stanley Livingston reached their goal, a circular accelerator capable of produce protons with 1 MeV [63].

In 1939 Lawrence was awarded with the Nobel Prize of Physics "*for the invention and development of the cyclotron and for results obtained with it, especially with regard to artificial radioactive elements*", and the scientist said that at the time of this invention he was "*overjoyed at the richness of the domain in the nucleus accessible to particles of several million electron volts energy*" [64, 65].

Due to their energy variability, energy precision and resolution, as well as due to the growing availability of higher energies for different kinds of projectiles, these equipments had a rapid and wider diffusion and availability and started to be applied in nuclear physics fundamental research and also in industrial and medical applications [66].

2.3.1 Cyclotron physics and operation

Cyclotrons are versatile devices used to produce accelerated ion beams which find application in a number of fields increasing each day. In the specific field of medicine, or more specifically in medical physics, their use is fundamental both for diagnosis and therapy. When citing diagnostic studies, it is important to emphasize that they are performed using suitable radionuclides (either pure gamma emitters or positron emitters) - whereas the former are produced using both nuclear reactors and cyclotrons, the latter, being proton-reach, are almost all produced at a cyclotron via charged-particle-induced reactions (with exception for some generator-produced radionuclides). On the other hand, hadron therapy is generally carried out either directly by accelerated ions themselves or by neutrons generated as secondary products in cyclotron induced reactions, being an example of another important application of cyclotrons in medicine [67].

As it was briefly introduced in the previous sub-sections of this work, radionuclide production using cyclotrons is very important for the Nuclear Medicine field, and specifically for the production of radionuclides used in PET imaging. Understanding the physics underlying the cyclotron operation is a topic of major interest when studying this field of science and development.

Charged-particle accelerators, which include cyclotrons and other devices such as linear accelerators, are efficiently used to accelerate electrically charged particles such as protons, deuterons and α particles to very high energies. Generally, a cyclotron consists of a pair of hollow, semicircular metal electrodes (called *dees* because of their shape), separated by a narrow gap (where the acceleration occurs), and positioned between the poles of a large electromagnet, with an ion source (used to generate the ions to be accelerated) near the center of the *dees*,

as it is shown in Figure 2.1. All these components of the device are contained in vacuum condition at pressures around 10^{-3} Pa (~10^{-8} atm) while in operation [22].

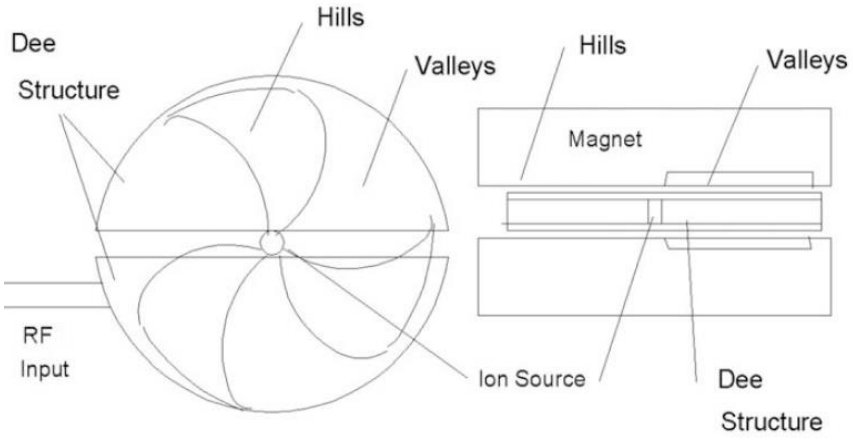

Figure 2.1 – Schematic representation of cyclotron components.

Source: International Atomic Energy Agency, "Technical Report Series No465 - Cyclotron Produced Radionuclides: Principles and Practice," ed. Vienna: IAEA, 2008, pp. 59-72.

Broadly, cyclotrons are devices that use a fixed magnetic field to constrain charged particles to nearly circular orbits that are synchronous with a radio frequency (RF) accelerating field. The charged particles repeatedly traverse the electric field produced by the RF electrodes, increasing in energy at each orbit [68].

Of course, with the natural evolution and scientific development, actual cyclotrons are quite different from the original ones. The classical cyclotron invented by Lawrence was simple in concept and construction, and it was based on the physical principles that charged ions are accelerated with electric fields and confined or focused by magnetic fields.

Fundamental frequency and higher order harmonics of RF fields may be used for acceleration of charged particles in a cyclotron. When the RF field is coupled to the *dees*, electric field gradients are produced. When the particle enters and leaves a *dee* it gains velocity and energy, due to the electric field, and the total energy gain of a particle crossing the accelerating gap depends on its charge, the amplitude of the potential difference, the phase relationship of the particle to the electric field and the path length between the electrodes [60]. After particle generation, a high frequency alternating voltage is generated by a high-frequency oscillator, typically in values around 30-40 kV and 25-75 MHz, respectively [22, 68].

The magnetic field of the cyclotron does not contribute to increase the energy of the ions to accelerate. Its function is to direct them to the region between the electrodes, that is where the electric field is felt. However, an important feature is that the value of the magnetic field should be such that the ion completes the semi-circle inside the *dee*

during the electric field oscillation period (time of the inversion of the oscillating electric field). This condition is called resonance condition and guarantees that the particle is accelerated always when crosses a *dee* [69].

The capability of the cyclotron machine to match the electric field RF with the frequency of revolution, called resonance condition, was the most brilliant insight of Lawrence in the invention of the cyclotron.

The orbit period of a particle of charge *q*, mass *m* and velocity *v* traveling in a circle in a uniform magnetic field *B* normal to the particle velocity is constant and its inverse is designed by cyclotron frequency. This lead to the fact that only the radius *R* of the orbit increases with particle momentum (*mv*) [69]. In this context, the radius *R* of the orbit is given by:

$$R = \frac{mv}{qB}. \qquad \textbf{Eq.2.11}$$

In the other hand, the period of each particle orbit could be given by

$$T = \frac{2\pi m}{qB}, \qquad \textbf{Eq.2.12}$$

showing that the frequency of a charged particle in a magnetic field is independent of the radius of its orbit.

However, it is also important to note that the particle must cross the gap between the *dees* at a given time interval or it will not be accelerated [60]. This is achieved applying a sinusoidal oscillating voltage on the *dees* that match the cyclotron resonance condition and accelerates the particles twice per each complete orbit, causing them to gain energy while increasing their orbit radius [69]. This condition is dependent on the orbital frequency and could be expressed as

$$\frac{1}{\omega} = \frac{r}{v}, \qquad \textbf{Eq.2.13}$$

where ω is the angular velocity, *r* is the radius in medium plane and *v* is the orbital velocity.

The magnetic field is responsible for the particle trajectory in the *dees* and it must be precisely constant to guarantee a constant orbit frequency that matches the constant RF electric field frequency [69]. This condition constitutes a state called resonance condition, being important to assure that each particle arrive at the acceleration gap when the RF voltage is near its peak value – as it was already reported.

Obviously, the condition of resonance and the other fundamental physical processes of cyclotron functioning are crucial and depend on the appropriate application. For instance, one of the most critical design issues for cyclotrons is the orbital stability of the circulating beam during the acceleration process, considering that all accelerated particles must remain focused in the spatial dimensions and in phase, preventing a particle to get lost on the magnet

poles or *dee* structures when circulating. In this context, both electric and magnetic restoring forces are important in the cyclotron to keep the beam centered in the correct orbit [69].

Apart from the discussion on the fundamental physics of the cyclotron, attention should also be given to the beginning of the process, i.e., to the ion generation. There are essentially two types of ion sources with different operating characteristics: internal and external. The internal sources are more common in commercial cyclotrons available nowadays. Charged ions are usually produced by the electric arc discharge in a gas yielding plasma. Two options are available to produce the electric discharge: the hot cathode and the cold cathode. In the hot cathode type a heated filament is used to maintain the arc, while in the cold cathode type once the discharge has been initiated no hot filament is used to maintain the plasma during normal operation of the ion source [60].

Another important aspect of cyclotron functioning is the vacuum system of the device. The inside the cyclotron must be maintained at a high level vacuum allowing the particles to travel in a free path in order to get an effective acceleration. Specifically, when talking about vacuum inside the cyclotron tank, values between $1x10^{-4}$ and $1x10^{-9}$ Pa are common, depending on the charge of particle aimed to be accelerated, whether the ion source is internal or external and also the type of cyclotron. To ensure this pressure condition there are three major types of vacuum pumps commonly used in cyclotrons: the ones based on oil diffusion, turbomolecular pumps and cryopumps [60].

Following the normal circuit of a particle inside a cyclotron, and after passing from the ion source to particle acceleration inside the *dees* (even exploring physical conditions needed to a normal circulation – as the vacuum and the magnetic field), attention should be paid to beam extraction systems used. It is important to separate two types of beam extraction systems that have a huge correlation with cyclotron properties and, more specifically, on particle charge: i) when particles are positively charged, the extraction of particles is carried out electrostatically (using deflectors); ii) when the negative ion of the projectile particle is used, extraction is carried out by stripping electrons off the negatively charged ions (using thin stripper foils) and allowing the magnetic field to reverse the beam path and to transport it out of the cyclotron [60]. Figure 2.2 illustrate these two different approaches.

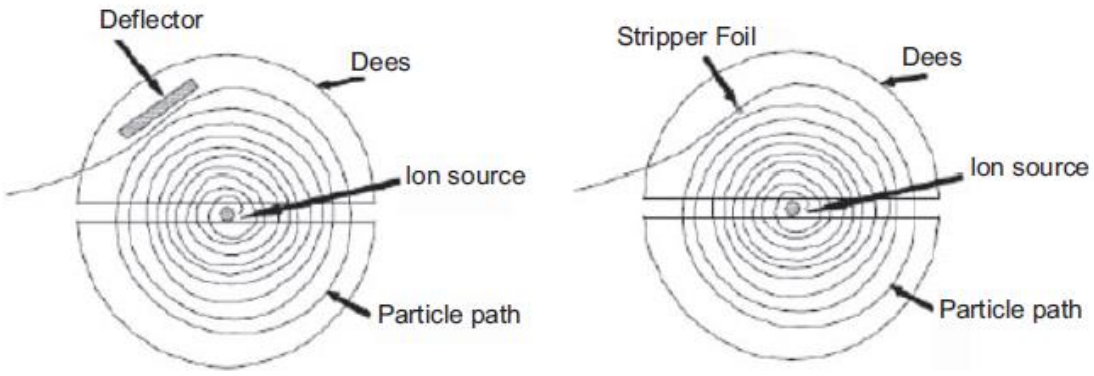

Figure 2.2 – Cyclotron beam extraction systems: electrostatic deflectors (left) and stripper foils (right).

Source: International Atomic Energy Agency, "Technical Report Series No465 - Cyclotron Produced Radionuclides: Principles and Practice," ed. Vienna: IAEA, 2008, pp. 59-72.

Apart from the general operational characteristics of a cyclotron, actual trends of research and development include a better knowledge about beam dynamics (specially in high intensity conditions), improvement of ion sources to obtain increased cyclotron performance related with intensity and energy of accelerated ions, increased capacity of injection and extraction of the beam, among other structural and functional improvements [70].

Maximum energy of accelerated particles extracted is, of course, one of the most relevant factors to characterize cyclotrons. This energy of particles accelerated in a cyclotron and extracted at a radius *R* is given by

$$E = \frac{1}{2}mv^2 = \frac{(qBR)^2}{2m}. \qquad \textbf{Eq.2.14}$$

showing that it is proportional to square of *B* and *R*[71].

According to the International Atomic Energy Agency [60], a possible classification of cyclotrons could be based on accelerated particle type and maximum energy of those particles, as it is shown in Table 2.3.

Table 2.3 – Classification of cyclotrons according to particle type and energy.

Source: International Atomic Energy Agency, "Technical Report Series No465 - Cyclotron Produced Radionuclides: Principles and Practice," ed. Vienna: IAEA, 2008, pp. 59-72.

Classification	Particle type	Particle energy (in MeV)
Level I	Single particle (protons or deuterons)	10
Level II	Single or multiple particle	20
Level III	Single or multiple particle	50
Level IV	Single or multiple particle	70-500

Although the widely accepted applicability of this classification, it could be cited that there are alternative classifications, and other authors prefer a more detailed approach, as the case presented in Table 2.4 from Qaim [72].

Table 2.4 – Alternative classification of cyclotrons according to particle type and energy.

Source: S. M. Qaim, "Nuclear data relevant to the production and application of diagnostic radionuclides," *Radiochim. Acta,* vol. 89, 2001.

Classification	Particle type	Particle energy (in MeV)
Level I	Single particle	≤ 4
Level II	Single particle	≤ 11
Level III	Single or two particle	≤ 20
Level IV	Single or multiple particle	≤ 40
Level V	Single or multiple particle	≤ 100
Level VI	Single particle	≥ 200

To analyze the distribution of the available cyclotrons according to its energy, an international survey conducted by the International Atomic Energy Agency [48] showed the preponderance of low energy cyclotrons, mainly those that allow maximum proton energies between 10 and 20 MeV – useful for diagnostic radionuclide production for Nuclear Medicine – Figure 2.3.

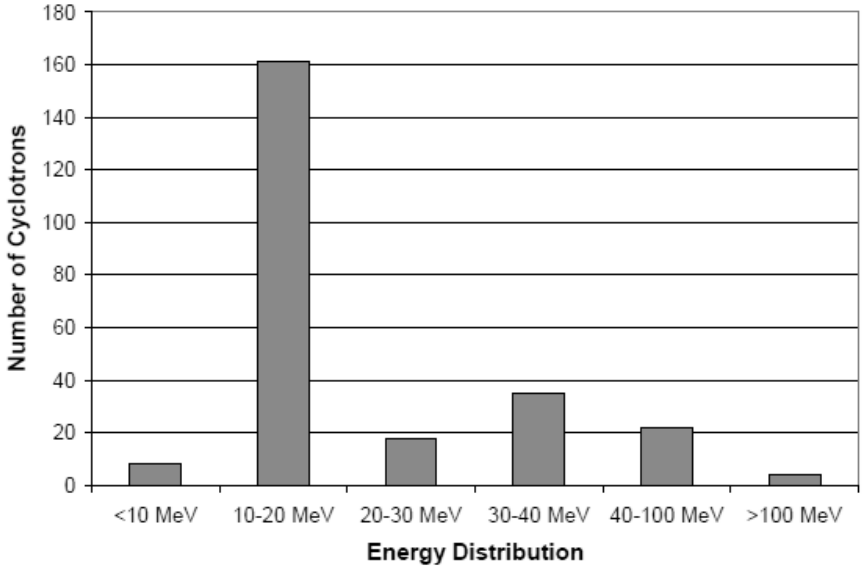

Figure 2.3 – Worldwide distribution of cyclotron maximum proton energies.

Source: International Atomic Energy Agency, "Directory of Cyclotrons used for Radionuclide Production in Member States - 2006 Update," ed. Vienna: IAEA, 2006.

In the other hand, commercial cyclotrons for isotope production could also be classified with respect to the method of ion production, technique of beam extraction from the cyclotron (or absence of extraction), intensity of accelerated ion beams, and other specific properties or features [73].

In this work focus will be devoted for commercial/industrial cyclotrons applied to PET radionuclides production. However, before exploring that type of cyclotrons, it is also important to correctly define the personal mean of this classification. A commercial (read as no fundamental research aimed) cyclotron for PET radionuclide production could be summarized according to some of its main technical features such as: i) capability of accelerating negative ions (H^-); ii) beam extraction using stripper foils; iii) fixed beam energy between 10–18 MeV, or 10-24 MeV mainly if the installation is intended for production of many isotopes, large-scale production and/or for research purposes; iv) fixed frequency of RF generator; v) two or four *dees* placed in valleys; vi) internal ion source(s); vii) possibility of adjust the beam position on target; viii) possibility of multi-target irradiations; ix) compact radiation shielding around the device ("self-shielded" cyclotron); x) maximum level of automation and simplicity in maintenance. Indeed, it is possible to find different opinions in the literature and also in the exploration of the field in daily practice about the

"best machine" to use, however one should emphasize the need to separate commercial-oriented opinions from rigorous scientific and technical analysis.

To analyze the wide range of possibilities and the fact that there are several manufacturers of these devices, some of the most common cyclotrons for radionuclide production are listed in Figure 2.4, indicating the manufacturer and some important technical details.

Company	Cyclotron model	Particles	Energy (MeV)	Beam current (μA)
ACSI	TR14	H^-	14	>100
ACSI	TR19/(9)	$H^-/(D^-)$	19/(9)	>300/100
ACSI	TR24	H^-	24	>300
ACSI	TR30/(15)	$H^-/(D^-)$	30/(15)	1600/400
ABT	Tabletop	H^+	7.5	5
Best	BSCI 14p	H^-	14	100 (400)
Best	BCSI 35p	H^-	15–35	1500
Best	BSCI 70p	H^-	70	800
CIAE	CYCCIAE14	H^-	14	400
CIAE	CYCCIAE70	H^-	70	750
NIIEFA	CC-18/9	H^-/D^-	18/9	100/50
EUROMEV	Isotrace	H^-	12	100
GE	MINItrace	H^-	9.6	>50
GE	PETtrace	H^-/D^-	16.5/8.6	>100/65
IBA	Cyclone 3	D^+	3.8	60
IBA	Cyclone 10/5	H^-/D^-	10/5	>100/35
IBA	Cyclone 11	H^+	11	120
IBA	Cyclone 18/9	H^-/D^-	18/9	150/40
IBA	Cyclone 30	H^-/D^-	30/15	1500/?
IBA	Cyclone 30XP	$H^-/D^-/^4He^{++}$	15–30/7.5–15/30	350/50/50
IBA	Cyclone 70 (Arronax)	$H^-/D^-/H_2+/He^{++}$	30–70/15–35 /17.5/70	2 × 350/50/50/35
KIRAMS	KIRAMS-30	H^-	15–30	500
KIRAMS	Kotron-13	H^+	40372	100
Siemens	Eclipse RD	H^-	11	2 × 40
Siemens	Eclipse HP/ST	H^-	11	2 × 60
Sumitomo	HM-7	H^-/D^-	7.5/3.8	
Sumitomo	HM-10	H^-/D^-	9.6/4.8	
Sumitomo	HM-12/S	H^-/D^-	12/6	>60/30
Sumitomo	HM-18	H^-/D^-	18/10	>90/50

Figure 2.4 – Description of some common commercial cyclotrons used for radionuclide production.

Source: P. Schmor, "Review of Cyclotrons for the Production of Radioactive Isotopes for Medical and Industrial Applications," *Reviews of Accelerator Science and Technology,* vol. 4, pp. 103-116, 2011.

2.3.2 Cyclotron targetry and target chemistry

There are several radionuclides that could be produced in cyclotrons, applying the physical principles of its operation and the appropriate nuclear reactions induction. From now on, in this section, attention will be devoted to the local where the nuclear reactions take place: the target.

Targetry is a field of cyclotron sciences with the goal to place the target material into the beam, keep it there during irradiation, and remove the product radionuclide from the target material quickly and efficiently [60].

Cyclotron targets could be classified according to its localization in the cyclotron (internal or external) and according to its physical state (solid, liquid or gaseous). Although internal targets were the first to be designed and used, and even considering that they are still used in a short number of applications, external targets are the most common nowadays, independently of their physical state.

In Table 2.5 it is possible to observe some examples of the different types of cyclotron targets used for radionuclide production.

Table 2.5 – Examples of radionuclide production routes and list of common targets used.

Target material	Product	Nuclear reaction	Target type
^{14}N	^{11}C	^{14}N (p,α) ^{11}C	External - Gaseous
^{18}O	^{18}F	^{18}O (p,n) ^{18}F	External - Liquid
^{64}Ni	^{64}Cu	^{64}Ni (p,n) ^{64}Cu	External – Solid
^{203}Tl	^{201}Pb $\longrightarrow$ ^{201}Tl	^{203}Tl (p,3n) ^{201}Pb	Internal – Solid

Solid targets are not yet the most frequent type of cyclotron targets for radionuclide production, either because of technical limitations or because of the radionuclides likely to be produced with this approach. However, if the target material is a metal (typically to produce metallic PET radionuclides) this is the most common approach and in this work focus will be given to it.

The first consideration in the design of a cyclotron target should be devoted to heat deposition by accelerated charged particles in the target, where the temperature can reach values up to 1000 ˚C. Because of that, water or helium cooling of the cyclotron target are commonly adopted [46].

While target refrigeration is a general consideration and could be based on the irradiation conditions and on target design, other technical details are dependent of each target material, as it is the case of target material deposition. A cyclotron solid target must fit some technical requirements such as homogeneity in all its surface, strong adhesion to the substrate (even at irradiation temperatures) and easiness of industrial production [60]. Techniques most often applied to deposit the raw material in an appropriate substrate include vacuum deposition, electrodeposition, thermal melt and powder compression, with a clear predominance of electrodeposited (via electroplating) targets [74].

Targets should also be very pure, i.e.: target constitution should be based on monoisotopic composition or at least based on enriched isotope constitution, to avoid contaminant production. Solid targets could be in the form of a metallic foil (for example: copper, aluminum, uranium, vanadium,…) or powders in different chemical states (for example: oxides, carbonates, nitrates, and chlorides) [46].

After irradiation, solid targets must suffer a process of chemical treatment, normally dissolution, to extract the radionuclide product and separate it from other possible contaminants (radioactive or non-radioactive chemical reagents).

2.4 Study of radionuclide production processes

As it was already presented and explored in previous sections of this work, Nuclear Medicine diagnostic imaging techniques can provide information about physiological and biochemical processes, relying on the use of appropriate radiopharmaceuticals. Actually, more than 2700 nuclides are known, of which only approximately 270 are stable, while the rest are radionuclides. In PET imaging only positron-emitting radionuclides are required, and

only a few positron emitters are being suitably used in the routine clinical practice of Nuclear Medicine, including the most common examples of ^{11}C, ^{18}F and ^{68}Ga – even considering that this tendency is predictably changing in the near future with an increased number of radionuclides explored and used.

Independently of the radionuclide(s) under consideration, it is unequivocally true that Nuclear Medicine rely on an appropriate supply of radionuclides, reason why the dedicated study of radionuclide production should be implemented. In this sub-chapter the principal goal is to provide a general overview of the importance of study radionuclide production processes to its reliable application and dissemination in an industrial manner.

2.4.1 Industrial radionuclide production issues

Radionuclides could be produced in different environments and there are some differences between a laboratorial environment and an industrial environment that should be mentioned. Although a laboratorial process of radionuclide production could be possible and viable to fit the goals established, it do not mean that the same process could be directly translated to an industrial environment and implemented globally.

In this context, it is possible to separate these two different approaches based on some specific requirements of an industrial process:

- ✓ Feasibility and reliability;
- ✓ Easiness and reproducibility;
- ✓ Efficiency and cost-effectiveness;
- ✓ Reduced time consume;
- ✓ Execution using standard equipment;
- ✓ Capability to be standardized and automatized;
- ✓ Safety;

Even considering that all processes developed aim to fit these requirements, some laboratorial approaches to radionuclide production require excess of manual intervention, without automation and standardization, while others need for specific and even “exotic” dedicated equipments and some others are based on several steps that increase the time needed to its execution and reduce their efficiency and cost-effectiveness. The message to take from this explanation is that a possible/feasible process performed in a research environment or in a small-scale/local laboratory is not necessarily a reliable and efficient process to be implemented in terms of global industrial radionuclide production.

Along with these insights emerge concepts such as applied research and design science research (that initially were applied only in informatics and information systems research), in whose research and innovative projects are designed to solve complex problems and to develop new solutions instead of studying or explaining a specific interaction or behavior [75]. So, for the development of industrial processes of radionuclide production, there is the need of innovation that departs from theoretical background already existent and travels in the direction of new solutions, new tools and new knowledge with a direct and measurable impact.

2.4.2 Excitation functions and production process optimization

The description of an industrial process of radionuclide production involves the schematization of the complete process needed for the production of a specific radionuclide, including the nuclear reaction data, target to be used, irradiation conditions, cyclotron technical requirements and radionuclide extraction and purification procedure.

In such a context, nuclear reaction data is the basis for the design of the rest of the process. A deeper analysis on this topic could explicit that the rate of production of a radionuclide is dependent on the number of incoming bombarding particles, the number of target nuclei bombarded and the cross-section of the chosen reaction, reason why the optimization of a production route need for the knowledge about threshold energy for the selected reaction, energy with maximum yields, chemical form of target/product material, physical form of target/product material and separation and purification aspects [76].

Focusing in the reaction channel selected, i.e.: appropriate nuclear reaction for the production of the desired product, the selection of the irradiation conditions and target properties, including beam energy and energy degradation over the target should occur.

While the cross-section data represents the probability that a nuclear reaction will occur through a certain reaction channel, it is more often used the study of the excitation function to understand the overall behavior of that reaction channel. In charged particle induced reactions in cyclotrons there is a rapid degradation of the projectile energy in the target material, the energy range covered within the target is relatively broad and the reaction cross section may vary rather rapidly with energy [59]. Excitation functions act as a way to look at the reaction channel feasibility along all the energy spectrum of projectiles available in a particle accelerator. Thus, the creation of a production route is dependent on the nuclear reaction, overall excitation function and target yields [59, 72]. Obviously, the use of reliable data is a mandatory requisite, reason why one of the worldwide regulatory bodies on radioactive materials related issues developed a compilation of nuclear data in an online database [77, 78].

Let's take the example of the production of the well-known ^{18}F used in PET imaging.

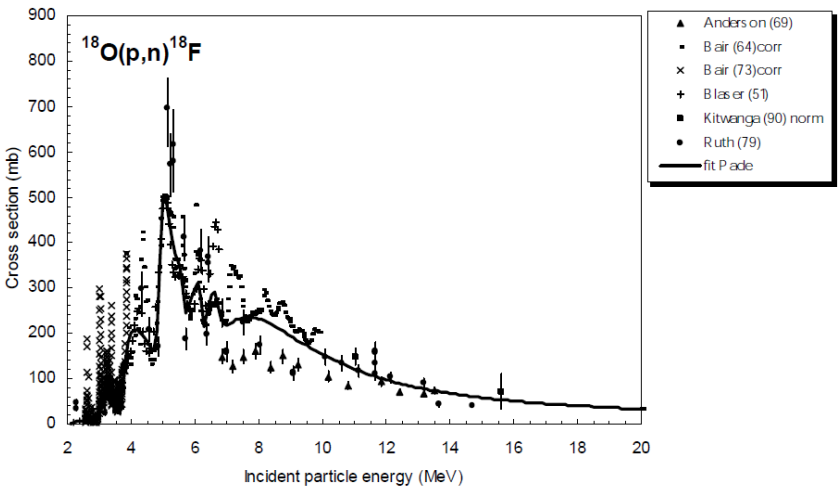

Figure 2.5 - Experimental data considered for the definition of excitation function of $^{18}O(p,n)^{18}F$ nuclear reaction.

Source: International Atomic Energy Agency, "IAEA Tec Doc 1211 - Charged particle cross-section database for medical radioisotope production: diagnostic radioisotopes and monitor reactions," ed. Vienna: IAEA, 2001

Figure 2.5 illustrates the variation of experimental cross-section data in function of the incident proton beam energy found in 6 different reliable experimental papers on the ^{18}F production bombarding ^{18}O with protons, and presents the recommended excitation function curve fitted from the experimental data. Here it is possible to verify that this reaction has a very low energy threshold (≤ 2 MeV) and that it reaches a peak value around 6 MeV.

Following the example presented above, Figure 2.6 presents the calculation of yield obtained using this reaction channel, indicating the amount of activity that could be produced in an irradiation following these conditions. Note that yields are typically calculated using thick targets, reason why the beam energy is degraded over the target used. This is a demonstration of the application of activation equations in a specific example and these data together with notions about chemical and physical forms of target material and product desired (liquid state for both) lead to the development of a globally accepted and disseminated process for the production of ^{18}F that is undertaken over the whole world, from small-scale to large-industry laboratories, with very good results.

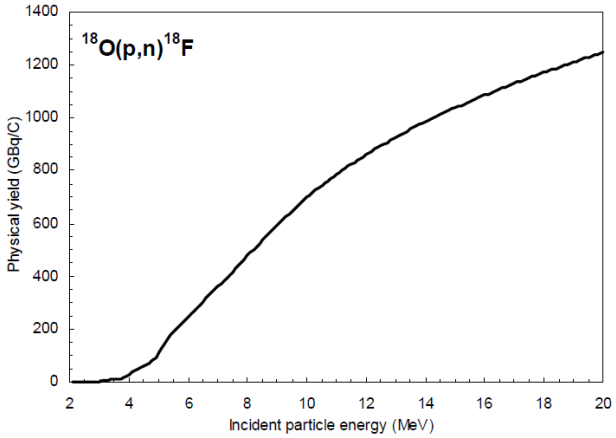

Figure 2.6 – Yield of ^{18}F calculated from the recommend cross-section data.

Source: International Atomic Energy Agency, "IAEA Tec Doc 1211 - Charged particle cross-section database for medical radioisotope production: diagnostic radioisotopes and monitor reactions," ed. Vienna: IAEA, 2001

Analytically, given an excitation function, the maximum yield of a product using a certain target could be calculated by

$$Y = \frac{N_L.H}{M} I(1-e^{-\lambda t}) \int_{E1}^{E2} \left(\frac{dE}{dx}\right)^{-1} \sigma(E) dE \,, \qquad \textbf{Eq.2.15}$$

where N_L is the Avogadro number, H the enrichment or isotopic abundance of the target nuclide, M the mass number of target element, I the projectile current, $\frac{dE}{dx}$ the stopping power, $\sigma(E)$ the cross-section at energy E, λ the decay constant of the product and t the time of irradiation performed.

To finalize this topic let's just look at another interesting example; the production of ^{123}I via $^{124}Te(p,2n)^{123}I$ nuclear reaction.

In addition to the simple examination of the excitation function and possible yields of a given nuclear reaction it is also very important to be aware on the importance to analyze competitive reactions that could lead to isotopic impurities in the production process.

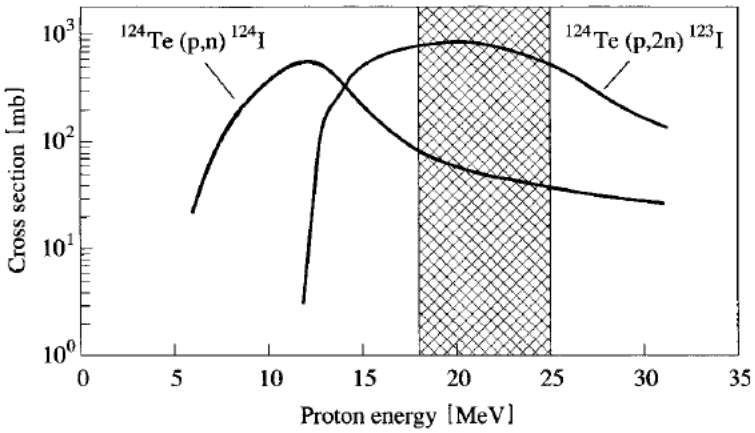

Figure 2.7 – Excitation functions of proton induced reactions on ^{124}Te.

Source: S. M. Qaim, "Nuclear data for medical applications: an overview," *Radiochim. Acta,* vol. 89, pp. 189-196, 2001.

A look at Figure 2.7 reveals the situation mentioned in the last paragraph. The desired reaction channel begin in energies around 12 MeV with a rapid increase of cross-section with the increase of projectile energy. However, in proton energies up to 15 MeV a concurrent reaction channel, $^{124}Te(p,n)^{124}I$, has also a very high cross-section, leading to a direct competition and to the concurrent production of this contaminant. In this specific situation, the better solution encountered is the use of the energy range between 18 and 25 MeV, in which the desired cross-section has high values with relatively low cross-sections for contaminant production. Indeed, in routine application of this nuclear data, a procedure with a selected energy of incident protons of 25 MeV was designed, using solid targets that degrade beam energy to 18 MeV, achieving production yields in the order of 565 MBq/μA with only 1% of ^{124}I impurity [59].

More than in fundamental Nuclear Physics or in fundamental Nuclear Medicine, it is here, in the correlation of all these factors and in its integration in the development of industrial solutions that radionuclide production becomes a complex process and requires the intervention of multiskilled professionals, requiring multidisciplinary teams dedicated to this field and working in close collaboration with (radio)pharmaceutical industry players. The work here presented aims to integrate all the insights discussed until now and to play a role in the demonstration of how experimental nuclear data could be obtained, treated and applied in radionuclide production research.

3. Monte Carlo simulation codes to plan an activation experiment

Preliminary study and optimization of radionuclide production processes is a complex, rigorous, time consuming and expensive task. Often this process must include information from nuclear physics to nuclear chemistry, and normally it begins in the investigation and characterization of excitation functions of nuclear reactions that could be used as feasible production routes. Normally, experimental data collection begins with the experimental determination of those excitation functions in experiences commonly named activation experiments.

In order to maximize the information available with the minimum spent of resources, as also to prevent some completely erroneous choices and/or the sequential repetition of experimental approaches, it is recommended to plan with maximum detail every activation experiment to be executed. Although it is widely known the usefulness of Monte Carlo methods for the planning of experiments and even considering that they are very often common in scientific literature, there is a certain lack of available published reports describing the application to activation experiments, allowing the understanding of the kind of information that they could provide and its reliability.

On this Chapter it will be presented the ideal methodologies to plan activation experiments using Monte Carlo simulation codes, having always the specific case of the study of ^{45}Ti production as the example of application.

3.1 Basic concepts on Monte Carlo simulation codes

Monte Carlo methods is a broad definition that includes a variety of different tools, simulation codes and computational applications. Generically, a Monte Carlo method could be defined as a numerical solution to a problem that models objects interacting with other objects or their environment, based upon simple object-object or object-environment relationships [79]. According to the available history, the first reference to a Monte Carlo method is attributed to Comte de Buffon who had proposed in 1777 an approach with this philosophy to evaluate the probability of tossing a needle onto a ruled sheet, many years before the appearance of automatic calculating machines or computers [80].

In this sense, these methods represent attempts to model natural phenomena through the direct simulation of essential dynamics of the system in question. Essentially it could be considered a simple approach to find a solution to a macroscopic system through the simulation of its microscopic interactions, where the solution is determined by random sampling of the relationships, or the microscopic interactions, until the result converges [81]. In terms of functioning, the solution determination involves repetitive calculations and successive iterations. Often the interactions simulated can be modelled mathematically and the solution is nowadays calculated on a computer, reason why its determination is much faster than in the past and with less inter-operator variability [79].

Although Monte Carlo methods could give approximate solutions for a given problem they should not replace experimentation in a systematic way. Thus, Monte Carlo simulation could provide very useful insights to plan, verify and complement experimental assays – Figure 3.1.

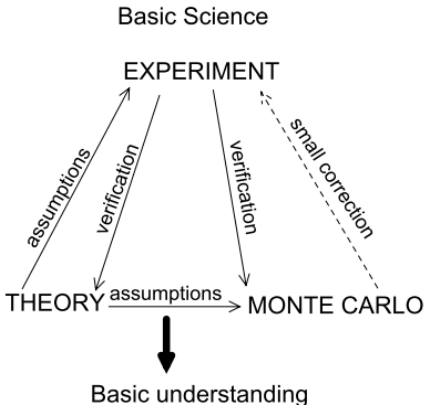

Figure 3.1 – Relationship between Theory and Monte Carlo approaches.

Source: A. F. Bielajew, *Fundamentals of Monte Carlo method for neutral and charged particle transport*. Michigan, USA: The University of Michigan, 2001

There are so many different applications of these methods, from social sciences, finance and quantum chemistry to nuclear physics, among others. But what should really be understood is the fact that Monte Carlo determination is a way to solve complex real life problems within a relatively short time – Figure 3.2.

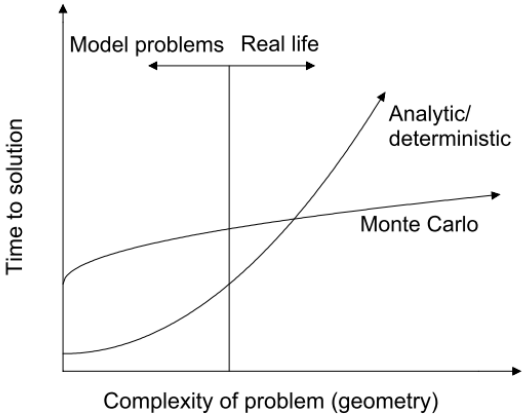

Figure 3.2 – Comparison between analytic methods and Monte Carlo methods.

Source: A. F. Bielajew, *Fundamentals of Monte Carlo method for neutral and charged particle transport*. Michigan, USA: The University of Michigan, 2001

There are a couple of reasons that justify the use of Monte Carlo methods in nuclear physics research: (i) existence of mathematical models of several phenomena under study, that allow modelling and simulation of different conditions; (ii) difficulties to perform exhaustive experimental studies, due to equipment and resources needed, but also due to the economic constraints involved on its execution. In the next sections of this work it will be presented the application of conventional Monte Carlo methods to plan an activation experiment.

3.2 Methodology of application of Monte Carlo simulation codes

Simply, the planning of an activation experiment could be systematized in three main steps: i) conceptualization; ii) design; and iii) simulation, according to the schematic representation of Figure 3.3.

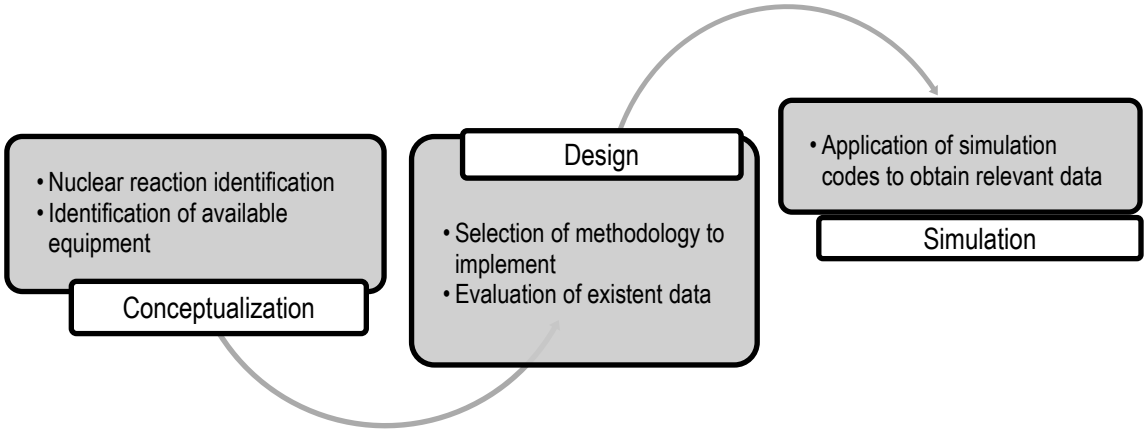

Figure 3.3 – Schematic representation of the main phases of an activation experiment planning.

To follow the diagram presented and to organize the different tasks that should be performed before the final task of simulation, the design of the experiment will be divided in three different main topics: i) Preliminary study of nuclear reaction excitation functions; ii) Study of the proton beam energy degradation; and iii) Study of the proton beam range and dispersion.

3.2.1 Preliminary study of nuclear reaction excitation functions

If experimental data are missing, a mean to obtain a good estimation of the calculation of cross-sections variation is the use of one of the available computer codes based on Monte Carlo simulation [82].
Firstly, a literature review was performed to collect nuclear reactions that allow the production of ^{45}Ti. This data collection was followed by the selection of the ones that could take place in cyclotrons, and mainly in low energy cyclotrons. Selected reaction will be presented and, to obtain a general overview of the reactions cited, *i.e.*, cross-section values for different incident proton energies, it was also indirectly used the simulation code TALYS, following the consultation of an online freely available library named TENDL-2011 (Talys Evaluated Nuclear Data Library) [83].

3.2.2 Study of the proton beam energy degradation

Considering that in an activation experiment following the stacked foil technique several foils are placed in front of the beam trajectory, it is mandatory to understand the energy degradation over the stacked foil. This study is also

important to obtain a good approximation of the beam energy when reaching each foil and therefore to determine the total number of foils needed to degrade the beam totally.

These results could be analytically obtained with mathematical calculations, however it is faster to use an optimized methodology as it is the case of the code SRIM (Stopping and Range of Ions in Matter) [84, 85].

In this simulation, several possibilities were analyzed, including stacks only constituted by scandium foils, and different configurations including scandium foils and scandium foils intercalated with copper monitor foils, in the way to find the most interesting experimental set-up for the purpose intended. Note that all the simulations were based on a foil thickness of 100 μm.

3.2.3 Study of the proton beam range and dispersion

While the energy degradation could give an idea about the longitudinal range of accelerated protons through a stacked foil setup, the understanding of the specific behavior of ions in the stack and the conclusions about its range and, consequently, about dimensions needed for each foil and for the experimental apparatus should be obtained via another kind of Monte Carlo approach. Here emerges the usefulness of Monte Carlo methods used in the transport codes for charged particles, in which it is possible to simulate interaction of the charged ion beams with matter. A typical example of these codes is SRIM/TRIM (Stopping and Range of Ions in Matter/Transport of Ions in Matter) [84, 85].

To improve validity and precision of the results a supporting sub-routine was also applied to the standard SRIM code, namely the SSSM or S^3M (SRIM Supporting Software Modules), that allow the simulation of a realistic beam using appropriate input parameters [86]. Even considering that each cyclotron has a set of specific parameters and performance characteristics, which are also dependent on operation and maintenance, a cyclotron beam analog of the one predicted to be used in experiments was simulated according to information available in the literature [87-89] –Table 3.1.

Table 3.1 – Input parameters for beam generation in SSSM/SRIM.

Parameter	Value
Max Energy (MeV)	18
ΔE/E (%)	1,1
n (n.sigma)	1
Y (total, mm)	5
Y (RMS, mm)	1
Z (total, mm)	5
Z (RMS, mm)	1
dY/dX (total, mrad)	12
dY/dX (RMS, mrad)	1
dZ/dX (total, mrad)	17
dZ/dX (RMS, mrad)	1
EPS Y (PI.mm.mrad)	28
EPS Z (PI.mm.mrad)	17
alpha	+

Some of the cited beam parameters are illustrated in Figure 3.4. Just as a guiding line, elliptical beam contours are determined by the maximum beam radius, maximum beam divergence and the total geometrical emittance, from which the Twiss parameters are calculated [90].

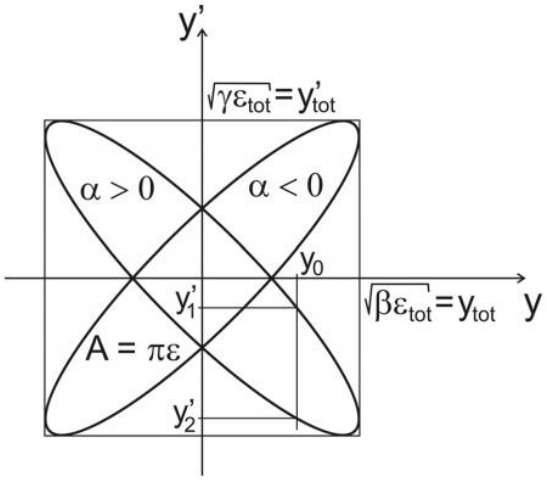

Figure 3.4 – Emittance diagram illustrating Twiss parameters, total geometrical beam emittance, maximum beam extent, radius and maximum beam divergence.

Source: M. Pavlovič and I. Strasik, "Beam transport with scattering using SRIM supporting software routines codes," in *EPAC08*, Genoa, Italy, 2008, pp. 1767-1769.

3.3 Results and discussion on the application of Monte Carlo simulation codes

The next sub-section is still divided in the above mentioned three topics and aims to present simultaneously the results obtained with the Monte Carlo simulations performed in this specific context while gives an overview on the role of these simulations in the appropriate planning of activation experiments.

3.3.1 Preliminary study of nuclear reaction excitation functions

The excitation functions, which represent the variation of cross-sections for a particular reaction in order to the incident energy, can be used in radioisotope production to determine the ideal particle energies required for a reaction, calculate the radioisotope production yield expected for a given nuclear reaction and a specific target, and to calculate the predicted production of radionuclidic impurities [59, 72, 82].

Throught the literature review it have been identified three different nuclear reactions that allow production of ^{45}Ti, namely:

- ✓ ^{45}Sc(p,n)^{45}Ti;
- ✓ ^{45}Sc(d,2n)^{45}Ti;
- ✓ ^{46}Ti(p,d)^{45}Ti

Deuteron-based reactions are typical examples of medium to high energy induced reactions, and the deuteron irradiation of Scandium lead to sufficient yields of ^{45}Ti production only in energies above 20 MeV – needing for a robust cyclotron instead of a simple low energy ("medical") cyclotron [91].

The proton irradiation of natural Titanium is a very ineffective process for the generation of ^{45}Ti and it was merely cited to list the possible routes that were studied. The reaction is just useful in fundamental research studies about level density and gamma-ray strength functions of the isotope [92].

Considering these exclusions, the remnant is the proton irradiation of Scandium. This route is possible at low energies and deserve a dedicated study of its feasibility.

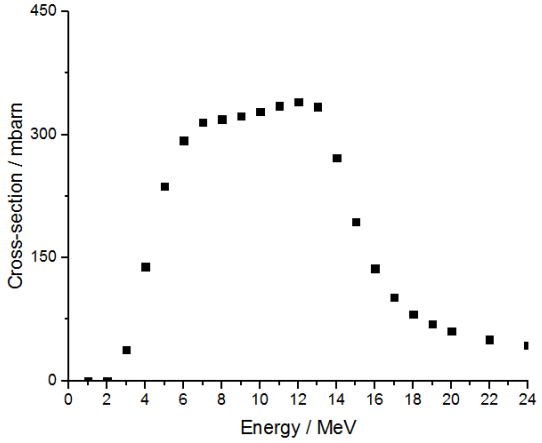

Figure 3.5 – Graphical representation of TALYS-based excitation function of the nuclear reaction ^{45}Sc(p,n)^{45}Ti.

Figure 3.5 presents the excitation function of the main reaction under study. Here it is possible to verify that the reaction becomes possible since energies of about 3 MeV (threshold energy), with a rapid increase in its cross-section until the *plateau* that is reached in energies between 6 and 14 MeV. Incident energies higher than 14 MeV appear to have a reduction of the cross-section value. Together, these facts lead to the theoretical feasibility of the induction of this reaction in low energy cyclotrons. Considering the most common cyclotron devices available worldwide and the simulated excitation function here under consideration, an experimental study of the excitation function of this reaction in energies up to 18 MeV is suggested.

Figure 3.6 adds another important data set, enhancing the behavior of various proton-induced nuclear reactions that could lead to the production of contaminants in the energy range common for "medical" cyclotrons. The careful observation of the simulated excitation functions allows the perception that the *p,n* reaction is the more favorable (typical for low energies) and that it has a superior cross-section value for all the energy range considered here. Thus, the use of this production route appears to provide simultaneously high amounts of ^{45}Ti with reduced level of radionuclidic impurities.

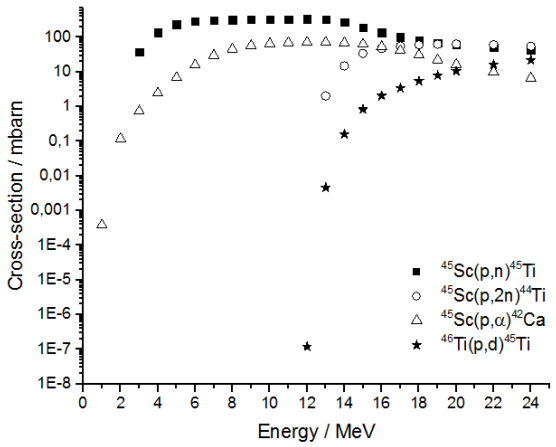

Figure 3.6 - Graphical representation of TALYS-based excitation functions of proton induced nuclear reactions for production of ^{45}Ti and some competitor nuclear reactions.

3.3.2 Study of the proton beam energy degradation

Interaction of charged particles with matter are dominated by Coulomb dispersion, both by atomic electrons and by the protons of nuclei. In this sense, for a given particle, its energy transfer is inversely proportional to target atomic mass, being electron interactions the ones that contribute much for energy loss. The physical concept of stopping power (or energy loss), dE/dx, aims to balance the energy loss by a particle in its trajectory [93].

Analytically, the stopping power could be calculated by the Bethe-Bloch equation

$$-\frac{dE}{dx}=\frac{4\pi}{m_e c^2}\frac{nZ^2}{\beta^2}\left(\frac{e^2}{4\pi\varepsilon_0}\right)^2\left[\ln\left(\frac{2m_e c^2\beta^2}{I\,(1-\beta^2)}\right)-\beta^2\right], \qquad \text{Eq.3.1}$$

where Z is the atomic number, n is the electron density of the target, c is the speed of light, m_e is the electron rest mass, ε_0 is the vacuum permittivity, I is the ionization potential of the target material and β is the fraction of the particle velocity compared to c ($\beta=v/c$).

This equation could only be used if the charged particle velocity is higher than the velocity of orbital electrons of the matter (target), and the final result of the stopping power is dependent on the target mass and atomic number (Z).

Analytical methods are very often substituted by rapid simulation and automatic calculations performed by SRIM – a code to perform stopping power calculation based on the Bethe-Bloch formula [84, 85].

Initially it was simulated an irradiation of a Scandium target with 18 MeV protons (Table 3.2).

Table 3.2 – SRIM simulation of beam energy degradation in a stack of 100μm scandium foils irradiated with 18 MeV protons.

Foil	Energy in (MeV)	Stopping power (keV/μm)	Energy out (MeV)
1	18,00	5,84	17,41
2	17,41	6,00	16,81
3	16,81	6,16	16,19
4	16,19	6,34	15,56
5	15,56	6,54	14,91
6	14,91	6,76	14,23
7	14,23	7,01	13,53
8	13,53	7,29	12,80
9	12,80	7,60	12,04
10	12,04	7,96	11,24
11	11,24	8,39	10,40
12	10,40	8,91	9,51
13	9,51	9,53	8,56
14	8,56	10,32	7,53
15	7,53	11,37	6,39
16	6,39	12,81	5,11
17	5,11	15,08	3,60
18	3,60	19,35	1,67
19	1,67	32,56	0

From data in Table 3.2 it is possible to verify that the entire energy of a 18 MeV is absorbed by 19 sequential Scandium foils, thus allowing the conclusion that a stacked foil with this constitution is possible and separate the analysis of cross-section data in 19 energy points.

Nevertheless, it is quite common to try to economize experimental runs reducing the total amount of enriched (and expensive) target material, reason why it were simulated other schemes for the desired stacked foil. Table 3.3 illustrates the better compromise found, with the inclusion of 11 scandium foils (Sc foils) and 3 copper degrader foils (Cu foils).

Table 3.3 - SRIM simulation of beam energy degradation in a stack of of 100μm scandium-copper foils irradiated with 18 MeV protons.

Foil	Energy in (MeV)	Stopping power (keV/μm)	Energy out (MeV)
Sc 1	18	5,85	17,42
Sc 2	17,42	6,00	16,82
Sc 3	16,82	6,16	16,20
Sc 4	16,20	6,34	15,56
Cu 1	15,57	17,42	13,82
Sc 5	13,82	7,17	13,11
Cu 2	13,11	19,79	11,13
Sc 6	11,13	8,46	10,28
Cu 2	10,28	23,67	7,91
Sc 7	7,91	10,94	6,82
Sc 8	6,82	12,23	5,60
Sc 9	5,60	14,12	4,18
Sc 10	4,18	17,44	2,44
Sc 11	2,44	25,34	0,00

3.3.3 Study of the proton beam range and dispersion

Another aim of this study was to analyze beam range and dispersion over the stacked foil planned to be implemented. To achieve this it was used again the SRIM/TRIM code – Table 3.4.

Table 3.4 – Range and dispersion of 18 MeV protons in a stack of 100µm scandium-copper foils simulated with SRIM/TRIM.

Longitudinal range	Longitudinal Straggling	Lateral range	Lateral Straggling	Radial range	Radial Straggling
1260 µm	35.6 µm	43.8 µm	58.0 µm	69.6 µm	46.1 µm

In addition to information about range it is also presented information about straggling in the different dimensions (longitudinal, lateral and radial) - that is a measure of the variance of obtained data. However, it is also very important to clarify that SRIM/TRIM do not simulate a beam of particles, instead it simulates several monoenergetic particles with the same origin and follows its interaction with the stack of foils [84, 85].

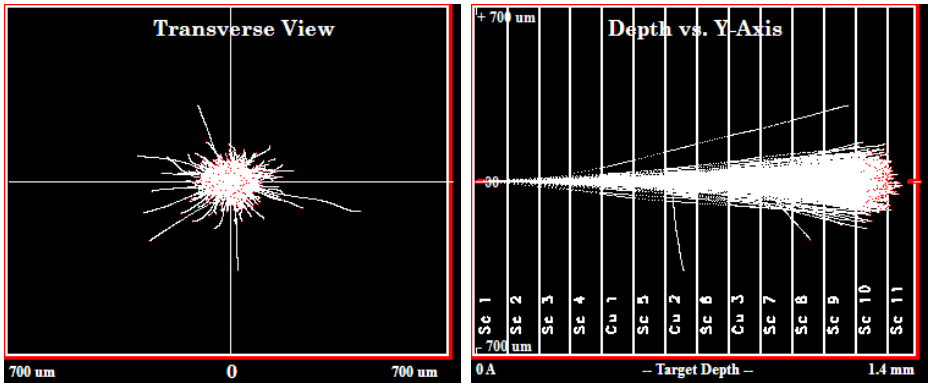

Figure 3.7 – SRIM/TRIM graphical outputs: transversal view of ions in the last foil of the stack (left); and longitudinal trajectories of ions simulated over the entire stack (right).

In what concerns with the longitudinal range of accelerated ions, beam energy is the main influence on it, and so this topic was already known from the beam energy degradation study, even considering that data obtained here is more robust and detailed. It is also widely known that SRIM/TRIM code is often used to calculate various physical quantities related to ion implantation, energy deposition and other effects of interaction of ions with matter and it is very a well stablished and recognized code in the community of ion-beam users [84]. Among several different results generated by SRIM, there are some quantities related to ion interaction with the target, for whose the standard SRIM code here applied uses a simplified “beam” model, i.e.: simulation of particles that start at the same position, with the same angle and with the same energy, as it was already briefly said, and what is called a mono-energetic, point-like, zero-emittance beam in ion-optical terminology. This fact leads to results that do not take in account particle distributions in a real beam, denying the consideration of full ion beam interactions with matter in a realistic way, what has a major impact in lateral and radial distribution outputs [94].

The recognition of these limitations, together with the goal to obtain realistic beam implantation Monte Carlo studies for different applications, are the main reasons for the appearance of supporting routines for SRIM/TRIM, namely the *SRIM Supporting Software Modules* (SSSM or S^{3}M) [86, 94].

In such a context, and to improve simulation results already obtained with the standard SRIM code, it was generated and implemented a beam with characteristics resemblant to the IBA Cyclone 18/9 cyclotron. The values of the parameters and properties used for the simulation were already presented in Table 3.1. Data presented in Table 3.5 allows the comparison of the simple SRIM simulation with the improved SSSM simulation of the beam implantation in the scandium-copper stacked foil under study.

Table 3.5 – Comparison of simulated range and dispersion of 18 MeV protons (SRIM/TRIM) and 18 MeV real beam (S^{3}M) implanted in a stack of 100μm scandium-copper foils.

Methodology	Longitudinal range	Longitudinal Straggling	Lateral range	Lateral Straggling	Radial range	Radial Straggling
SRIM/TRIM	1260 μm	35.6 μm	43.8 μm	58.0 μm	69.6 μm	46.1 μm
S^{3}M→SRIM/TRIM	1260 μm	82.3 μm	820 μm	1001 μm	1260 μm	625 μm

Note that a fair direct comparison between SRIM/TRIM and S^{3}M is not possible, because of the intrinsic differences on the simulation algorithm implemented in what relates to beam origin and beam dimensions. Even so, and despite some beam parameters could not be considered optimized, the generated beam could be seen as a good approximation, representing almost in all the known characteristics the cyclotron beam planned to be used in experiments. In this sense, it is clear the impact of the real beam simulation in almost all parameters related with its implantation, with the exception of the longitudinal range – exclusively dependent on the beam energy, so, already simulated in an optimized situation. However, even in the longitudinal straggling it was found a slight difference, due to the inclusion in S^{3}M of beam energy spread (instead of a complete monoenergetic situation considered for the standard simulation). This simulation also confirms what was predicted for the increase tendency of the lateral and radial range, result of the increase of the effective size of the beam implanted (since its origin).

The specific role and application of these results, in addition to the fundamental understanding of beam interaction with the target, is the possibility to design the target (in this case, foils) to meet one of the most important requisites of these experiments; include the entire beam inside the target (even in the last foil – with most dispersion). So, the range and straggling here obtained will be set as minimum limits for target size.

3.4 Final considerations on the application of Monte Carlo simulation codes

To conclude this section, and according to what was predicted, Monte Carlo methods have revealed an enormous importance on the planning of an activation experiment.

In a general overview:

- ✓ Nuclear reaction model simulation codes allow the user to obtain a generic perspective of the excitation functions of reactions under study, extracting relevant information such as the threshold energies and the cross-section variation across different projectile energies;
- ✓ The planning of a stacked foil experiment should be carefully executed to economize resources and to prevent technical errors;
- ✓ SRIM code should be considered as a versatile approach that generates useful information, being very important for the study of beam energy degradation;
- ✓ For the detailed characterization of beam interaction with the stacked foil, SRIM should be complemented with the sub-routine SSSM, allowing the simulation of the implantation of a real beam, with a critical impact on beam size on its origin and on lateral and radial range after implantation;

4. Radiation detection and quantification using Gamma-ray spectroscopy

Among the extensive experimental techniques used in nuclear physics research, and even considering completely different focus of attention, there is a relatively common factor that is the need to detect and/or quantify radiation. From the various kinds of radiation, gamma rays are the most penetrating form of electromagnetic radiation with natural origin, resulting from different ways of decay of radioactive elements, such as isomeric transition, positron emission or electron capture.

In this sense, gamma-ray spectroscopy is presented as a powerful tool for studies of characterization, identification and quantification of radiation, environmental radiation monitoring, materials study, among other more uncommon applications. In such a context, the use of gamma-ray spectroscopy as the detection and quantification tool for the activation experiments executed under the scope of this Thesis appeared as the smartest option.

To correctly explain and analyze any kind of radiation detection methodology it is often used the strategy to begin with theory about radiation interaction with matter. Here it will be followed the same strategy, even considering that this Chapter is a secondary focus of this work, aiming only to introduce some basic principles of radiation detection by gamma spectroscopy, wanting to act as a short theoretical introduction about one of the most important experimental tools that was used on this Thesis. To illustrate some of the theoretical notions that will be covered, real experimental examples will be shown.

4.1 Gamma radiation interaction with matter

Radiation emission is often the simple release of energy by a given system as it moves from one state (instable) to another (more stable). Gamma-rays are examples of this rule.

Gamma photon interaction with an atom could result in its absorption or scattering, with or without loss of energy. However, these photons are able to travel some distance in matter before interacting with an atom, being the total penetration distance governed statistically by a probability per unit path length, that depends on the specific medium traversed and on the photon energy, and is generally expressed in the form of an interaction cross section [56, 95].

When penetrating an absorbing medium, photons could experience various interactions, either with the nuclei of the absorbing medium or with orbital electrons of the absorbing medium. Considering the interactions with nuclei, they may be direct photon-nucleus interactions (e.g.: photodisintegration) or interactions between the photon and the electrostatic field of the nucleus (e.g.: pair production). The photon-orbital electron interactions are intrinsically related with the balance between photon energy and electron binding energy. In such context, interactions with a loosely bound electron, with a binding energy that is small when compared to the photon energy, lead to Thomson scattering, Compton effect or triplet production, while an interaction with a tightly bound electron, with binding energy only slightly smaller than the photon energy, lead to photoelectric effect [56].

Although a larger number of interactions between gamma photons in matter are possible, only three major types play a critical role in radiation detection and measurement (photoelectric effect, Compton effect and pair production) [96].

The photoelectric effect is a specific process of atomic absorption in which an incident photon energy is totally absorbed by an atom. Consequently, a photon with less energy is emitted and this energy difference is used to eject an orbital electron from the atom. The ejected electron is called a photoelectron, and has a kinetic energy that is equal to the difference between the incident photon energy and the binding energy of the electron shell from which it was ejected [22].

There is no single mathematical expression for the evaluation of the probability of photoelectric absorption per atom (τ_a) that covers all ranges of the photon energy and the atomic number of the absorbers. According to some authors [96, 97] a possible approximation is given by

$$\tau_a \cong const \frac{Z^n}{E_\gamma^{3.5}}, \qquad \textbf{Eq.4.1}$$

where the exponent n could have values between 4 and 5, Z means atomic number of the absorber and E_γ the energy of the incident photon. This relation emphasizes the high dependence of the probability of occurrence of this effect with the atomic number of the absorber. Also, it indicates the predominance of the effect for low photon energies.

A schematic representation of this process is shown in Figure 4.1.

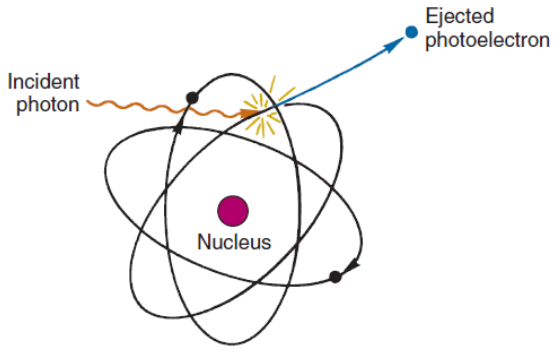

Figure 4.1 – Schematic representation of the photoelectric effect.

Source: S. R. Cherry, J. A. Sorensen, and M. E. Phelps, *Physics in Nuclear Medicine*, Fourth ed.: Saunders, 2012. p.74.

Another interaction mechanism is the Compton scattering. Compton scattering is typically an interaction between a photon and a loosely bound outer-shell orbital electron of an atom. Here, the photon is deflected through a specific scattering angle (θ), while part of its energy is transferred to the recoil electron; thus leading the photon to lose some energy in the process. To occur this interaction mechanism, the incident photon energy should greatly exceed the binding energy of the electron [56, 95, 96].

The mathematical expressions that make the relation between the energy of the scattered photon, the energy transferred to the recoil electron and the scattering angle could be derived by writing simultaneous equations for the conservation of energy and momentum [96].

Thus, the scattered photon will have an energy ($h\nu'$) that is

$$h\nu' = h\nu \frac{1}{1+\varepsilon(1-\cos\theta)}, \qquad \textbf{Eq.4.2}$$

while the energy of the recoil electron (E_K) is

$$E_K = h\nu \frac{\varepsilon(1-\cos\theta)}{1+\varepsilon(1-\cos\theta)}, \qquad \textbf{Eq.4.3}$$

where ε is equal to $h\nu/m_e c^2$, h is the Planck constant, ν is the photon frequency, m_e is the mass of the electron and θ is the scattering angle.

The amount of energy transferred to the recoil electron in Compton scattering can range from nearly zero (for $\theta \approx$ 0 degrees) up to a maximum value (for $\theta \approx$ 180 degrees - backscattering events). The residual energy (energy of scattered photons) is inversely proportional to the energy of the recoil electron, and is minimum for backscattering events and maximal for $\theta \approx$ 0 degrees collisions [22].

In what regards to the probability of this kind of interaction between a photon and an electron, there is a quantity called differential scattering cross section ($d_e\sigma$) that is the probability per unit solid angle in steradians (sr) that a photon, passing normally through a layer of material containing one electron per square meter, will be scattered into a solid angle $d\Omega$ at an angle θ [95]. The integral of this differential cross section over all solid angles ($d\Omega = 2\pi \sin\theta\, d\theta$) is called Compton collision cross section (σ_a) and it gives the probability that the photon will have a Compton interaction [95]:

$$\sigma_a = 2\pi \int \frac{d_e\sigma}{d\Omega} \sin\theta d\theta . \qquad \textbf{Eq.4.4}$$

A schematic representation of this process is shown in Figure 4.2.

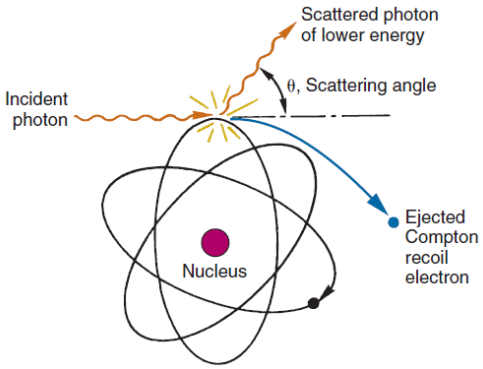

Figure 4.2 - Schematic representation of the Compton scattering effect.

Source: S. R. Cherry, J. A. Sorensen, and M. E. Phelps, *Physics in Nuclear Medicine*, Fourth ed.: Saunders, 2012. p.75.

Finally, pair production occurs when a photon interacts with the electric field of a charged particle (being the atomic nucleus the most common example, right followed by electrons). In this process the photon is totally absorbed and a positron-electron pair is produced. Considering the positron and electron rest masses, the minimum photon energy for this phenomenon of interaction is 1022 keV. The difference between the incident photon energy and the energy threshold of 1022 keV is furnished as kinetic energy to the positron and to the electron [22]. For the majority of photon energies involved in the context of the research project here presented pair production has no (or has very low) probability of occurrence. This process could be schematically seen in Figure 4.3.

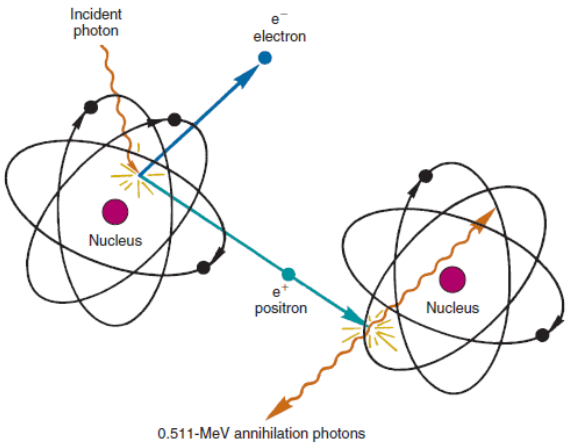

Figure 4.3 - Schematic representation of the pair production interaction phenomenon.

Source: S. R. Cherry, J. A. Sorensen, and M. E. Phelps, *Physics in Nuclear Medicine*, Fourth ed.: Saunders, 2012. p.77.

As it was briefly cited before, the probability of a photon to undergo a specific interaction phenomena depends on its energy and on the atomic number of the absorber (schematic representation in Figure 4.4).

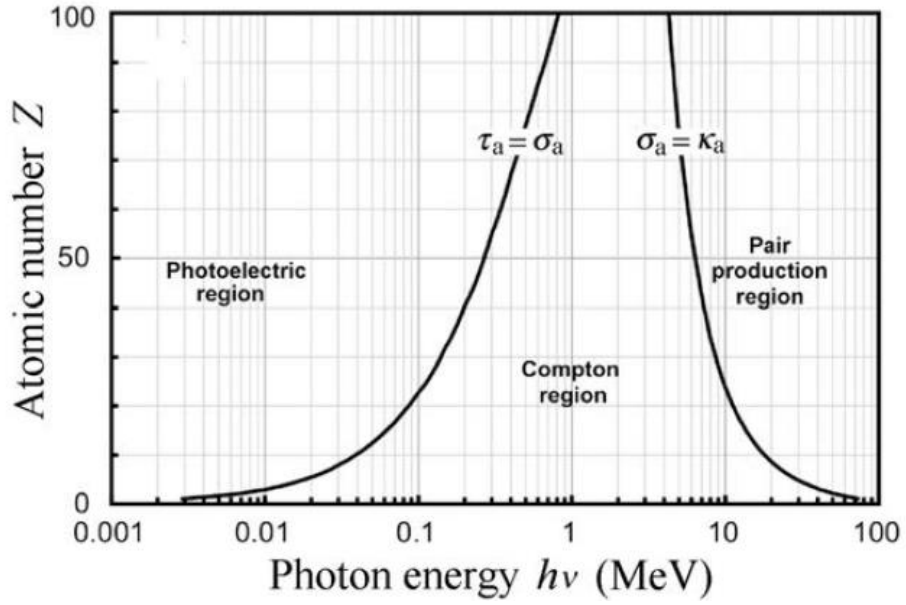

Figure 4.4 - Schematic representation of the relative predominance of the three main processes of photon interaction with matter.

Source: E. B. Podgorsak, A. L. Kesner, and P. S. Soni, "Basic Physics for Nuclear Medicine," in *Nuclear Medicine Physics: A Handbook for Teacher and Students*, D. L. Bailey, J. L. Humm, A. Todd-Pokropek, and A. v. Aswegen, Eds., ed Vienna: IAEA, 2014, pp. 46.

Together, these phenomena could explain photon interactions with matter, being responsible for energy deposition in a variety of situations, including the ones involved in the radiation energy deposition in the human tissues and cells (dosimetry) or, more related with the context here considered, in the deposition of energy in radiation detectors.

4.2 Introduction to radiation detection and quantification

The emission of ionizing radiation obeys quantum theory rules. As a result, it is only possible to talk about the probability that a certain emission take place, and if it is attempted to predict the number of particles or photons emitted by a given nucleus, there is always a probability, not a certainty, about the emissions in the next unit of time. Thus, the actual number of particles emitted per unit time is different for successive runs. Therefore, one can only determine the average number of particles emitted and that average, like any mean value, carries a variance. It represents a specific level of uncertainty, an error in the estimation and/or measurement of the mean value. The quantification of this error is an integral part of any radiation measurement [98].

When talking about measurement errors it is of indubitable interest the discussion of two related concepts: accuracy and precision. Accuracy tells how close a measurement is from the true value of the variable measured, while precision means the capacity to obtain the same value of the variable in independent measurements [98]. The relationship between these concepts is schematically represented in Figure 4.5.

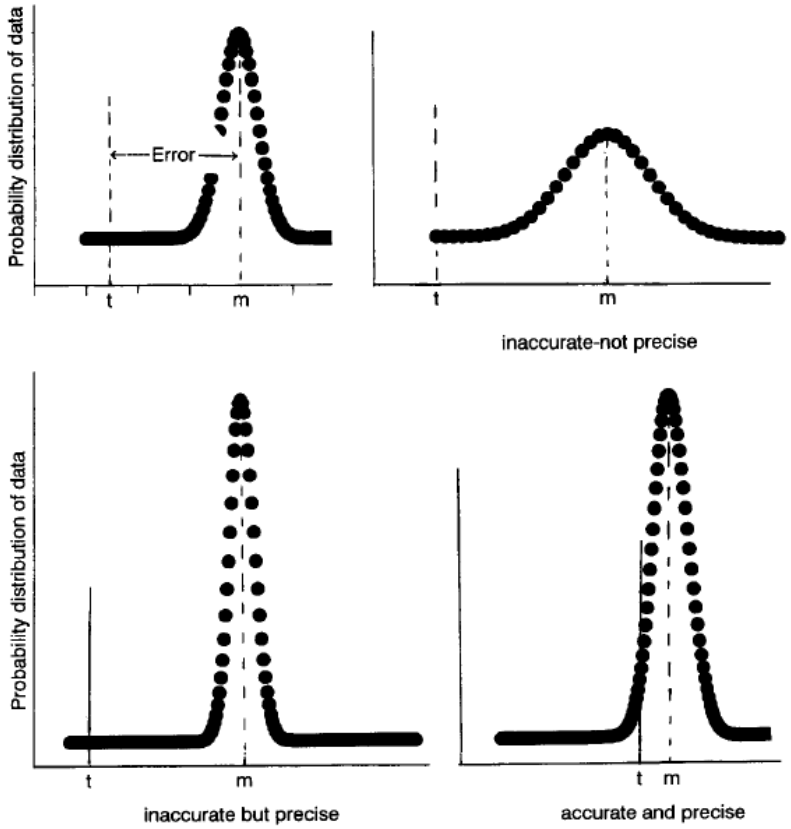

Figure 4.5 – Schematic representation of precision and accuracy of measurements.

Source: N. Tsoulfanidis, *Measurement and Detection of Radiation*, Second Edition ed.: Taylor & Francis, 1995. p.4

After understanding the concepts underlying the uncertainties in radiation detection and quantification, attention should be paid to the process of detection and to the basic constitution of the instruments applied.

As it was described in the previous sub-chapter, when radiation interacts with matter it interacts with atoms and could transfer energy to them. Energy transfer results in one of the two possible effects: ionization and/or excitation. Both of these interaction processes are involved in the process of radiation detection, even if the ionization process could be considered as the primary event [22].

It is also very important to clarify the two most important components of a radiation detection instrument: the counting system and the detector [98].

Given this, counting systems could be divided in two big groups: i) pulse-type systems, in whose the output consists in one pulse per particle detected; ii) current-type systems, in whose the output is an average resulting from many particles [98].

Radiation detectors could be divided in several different classes, such as: i) gas-filled detectors; ii) scintillation detectors; iii) semiconductor detectors; and iv) other (specific for a given application) that could include spark chambers, bubble chambers, photographic emulsions, thermoluminescent dosimeters, Cerenkov counters or self-powered neutron detectors [22, 98].

Although this topic could be much more explored, and in fact it deserves attention in the medical physics field, for the purpose here considered in this work it will not be deeply covered. Thus, the next sub-chapter will move directly for the gamma-spectra detection and analysis concepts.

4.3 Gamma-ray spectra: basic technical considerations on detection and analysis

When a gamma-ray interacts with a detector, it is needed energy deposition (via one of the above mentioned radiation interaction processes) and conversion of energy in an electron pulse. After appropriate pulse process and analysis, it hopefully results in its detection and accurate quantification. This process is the basic rationale for gamma-ray detection.

A radiation detection method could have energy resolution sufficient to perform spectroscopy (also called spectrometry). Spectroscopy is the aspect of radiation measurement that deals with measuring the energy distribution of particles or photons. In particular, gamma-ray spectroscopy is an analytical method that allows the identification and quantification of gamma-rays, in one single measurement, and with simple procedures, allowing also the study of specific radiation interaction mechanisms. In practical terms, the measurement gives a spectrum of lines that represent the number of counts (events) per second (amplitude – y axis position) in function of the energy (channel – x axis position) [98, 99]. Implementing appropriate efficiency calibration factors, number of counts per second could be converted to units of activity, while the appropriate energy calibration is required to allow the conversion from a channel number to an energy value.

The process of radiation detection begins in the detector, where the gamma-ray interaction produces a weak electrical signal that is proportional to the deposited energy. There are several generic types of gamma-radiation detectors (most of them already cited in the previous sub-chapter), but also several variations of size, shape, packaging configuration, performance, and price. Resulting from the conjugation of all these factors, the choice of an ideal detector must be evaluated having in account technical requirements of a specific application, but also the nontechnical requirements such as operational conditions, resources and budget availability [100].

In a general view, without a specific application considered, for a detector to act as a gamma-ray spectrometer, is must fit two important requirements: i) act as a conversion medium (high probability of gamma photon energy absorption, yielding fast electrons); and ii) act as a detector for those secondary electrons [96].

As a matter of fact, predicted response functions will vary according to the characteristics and properties of detectors used. For instance, in the past, scintillation detectors were the most common for use in gamma-spectroscopy. Sodium iodide (NaI) was the most used one, mainly due to its relatively high atomic number that ensured high levels of photoelectric absorption of gamma-radiation energy, resulting in high intrinsic detection efficiency and large photofraction.

Considering the availability of a NaI(Tl) scintillation detector in the *Physics Department of the University of Trás-os-Montes e Alto Douro* (Dept Física – UTAD), specifically a Scintillation Counter Leybold Didactic GMBH (LEYBOLD®), coupled to an High Voltage Power Supply of 1.5 kV (LEYBOLD®) and a multichannel analyzer,

CASSY 529780 (LEYBOLD®), it will be presented a series of examples of spectra collected with this setup. This is a demonstration of the ability of spectroscopy to study gamma-radiation emissions, explaining the steps involved in its application, in the way to describe the limitations underlying the utilization of a scintillation detector for gamma spectroscopy.

Figure 4.6 shows an energy spectrum of a ^{60}Co calibrated source with 3.6 kBq, obtained in a NaI(Tl) detector coupled to a multichannel analyzer.

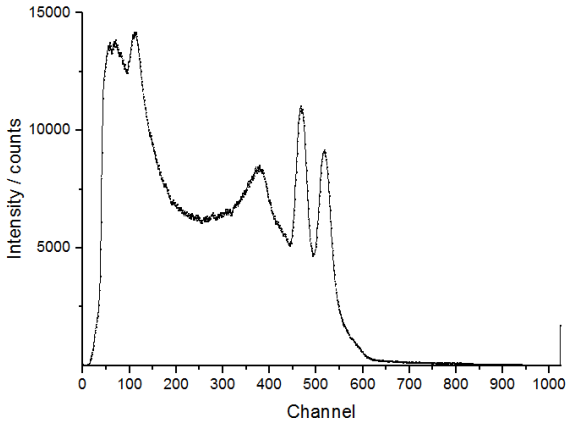

Figure 4.6 – Gamma spectrum of a ^{60}Co standard source obtained using a NaI(Tl) detector at *Dept Física - UTAD*.

This spectrum was used for energy calibration, resulting in the multichannel analyzer calibration that lead to the transposition of the channel number into energy value (Figure 4.7).

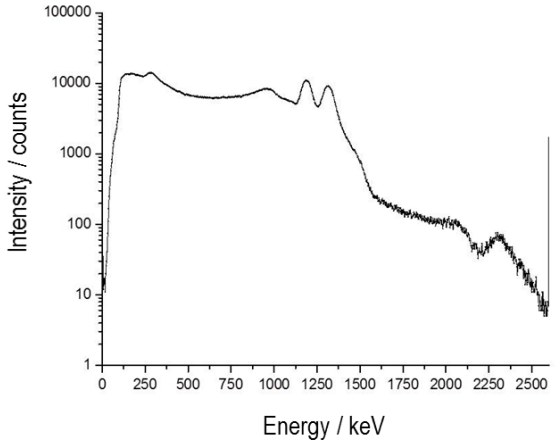

Figure 4.7 – Calibrated gamma spectrum of the ^{60}Co standard source obtained at *Dept Física - UTAD*.

Although the source used here, ideal sources should emit several different photopeaks, allowing the calibration of the detector in a wider range of energies.

The acquired spectra were processed and a Gaussian fitting curve was used to study each photopeak, leading to energy resolution values in the order of 5% - that are compatible to typical values referred for NaI scintillation detectors.

Another set of long spectra were acquired for a ^{22}Na source, a standard source of positrons, that allows one to study gamma spectra of positron emitters – focused in the context of this research.

According to Knoll [96], a typical spectrum of a radioactive source with a full energy-peak that is greater than 1022 keV (the case of ^{22}Na, with 1274 keV) could be represented as the Figure 4.8 shows.

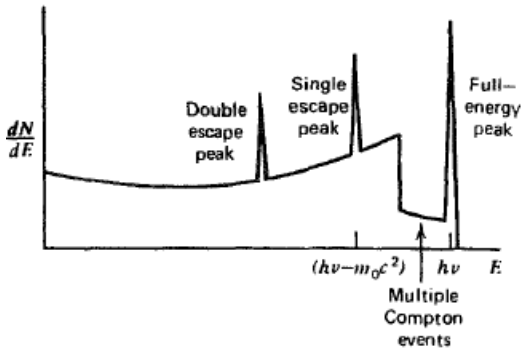

Figure 4.8 – Typical gamma spectrum of a source with a photopeak greater than 1022 keV, obtained in an intermediary size detector.

Source: G. F. Knoll, *Radiation Detection and Measurement*: John Wiley & Sons, 2000; p.316

This spectrum presents the full energy peak represented together with the events resulting from Compton effect, adding also a single escape peak (corresponding to the initial pair production interactions in which only one annihilation photon leaves the detector without further interaction), and a double escape peak (in which both annihilation photons escape from the detector) [96]. A real example of a spectrum like the one theoretically described is shown in Figure 4.9.

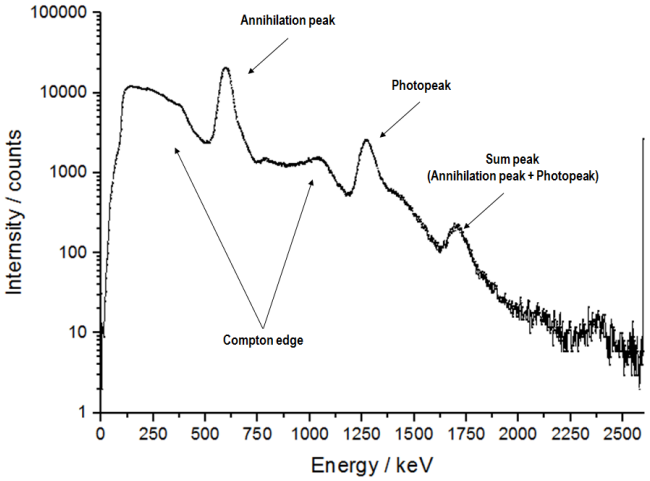

Figure 4.9 - Calibrated gamma spectrum of a ^{22}Na standard source obtained at *Dept Física - UTAD*.

The spectrum presented in Figure 4.9 was acquired using a standard ^{22}Na source with 0.2 kBq, using the same scintillation detector already cited.

At the date of the experiments, the aim of the experimental setup was to study radiation interaction mechanisms and to develop the ability to modulate the detector response functions via mathematical fitting of the obtained spectra. The rest of the experiments, and their respective mathematical treatment, will not be fully described here in this Thesis.

The spectra here presented serve only as examples of scintillation detectors based spectroscopy. Thus, it is possible to observe that scintillation counters have very poor energy resolutions, mainly due to the fact that the process of converting an incident radiation to light and then to an electrical signal is long and inefficient [96, 101].

As a note, and only to complicate the understanding of the detector response in a gamma-spectroscopy experiment, there are several factors that can include artifacts into the spectrum, and that should always be considered in its analysis. Examples of these factors are: secondary electron escape, Bremsstrahlung escape, characteristic X-ray escape, secondary radiations created near the source, the effects of surrounding materials, among other that are typical of certain experimental setups [96].

So, in such a context, the selection of the ideal detector should be according to the objective of the study desired. If the study of radiation interaction mechanisms using standard sources is the only aim of the experiment, the kind of experimental setup used here is enough. However, if the objective is the characterization of a heterogeneous sample consisting of several different radioactive sources, needing for appropriate identification of each energy considered, another kind of detector should be used.

Based on the limitations of scintillation detectors other materials for spectroscopic detectors were searched in order to find advantageous features to this technical application. For instance, semiconductor crystalline materials have two types of allowed energy bands for electrons that are of interest: i) the valence band; and ii) the conduction band. The lower band, known as the valence band, corresponds to outer-shell electrons that are bound to specific lattice sites within the crystal. The other band is known as the conduction band and represents electrons that are free to migrate through the crystal. In these materials, if an electron gain an energy that is equal or greater than the bandgap (gap of energy between the two bands) it will gain the ability to jump up into the conduction band. These excitation processes (gains of energies by the electrons) create also holes in the valence band, and the combination of electrons created in the conduction band with these holes are known as electron-hole pairs, and are used to carry electric charge generated. This mechanism is the rationale behind semiconductor-based radiation detection [101].

The use of semiconductor detectors have been suggested, because of their higher energy resolution. High purity germanium detectors (HPGe) are the most common examples used in gamma-spectroscopy, allowing high resolution spectroscopic analysis of radioactive sources or samples (see a possible example in Figure 4.10).

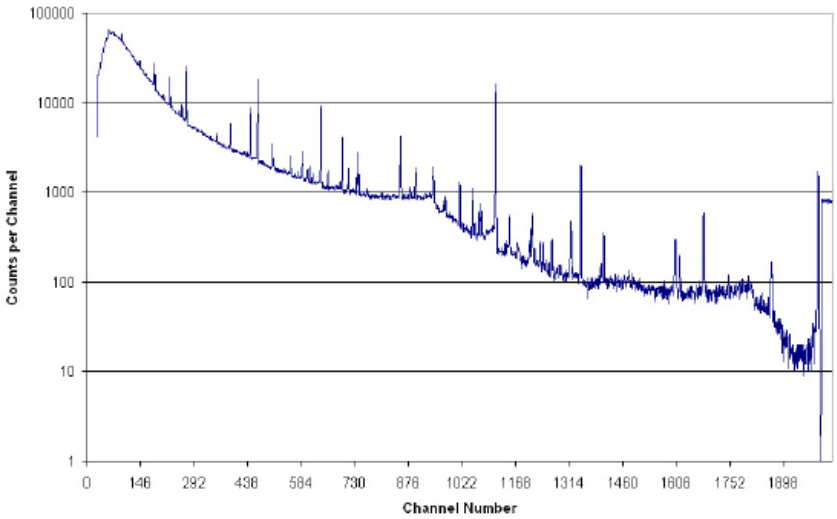

Figure 4.10 – Typical background spectrum using a semiconductor (HPGe) detector.

Source: I. Rittersdorf, *Gamma Ray Spectroscopy*. Michigan: University of Michigan, 2007. P.40.

To finalize the notions related with gamma spectra analysis, again depending on the purpose of the experimental setup under consideration, a simple or a deeper analysis of the spectra could be desired, resulting in the use of more simple or more robust automatic software products for gamma spectra analysis.

Independent of the complexity or the application, automatic software products for gamma spectra generation and/or analysis should begin the analysis with raw data, allowing their direct manipulation and the extraction of results in graphics. More specifically, the ideal software should include: i) spectra libraries; ii) tools for energy calibration; iii) tools for peak search; iv) mathematical tools for fitting and analysis; and v) tools for uncertainty calculation [102].

Having in account the specific requirements for these tools, during the gamma spectroscopy experiments already described in these sub-chapter, it was conceptualized a graphical user interface (GUI), based on the flowchart presented in Figure 4.11. In a basic overview, a software named Gamma Spectra Analyzer (GSA) was developed with the aim to allow automatic gamma-ray spectra generation and/or analysis. In other words, it was aimed to develop a platform that would be able to jointly generate standard spectra of some radioactive sources for a given detector, and/or analyze a given spectrum acquired in a specific detector. GSA was developed with MATLAB v7.10.0 (2010), that have a tool to create graphic user interface - GUI generation.

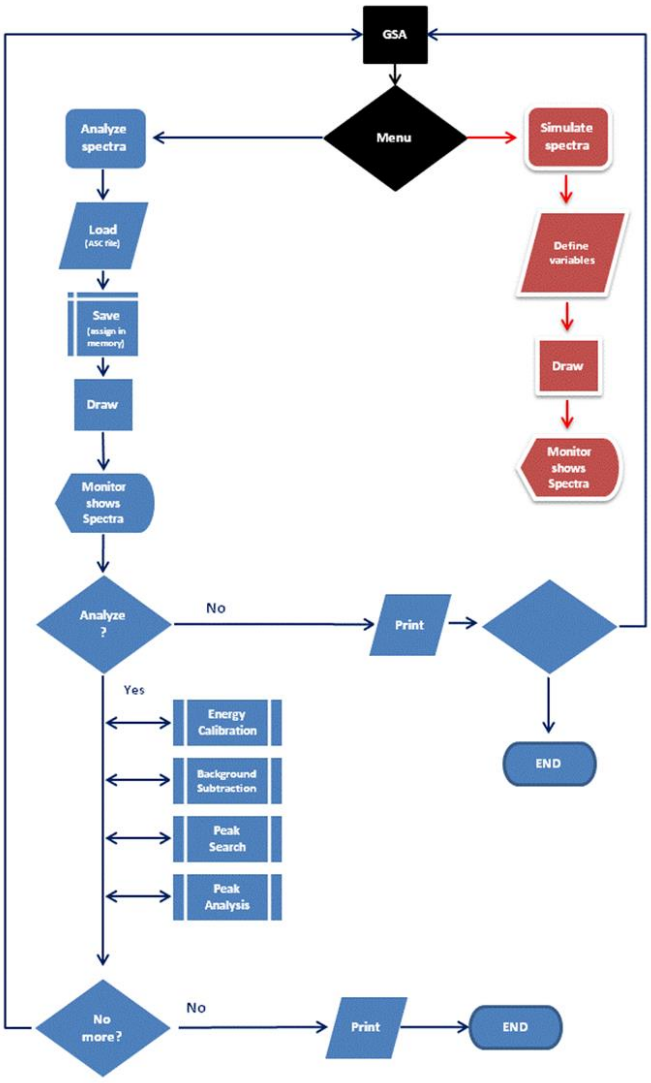

Figure 4.11 – Logic flowchart describing the overall functioning of the GSA software.

Basically, as it can be seen in the flowchart present in Figure 4.11, GSA allows two main functions: i) Analysis of spectra; ii) Simulation of spectra. Following each route described, the user would follow the steps in the way to succeed with the aimed task.

This software is not yet complete, but it already allowed simple characterizations of spectra in an easy and intuitive way [103]. Future work should be dedicated to the more advanced functions of spectra analysis and to more robust studies of validation.

Figure 4.12 illustrates the basic appearance of some user panels in the GSA program. As it is shown, the menus were designed with a very simple appearance. An existing raw spectrum could be loaded directly on the software to be analyzed with the specific tools implemented on the code (energy calibration, background subtraction, peak search and analysis), while a simulated spectrum could be generated based on the description of the radioactive source, detector properties and acquisition conditions.

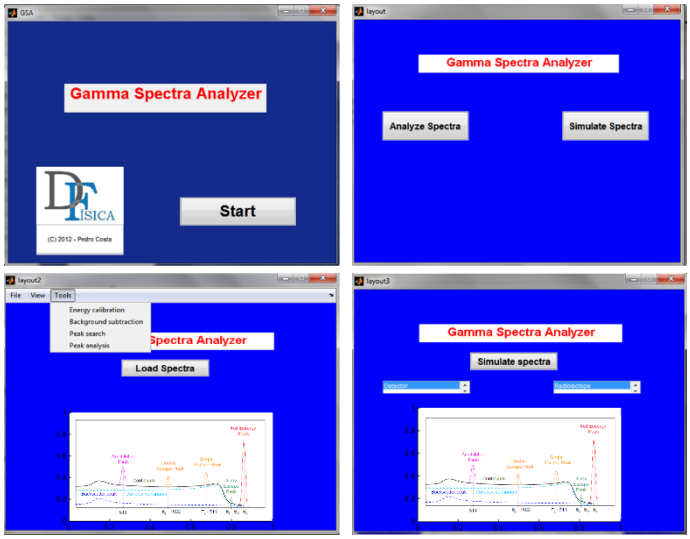

Figure 4.12 – GSA interface.

Thus, the software should serve as an intuitive and simple way to generate and analyze gamma spectra, combining the easiness of utilization with the deeper knowledge on the nuclear and radiation physics, allowing solid and robust results.

4.4 Gamma-ray spectroscopy: calibration and sources of error

The reliability of the measurements undertaken via gamma-ray spectroscopy is highly-dependent on the detectors stability and on its performance characteristics. Thus, to use this technique the protocol should include technical steps of calibration, namely for: i) energy range; and ii) efficiency [104].

For the energy calibration of an HPGe detector, the channel number scale should be carefully calibrated mainly in situations in whose it is expected that various peaks in the spectrum will be identified during the experiment. Thus, the energy calibration consists in the experimental determination of a function, usually a first or a second degree polynomial, describing the energy dependence of the channel number in the spectrum [105].

Calibration procedure requires the use of standard calibration sources used to add peaks with known energy values to the spectrum. Standard calibration sources often include multiple gamma-emissions, preferably within the range of energies that will be covered during the experiments, in order to account to possible nonlinearities of the channels response function in order to energy [96].

Considering that in high performance HPGe-based systems the uncertainty in the peak position can be equal to one part in 10^5, the uncertainty involved in this positioning is on the same order of magnitude of the uncertainty in the calibration energy standards – giving rise to the importance of the selection and definition of the energy of the standards to be used [96]. Some common examples of standard sources used for this procedure are: ^{22}Na, ^{57}Co, ^{60}Co, ^{137}Cs, ^{152}Eu, ^{192}Ir, ^{241}Am, among others. Figure 4.13 presents an example of an energy calibration curve

obtained in an HPGe system using certified spectrometric sources of ^{133}Ba, ^{137}Cs, ^{60}Co, ^{152}Eu, ^{22}Na and ^{241}Am, together with the use of the energy lines of the natural ^{40}K and ^{208}Tl.

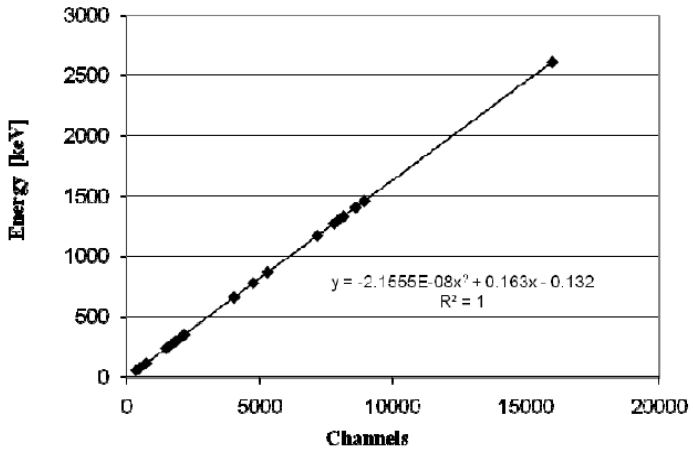

Figure 4.13 – Example of an energy calibration curve for HPGe-based spectroscopy.

Source: M. Saizu and M. Calin, "Basic aspects concerning the validation of the measuring method using a new spectrometric gamma system with HPGe detector," *Rom. Journ. Phys,* vol. 56, pp. 1108-1115, 2011.

In spectroscopy, the precise determination of the activity concentration of a given radionuclide requires the determination of the full energy efficiency. Efficiencies of HPGe detectors can be estimated from published measurements or calculations based on detectors of similar sizes and types, however the accuracy of these values will not be much better than 10-20% [96]. Therefore, a specific detection efficiency curve, also known as efficiency calibration, over the energy region of interest, should be experimentally established before a quantitative measurement [106].

The detection efficiency curve is a set of photopeak detection efficiencies over the energy region of interest for a given application. Similarly to the energy calibration procedure, in efficiency calibration a standard radioactive source is used to serve as a reference for the study of the response function of the detector. In analytical terms, absolute efficiency, ε, is the ratio between the number of measured emissions and the number of decay-corrected emissions of the standard source, and is determined in order to each gamma energy, E_i, using the equation

$$\varepsilon_i = \frac{n_i}{A.I_i}, \qquad \textbf{Eq.4.5}$$

where A accounts for the standard radionuclide source activity in Becquerel, n_i is the net count rate in the peak corresponding area for the energy E_i and I_i is emission intensity of photons with energy E_i.

This parameter depends not only on the detection system but also on some properties of the measured sample (size, density, physical state,…) and on the detection conditions (sample-detector distance, sample positioning, shielding,…) [96, 106, 107].

For an accurate determination of the absolute efficiency along a given energy interval, many photopeaks should be included in the calibration procedure, in order to correctly study the energy-dependent efficiency. To achieve this goal several sources could be used, while simplified methods propose the use of a source that emits many different gamma-energies, as it is the case of ^{152}Eu [96]. Table 4.1 present nuclear data about the gamma emissions of ^{152}Eu needed to incorporate in an efficiency calibration procedure. This set of gamma emissions, together with a convenient half-life (13 years) turned this source very popular and used in the field.

Table 4.1 – Nuclear decay data of ^{152}Eu.

Energy (keV)	Relative intensity
121.8	141.0 ± 4.0
244.7	36.6 ± 1.1
344.3	127.2 ± 1.3
367.8	4.19 ± 0.04
411.1	10.71 ± 0.11
444.0	15.00 ± 0.15
488.7	1.984 ± 0.023
586.3	2.24 ± 0.05
678.6	2.296 ± 0.028
688.7	4.12 ± 0.04
778.9	62.6 ± 0.6
867.4	20.54 ± 0.21
964.0	70.4 ± 0.7
1005.1	3.57 ± 0.07
1085.8	48.7 ± 0.5
1089.7	8.26 ± 0.09
1112.1	65.0 ± 0.7
1299.1	6.67 ± 0.07
1408.0	7.76 ± 0.08

After spectrum acquisition and analysis, absolute efficiency is calculated for each photopeak, allowing the determination of the efficiency in order to gamma energy, which is typically plotted for simple graphical interpretation (Figure 4.14).

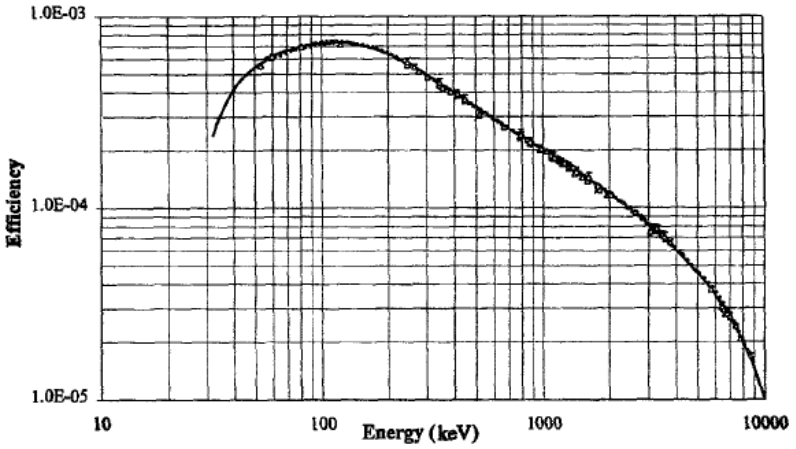

Figure 4.14 – Example of an efficiency calibration curve obtained in an HPGe system.
Source: G. F. Knoll, *Radiation Detection and Measurement*: John Wiley & Sons, 2000; p.316

Application of the equation 4.1 often requires taking into account some correction factors related with the measurement conditions. When these corrections are required, appropriate correction factors should be multiplied by the right side of the equation in order to obtain unbiased values of εi or A [108].

Measurement technical conditions that could imply correction factors include: detector properties and shielding, electronic pulse shaping, radioactive sources properties, peak parameters and/or procedure specifications. Therefore an important step to minimize uncertainties related with a spectroscopic measurement is to carefully select the experimental conditions in order to have corrective effects as low as possible (or, ideally, avoiding the need for corrections). Thus, the relative combined standard uncertainty associated with a result obtained by gamma-ray spectrometry will depend not only on the uncertainties on the main input parameters, but also on the correction factors applied during the calculations [108].

For instance, a critical factor that influences the detection efficiency is the detector-source geometrical arrangement, including detector-source distance and also the source shape and size, mainly in the case of volume samples. This factor is being discussed in the literature, pointing into the need to use similar conditions along the calibration tests and in the measurements undertaken [104, 107, 108].

Figure 4.15 presents several efficiency curves obtained with a point source at different distances of the detector window, and with three volume sources in the same container but with different density profiles.

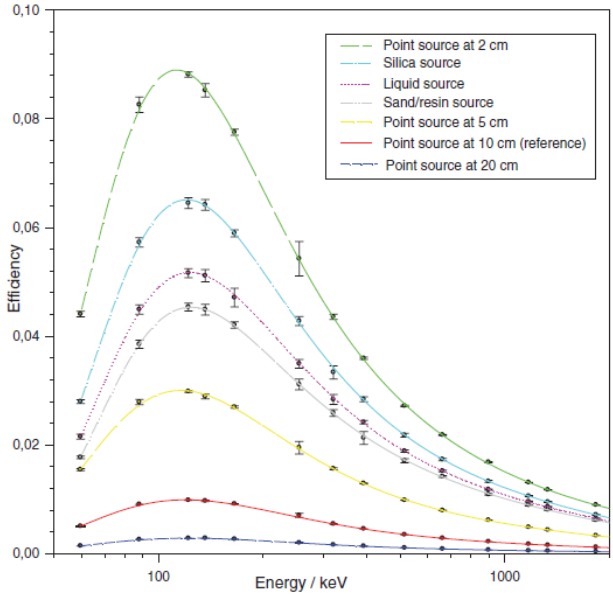

Figure 4.15 – Efficiency calibration curves of an HPGe detector and its relation with source-detector distance and sample configuration.

Source: M. Lépy, A. Pearce, and O. Sima, "Uncertainties in gamma-ray spectrometry," *Metrologia,* vol. 52, pp. S123-S145, 2015.

This graphical comparison highlight that differences between obtained curves are evident, being different the ratio between curves along the energy spectrum. These differences could be explained by the detection solid angle, influenced by the geometrical arrangement of the source and the detection system, but also due to self-attenuation effects and/or attenuation by the surrounding materials [108].

Aspects discussed here in this sub-chapter allow the conclusion that the efficiency in gamma-ray spectroscopy depends on the gamma ray energy, on the sample properties and on the detector characteristics, inducing that appropriate knowledge and control of these factors is mandatory for accurate results.

4.5 Final considerations on gamma-ray spectroscopy

To conclude this section, and following the theoretical background here presented, always complemented with some real experimental examples, in a general overview one should state that:

- ✓ Gamma-ray spectroscopy has multiple applications and could be based in several different experimental apparatus (different detectors or systems coupled to it);
- ✓ Scintillation-based spectroscopy allow a simple study of radiation interaction mechanisms, with high intrinsic efficiency, even considering low energetic resolution;
- ✓ Semiconductor-based spectroscopy in general, and HPGe spectroscopy in particular, appeared to solve some of the limitations of the scintillation detectors, allowing a much more powerful characterization of complex sources or radioactive samples;

- ✓ Considering that the nuclear activation experiments designed to be implemented under the scope of this Thesis involve the need of efficient quantification, but also appropriate identification of heterogeneous radioactive samples, HPGe spectroscopy is suggested as the ideal tool for radiation quantification;
- ✓ Special attention is needed in the energy and efficiency calibration of the HPGe system, due to its high impact on the obtained results;

5. Experimental determination of the excitation function of $^{45}Sc(p,n)^{45}Ti$ nuclear reaction

Knowledge of nuclear cross sections, excitation functions and theoretical predicted yields are essential to plan and optimize irradiation conditions and processes for radionuclide production, mainly when considering industrial large-scale production. After the appropriate description of the steps involved in the planning of the experimental component of this research project, the present section illustrates the experiments performed, and the analysis of the data collected, for the determination of the excitation function of the main nuclear reaction for the production of ^{45}Ti in low energy cyclotrons.

5.1 Introducing Titanium-45: what is it and how to obtain it?

Titanium is a transition metal with the atomic number 22, member of the group 4 and block *d* of the periodic table, with an atomic weight of 47.867 Da, density approximately equal to 4.5 g/cm^3 in standard ambient temperature and pressure (SATP), presenting a melting point of 1668 °C and a boiling point of 3287 °C.

Twenty five titanium isotopes are known, with mass numbers from 39 to 63; 5 of these nuclides are stable, 7 proton-rich and 13 neutron-rich isotopes [36]. The isotope here considered, Titanium-45 (^{45}Ti), has a physical half-life of 3.09 hours and decays predominantly by positron emission (85%), resulting in a β^+ maximum energy of 1040 keV, with an average energy of 439 keV. It was selected according to its favorable chemical properties that allow the possibility to label several different molecules and ligands (that will be covered in an appropriate section – Chapter 6**).** The nuclide is also interesting due to the set of physical properties that provide sufficient time for industrial production and medium-scale local distribution, and can lead to good quality images, even in dedicated fields such as preclinical imaging.

The first relevant reference to the production of ^{45}Ti could be attributed to a Japanese research group that irradiated 65 and 130 mg Scandium foils (0.127 and 0.254 mm thickness, respectively) with 99.9% purity following the reaction $^{45}Sc(p,n)^{45}Ti$ using 11.5 MeV accelerated protons, reaching yields of about 25 ± 2.0 and 48 ± 0.5 mCi/μA.sat respectively. The radionuclidic purity tests indicated only the presence of ^{45}Ti as a radioactive nuclide [109].

After several years without any published reference, the production of this radioisotope was reported by a group in the Washington University School of Medicine in St. Louis (USA) that followed the first steps took by the Japanese group. They reported the use of natural Scandium foils (0.250 mm thick, 100% abundant) that were screwed into aluminum targets and irradiated with 14.5 MeV protons with beam currents ranging from 3 to 10 μA during 30 minutes to 2 hours. The experimental program led to an accumulated production of 115 GBq (3.1 Ci) in 75 production runs, with an average yield of 422 ± 30.0 MBq/μAh [38]. The same group also agreed to a very good correlation of the obtained yields with the predicted values, always leading to the possibility to recover from the target around 95% of the ^{45}Ti produced, attaining always radionuclidic purity values better than 99.8% [110].

More recently, an Iranian group published a paper with experimental results regarding the test of targets associated with the production of ^{45}Ti. They tested two deposition methods to coat scandium oxide on copper substrates. These approaches were proposed to optimize the design of a dedicated target with chemical and physical properties that met the desired requirements, but no experimental irradiations with the obtained targets were demonstrated [37].

Last year, another research team, an Iranian group, obtained yields of about 403.3 MBq/ μAh after an irradiation of 1 h with 21 MeV protons at 20 μA, using a target based on 360 mg of Scandium (Sc_2O_3). The metallic oxide powder was pressed at 50-60 bar to obtain a pellet and then put into the appropriate aluminum shield for bombardment as a capsulated target. Their solution demonstrated another possible approach to targetry and cyclotron routine to obtain the radionuclide in study [111].

In short, all the teams focused in the study of the production of ^{45}Ti have reached similar production yields and radionuclidic purity values using the ^{45}Sc(p,n)^{45}Ti nuclear reaction, even following different targetry approaches. Tests reported ranged from foil-based targets to capsulated powder targets, and using different cyclotrons, from low energy (medical) cyclotrons to a medium energy cyclotron. Therefore, it seems to exist some consensus that this nuclear reaction ^{45}Sc(p,n)^{45}Ti is an effective route to produce ^{45}Ti and that the incident energy on the target should be around 14 MeV. However, it also seems to exist a clear lack of experimental results concerning the overall excitation function of this nuclear reaction. It lacks also a detailed technical analysis about the optimization of the irradiation conditions that justifies the experimental component of this research project.

5.2 Materials and methods

A nuclear reaction could be artificially induced irradiating the nucleus of a solid target with a beam of accelerated particles. Depending on the aim of the study in question, the reaction product could be analyzed online (in real time) or offline (after bombardment). The offline approach is called activation technique and it is based on the measurement of the residual nucleus that are collected in catcher foils (targets) and are identified by detection of the characteristic gamma rays of the nuclei [112]. Due to its selectivity, sensitivity and simplicity, offline activation analysis is one of the most commonly used techniques in applied nuclear physics research and specifically in the study of radionuclide production processes.

Activation experiments are often performed using a simplified method named stacked foil technique. In this experimental method several target foils can be simultaneously irradiated to study in “one-shot” the activation induced by different projectile energies. Of course, the validity of the method implies to assume some requirements such as: knowledge of the energy loss in each foil, constant beam intensity on the entire stack, capacity to isolate each foil to its neighbor, among other important technical considerations.

5.2.1 General aspects

The cyclotron used in the experiments here described is installed at ICNAS (*Instituto das Ciências Nucleares Aplicadas à Saúde* – Institute for Nuclear Sciences Applied to Health) of the University of Coimbra, manufactured by IBA (Ion Beam Applications, S.A., Belgium) and the specific model is named as Cyclone® 18/9 HC (Figure 5.1). This model is a fixed-energy cyclotron that is capable to accelerate protons up to 18 MeV and deuterons up to 9 MeV [87, 113].

Figure 5.1– Real photograph of the IBA Cyclone® 18/9 HC cyclotron installed at ICNAS.

As it is the normal procedure for cyclotron operations, all the experiments here described were conducted by a multidisciplinary team that included always the presence of at least one cyclotron physicist responsible for its operation and control. The team involved (physicists and nuclear medicine technologists) were always monitored in terms of radiation exposure by the use of personal dosimeters, and complemented with the use of other portable radiation detection equipment. All the experiments based on irradiations were performed during the night, before the normal industrial operations of the cyclotron used for medical purposes. This choice, allowed to minimize the radiation exposure for all the team involved in the data collection, complying with legal rules and ensuring real implementation of radioprotection principles.

Despite the cyclotron itself and all the quantification equipment (radiation monitoring detectors and HPGe detector) the other setup accessories needed were all manufactured *in house*, namely the target holder system and the

circular stacked foil holder system. The target holder system is an appropriate aluminum system to be connected directly to the cyclotron port and includes a collimator that guarantees a beam diameter of 10 mm and is adequately insulated.

The circular stacked foil holder is an aluminum device that was specifically designed to fully fit all the requirements of these experiments in what relates to its adaptation to the target holder system and to the foils projected to be used, including a spring to compress the foils and reduce dead spaces between each foil and its neighbor foil and a back cover made in copper to completely absorb the residual beam (Figure 5.2). Nevertheless, flexibility and versatility were always in mind while designing these instrument(s) in order to allow their use in future experiments.

Figure 5.2 – Some real photographs of the *in house* stacked foil holder. From left to right: dismantled pieces of the stacked foil holder; complete stacked foil holder connected to the adapter for the connection to the target holder; zoom of the back cover of the stacked foil holder; and complete overview of the connection to the cyclotron.

5.2.2 HPGe gamma spectroscopy

Activity measurements, or more specifically gamma spectroscopy analysis, took place on a high purity germanium detector (HPGe – Pop Top, GEM series, ORTEC®) coupled to a multichannel analyzer DSPEC jr 2.0™. All spectra were processed and evaluated using the software GAMMA VISION™ (ORTEC®). The detector was previously calibrated in terms of energy and efficiency using a standard source of ^{152}Eu. Calibration step was repeated in three different geometrical configurations (overhead the detector; 10 and 40 cm upward the detector) in such a way that the measurements could take place in any of the geometrical positions calibrated, avoiding the employment of geometrical interpolations in the evaluation of the measured data.

Sample positioning for quantification was undertaken carefully in such a way to guarantee reproducibility and maintenance of the detection conditions. The detector was kept in a region of the building presenting low background activity.

Produced activity was then obtained by the integral calculation of the area under the curve in each considered peak. Nuclear decay data needed for calculations (either for beam energy calibration as for the titanium production study) was found in the more reliable bibliographic sources and is described in Table 5.1.

Table 5.1 – Nuclear data relevant for gamma spectroscopy calculations.

Radionuclide	Half-life	γ energy	Abundance
^{62}Zn	9.19 h	596.56 ± 0.13 keV	26.0 %
		548.35 ± 0.11 keV	15.3 ± 0.8 %
^{63}Zn	38.5 min	669.62 ± 0.05 keV	8 %
^{65}Zn	244 days	1115.546 ± 0.004 keV	50.60 ± 0.24 %
^{45}Ti	3.08 h	720.22 ± 0.17 keV	0.154 ± 0.012%
^{44}Ti	63 years	67.9 keV	94.4 ± 1.4 %
		78.3 keV	96.0 %
^{44}Sc	3.93 h	1157.0 keV	99.9 %
^{44m}Sc	2.44 days	271.1 keV	86.7 ± 0.3 %

Note that uncertainty levels not presented are in the order of the last digit.

All the measurements intended for quantification purposes were performed in such conditions that guarantee dead time losses minor than 5% and counting uncertainties inferior to 1%.

5.2.3 Cross-section determination

Departing from the number of counts measured using the HPGe spectroscopy for the main peak of the produced radionuclide, initial activity (at the end of bombardment time) of each radionuclide was calculated having in account the efficiency calibration of the HPGe and the time passed between the end of bombardment and the HPGe spectroscopy time (using synchronized clocks). Cross-sections of each nuclear reaction for each studied beam energy, in square centimeters, σ_i, were calculated according to the equation:

$$\sigma_i = \frac{A}{IN(1-e^{-\lambda t})}, \qquad \textbf{Eq.5.1}$$

where A is the activity of the produced radionuclide in decays per second (Becquerel), I is the intensity of incident beam in particles per second, N is the number of target nuclei per square centimeter of target and $1-e^{-\lambda t}$ is named the growth factor of the produced radionuclide and takes in account the decay constant of the radionuclide, λ, and the duration of the irradiation, t.

The number of target nuclei per square centimeter of target, N, depends on quantities such as density of the target material, ρ, atomic mass of the material, A, relative abundance of the isotope, θ, and foil thickness, d, and it was calculated following the equation

$$N = \theta\left(\frac{\rho d}{A}\right)N_A, \qquad \textbf{Eq.5.2}$$

where N_A is the Avogadro's constant and is equal to $6.022x10^{23}$.

5.2.4 Preliminary beam energy calibration

Cyclotrons used for radionuclide production need to have their beam energy calibrated periodically, either as a good manufacturing practice and quality assurance test, but also as a necessary step for optimizing routine production yields, allowing to minimize impurities that result from concurrent energy-dependent nuclear reactions. Considering this fact, it was implemented a preliminary experiment in order to check beam energy of the ICNAS cyclotron used in the rest of the experiments.

A possible methodology to perform this task involves the study of a well characterized nuclear reaction (monitor reaction) in order to compare obtained results with the validated and tabulated data for that nuclear reaction. In this context, proton induced nuclear reactions on natural copper foils are among the most common monitor reactions. Thus, a stacked foil fully constituted by Copper foils (17 mm diameter, 100 μm thickness and 99.999% purity) was build and screwed into our in house developed target holder (Figure 5.3).

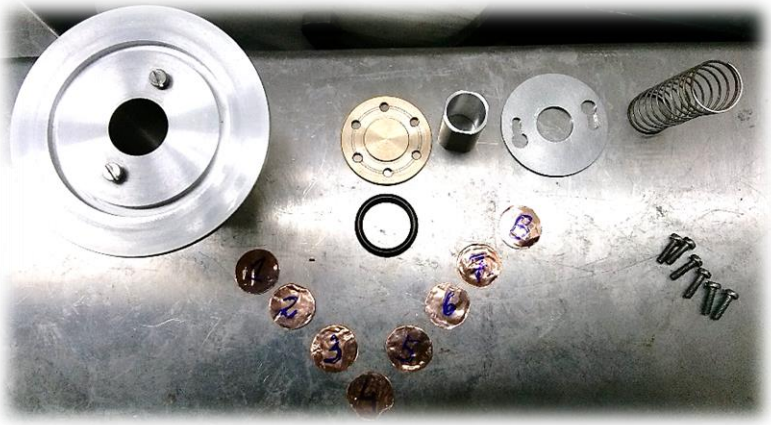

Figure 5.3 –Real photograph of the dismantled target holder and copper foils used for beam energy calibration.

According to the SRIM calculation of beam energy degradation over the stack, the use of 8 copper foils allows for the total beam energy absorption (Table 5.2).

The stack was irradiated with 18 MeV accelerated protons at approximately 0.5 μA during 5 seconds. After an appropriate cooling time, the target was took from the cyclotron bunker and each foil was kept in a shielded lead container until its activity quantification with a gamma spectrometer based on the HPGe detector. The acquisition of the spectra begun around 1 h post-EOB and end 24 h post-EOB. Information regarding tabulated cross-sections was found at the IAEA's online database – EXFOR [77].

Table 5.2 - SRIM simulation of beam energy degradation in a copper stack irradiated with 18 MeV protons.

Foil	Energy in (MeV)	Stopping power (keV/μm)	Energy out (MeV)	Mean Energy (MeV)
Cu 1	18.0	15.6	16.4	17.2
Cu 2	16.4	16.7	14.8	15.6
Cu 3	14.8	18.1	13.0	13.9
Cu 4	13.0	20.0	11.0	12.0
Cu 5	11.0	22.6	8.7	9.8
Cu 6	8.7	26.7	6.0	7.4
Cu 7	6.0	34.6	2.6	4.3
Cu 8	2.6	61.1	0	1.3

5.2.5 Foil preparation

In the main experiments performed, Scandium foils (99.5% enriched) with dimensions of 50x50 mm and 100 μm of thickness (Materion®) were manually cut in circular samples with approximately 17 mm diameter. The Copper (99.999% pure) foils with dimensions of 50x50 mm and 100 μm of thickness (Alfa Aesar®) were also manually divided in disks with the same diameter. Figure 5.4 presents real photographs of some samples used during these experiments.

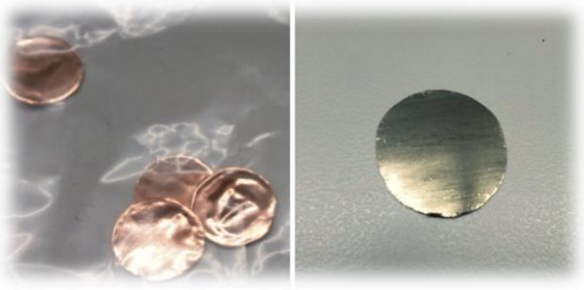

Figure 5.4 – Real photograph of some copper (left) and scandium (right) foils used in the experiments.

Cutting procedure was always performed with maximum careful for the maintenance of material integrity and homogeneity. Before and during all the experiments, these materials were stored according to manufacturer's recommendations, always assuring the use of gloves and tweezers to execute material manipulations. Apart from the properties already presented, one should also note that the uncertainty associated to thickness is indicated to be in the order of ± 10%.

5.2.6 Qualitative study of $^{45}Sc(p,n)^{45}Ti$ energy threshold

Before the beginning of the activation experiments, the theoretical value reaction energy threshold (~ 3 MeV) was tested using two independent unique-foil irradiations, using two different beam energies; under the threshold (2.5 MeV) and above threshold (5.0 MeV). To achieve these conditions, aluminum degraders were used, with thicknesses calculated using SRIM/TRIM. Degraders of 1571 μm and 1600 μm thickness, respectively for 5.0 and 2.5 MeV beam energies, were employed. In each experiment the degrader was placed right after the collimator of the target holder and before the Scandium foil.

Single irradiations of each foil were implemented with nominal beam current of 1 μA during 10 minutes, followed by qualitative analysis via gamma spectroscopy to check existence or not of ^{45}Ti activity.

5.2.7 Stacked foil irradiation

A stack constituted by eleven Scandium foils interspaced by three Copper foils was made and inserted into the *in house* holder already described, following the planning designed using the calculation based on the SRIM energy degradation study (See Table 5.3). The overall experimental results of this work were based on two complete independent irradiations, in whose the apparatus was connected to the IBA Cyclone® 18/9 HC and irradiated with a mean current of 0.6 μA during 100 and 550 seconds, resulting in integrated currents of 0.03 μA-h.

Table 5.3 - SRIM simulation of beam energy degradation in a scandium-copper stack irradiated with 18 MeV protons, with the indication of mean energy per foil.

Foil	Energy in (MeV)	Stopping power (keV/μm)	Energy out (MeV)	Mean Energy (MeV)
Sc 1	18.0	5.846	17.4	17.7
Sc 2	17.4	6.000	16.8	17.1
Sc 3	16.8	6.164	16.2	16.5
Sc 4	16.2	6.344	15.6	15.9
Cu 1	15.6	17.42	13.8	14.7
Sc 5	13.8	7.168	13.1	13.5
Cu 2	13.1	19.79	11.1	12.1
Sc 6	11.1	8.459	10.3	10.7
Cu 3	10.3	23.67	7.9	9.1
Sc 7	7.9	10.94	6.8	7.4
Sc 8	6.8	12.23	5.6	6.2
Sc 9	5.6	14.12	4.2	4.9
Sc 10	4.2	17.44	2.4	3.3
Sc 11	2.4	25.34	0	1.2

5.2.8 Data analysis

All the data collected was inserted in a Microsoft Excel 2013® database. Simple data analysis and processing was performed using Microsoft Excel 2013®. Statistical analysis and mathematical fitting of data was performed using Origin 2016®.

5.3 Results and discussion

The ideal description of an experiment should include a complete analysis and discussion of all the results obtained. In this sense, the next sub-chapters aim to present all data obtained and all the processing and analysis undertaken, complemented with the appropriate discussion and comparison of obtained results with published values (either theoretical or experimental).

5.3.1 HPGe calibration

The isotope ^{152}Eu was selected for calibration due to its emissions in a large energy spectrum, from around 100 to 1800 keV. The choice allowed the calibration to cover the full energy spectrum selected to the experimental measurements. ^{152}Eu standard source used is a point-like source that was calibrated on 15th of April of 1993 with 0.5 µCi (≈ 0.02 MBq). Examples of some spectra obtained are presented in Figure 5.5 and 5.6.

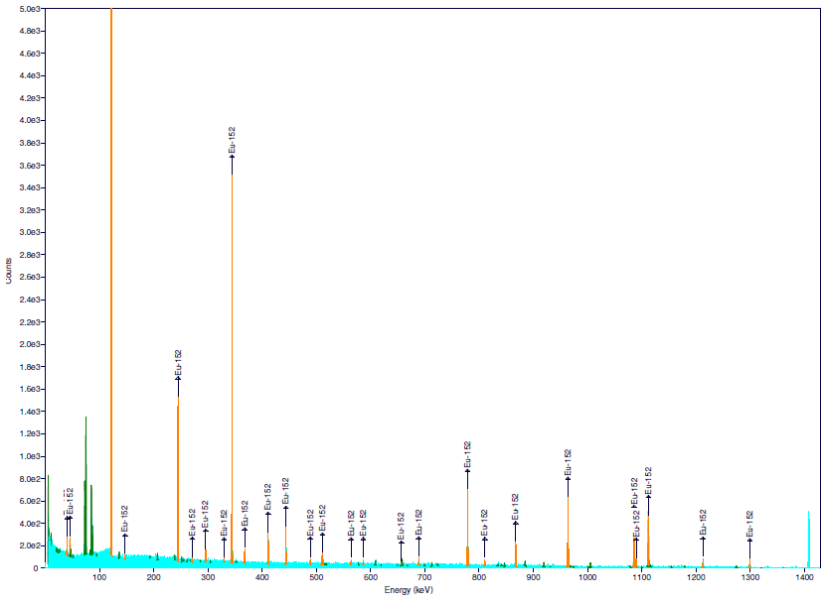

Figure 5.5 - Example of a gamma-spectrum of the ^{152}Eu source used for HPGe detector calibration (linear scale).

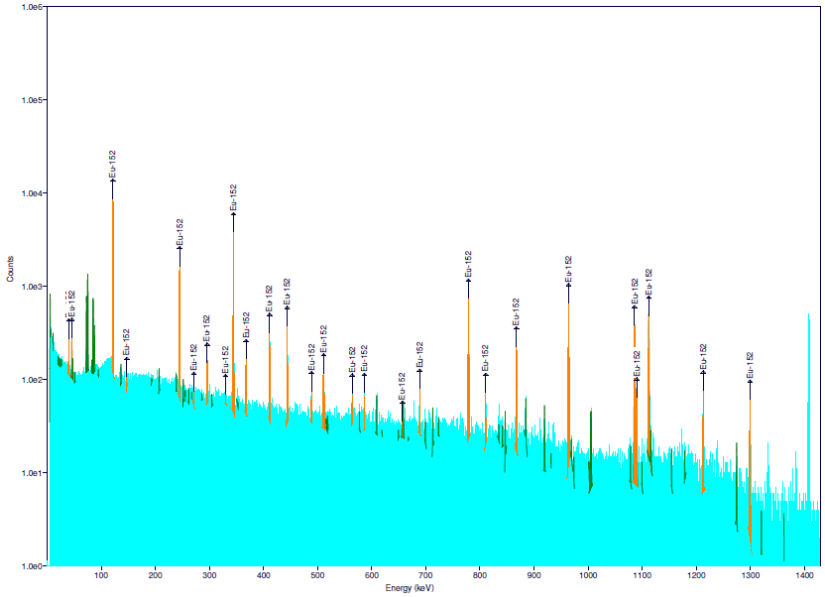

Figure 5.6 - Example of a gamma-spectrum of the ^{152}Eu source used for HPGe detector calibration (log scale).

This source allowed the energetic calibration of the multichannel analyzer of the detector. The same source was used for the efficiency calibration of the detector, allowing the automatic conversion of the number of events detected (counts) to units of activity of a given radionuclide in the radioactive source/sample measured (in Becquerel).

5.3.2 Beam energy calibration

The correct choice of a nuclear reaction to be used as monitor reaction implies the selection of an appropriate energy range, target (availability with maximum purity at reduced prices) and products (with ideal physical properties for gamma spectroscopy). Several beam monitor reactions have been extensively cited, explored, published and used for many years, including for example the following cases: ^{27}Al(p,x)^{22}Na, ^{27}Al(p,x)^{24}Na, ^{nat}Ti(p,x)^{48}V, ^{nat}Cu(p,x)^{62}Zn, ^{nat}Cu(p,x)^{63}Zn and ^{nat}Cu(p,x)^{65}Zn.

However, one should note that the reliable use of these methods requires always the access and experience in the application of a well calibrated detector system which typically entails an HPGe gamma-ray spectroscopy system. In this sense, using the activation equation(s) and if the cross-sections for the reaction of interest are well characterized, the beam energy may be determined by measuring the activity produced and having an accurate knowledge of the target thickness, the proton beam intensity and the decay constant of the produced radionuclide [114].

This approach was applied to several irradiations of single foils to adequately characterize beam energy of a cyclotron. However, instead of irradiating a single monitor foil it has been also previously proposed that it is preferable to use a stack of copper foils and then analyze every single foil by high resolution gamma-ray

spectroscopy for the isotopes ^{62}Zn, ^{63}Zn and/or ^{65}Zn. The use of this copper stacked foil technique for subsequent gamma-ray spectroscopy evaluation was proposed by J. H. Kim, et al. [115] and M. U. Khandaker, et al. [116], and consistently used in this field. In the other hand, more recently, to overcome the need for gamma-ray spectroscopy or high quality efficiency calibrations, there are also studies suggesting the irradiation of two monitor foils of the same material interspaced by an energy degrader with subsequent relative quantification [117]. This later method is characterized as a simple and independent method.

Comparing the two approaches here mentioned, the major drawback in evaluating the beam energy using the most common stacked foil technique is that it requires absolute quantification of the produced radioisotope activity and/or cross-section values. This can lead to a serious compromise in the obtained results by any incorrect or offset efficiency calibration for the gamma detector used. In the second approach, by carefully choosing both the monitor foil material and degrader thickness, the differential activation of the two monitor foils may be used to determine the beam energy (as illustrated in Figure 5.7). The major advantage of examining the ratio of two identical isotopes produced in two different foils (i.e. ^{63}Zn in foil 1/^{63}Zn in foil 2), as opposed to the evaluation of the ratio of different isotopes resulting from proton irradiation of a single copper monitor foil is that all detector efficiency calibration requirements are eliminated from the data analysis [117].

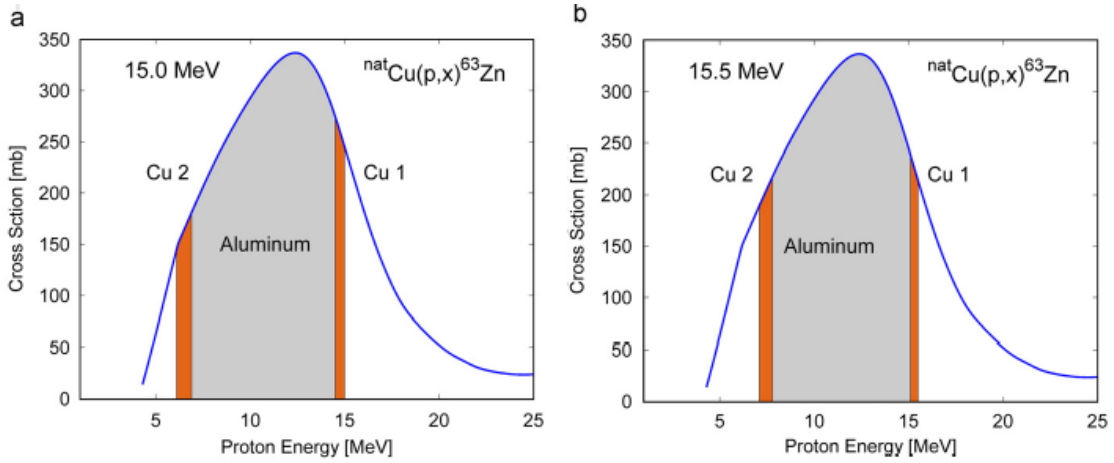

Figure 5.7 – Comparison of the ^{63}Zn activation in two 25 µm copper foils interspaced by an 875 µm aluminum degrader given incident proton energies of 15.0 MeV (a) and 15.5 MeV (b). As noted in the example, a small change in the incident energy can lead to a measurable change in the ^{63}Zn activity ratio.

Source: K. Gagnon, M. Jensen, H. Thisgaard, J. Publicover, S. Lapi, S.A. McQuarrie, and T. J. Ruth, "A new and simple calibration-independent method for measuring the beam energy of a cyclotron," *Appl. Radiat. Isot.,* vol. 69, pp. 247–253, 2011.

Since this activity ratio may be predicted using well known published recommended cross-section data, and considering that beam energy degradation could be studied using the Monte Carlo SRIM software package [84], data could be fitted using a second degree polynomial leading to the development of a simple lookup table for monitoring the proton energy given experimental evaluation of the activity ratio [114, 117].

In our experiment, an adapted version of the independent methodology proposed by K. Gagnon, et al. [117] was used. To achieve the cyclotron beam energy calibration, the irradiated stack of copper foils was studied in terms of the production of ^{63}Zn, using the copper foils both as monitor and as degrader foils (Figure 5.8).

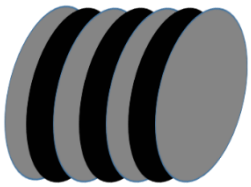

Figure 5.8 – Representation of the stack of copper foils, including 100 µm copper monitor foils (grey), interspaced by 100 µm copper degrader foils (black).

Activities of ^{62}Zn, ^{63}Zn and ^{65}Zn produced during the irradiation of the copper stacked foil were quantified using HPGe gamma spectroscopy and are shown in Table 5.4.

Table 5.4 – Activities of ^{62}Zn, ^{63}Zn and ^{65}Zn produced in the copper stack used for cyclotron beam energy calibration.

Foil	Product	Activity (Bq)
Cu 1	^{62}Zn	$1.6X10^{4}$
Cu 2	^{62}Zn	$6.1X10^{3}$
Cu 3	^{62}Zn	$1.7X10^{1}$
Cu 1	^{63}Zn	$1.4X10^{6}$
Cu 2	^{63}Zn	$2.8X10^{6}$
Cu 3	^{63}Zn	$3.3X10^{6}$
Cu 4	^{63}Zn	$3.7X10^{6}$
Cu 5	^{63}Zn	$2.5X10^{6}$
Cu 6	^{63}Zn	$4.8X10^{5}$
Cu 2	^{65}Zn	$8.7X10^{1}$
Cu 3	^{65}Zn	$2.8X10^{2}$
Cu 4	^{65}Zn	$3.4X10^{2}$
Cu 5	^{65}Zn	$2.7X10^{2}$
Cu 6	^{65}Zn	$7.4X10^{1}$

In Figure 5.9 it is shown an example of a gamma spectrum acquired with the HPGe detector including the ^{62}Zn, ^{63}Zn and ^{65}Zn peaks.

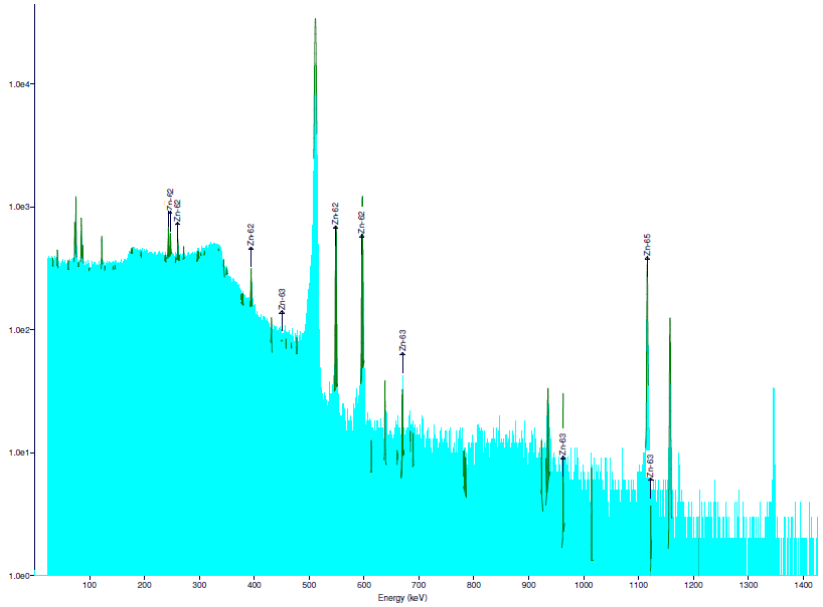

Figure 5.9 - Example of a gamma-spectrum of a Copper foil irradiated presenting production of ^{62}Zn, ^{63}Zn and ^{65}Zn.

Based on the properties of the stack of copper foils here described, the beam energy degradation predicted by SRIM and on the well-known tabulated values of the ^{nat}Cu(p,x)^{63}Zn nuclear reaction, it was built our lookup table for adjustment of the beam energy calibration model (Table 5.5) based on the second degree polynomial $E(MeV) = Ar^2 + Br + C$, where r means the experimental ratio between ^{63}Zn activity in the two copper monitor foils considered.

Table 5.5 – Fitting parameters for the adjustment of cyclotron beam energy calibration model.

Incident energy range (MeV)	Copper degrader thickness (μm)	Second order term A	First order term B	Constant term C
18.0-16.4	100	0.02878 ± 0.00002	-1.072 ± 0.005	10.33 ± 0.05
16.3-14.8	100	0.03099 ± 0.00006	-1.15 ± 0.02	11.0 ± 0.1
14.7-13.0	100	-0.01228 ± 0.00007	0.10 ± 0.02	1.9 ± 0.1
12.9-11.0	100	0.016 ± 0.002	-0.63 ± 0.04	6.8 ± 0.2

This model of adjustment requires at least a prediction on the cyclotron beam energy value for each foil (incident energy range), that could be achieved using SRIM. Considering SRIM prediction of the beam energy in the copper foils (nominal energy) it were calculated the calibrated energy values using experimental ratios of ^{63}Zn activity in copper foils studied (Table 5.6).

Table 5.6 – Cyclotron beam energy calibration results following ^{63}Zn activity experimental ratios.

Nominal energy	Experimental ratio	Calibrated energy
17.2	0.430	**17.0**
15.6	0.751	**14.9**
13.9	1.33	**12.9**

Calibrated energies calculated according to the model were plotted against nominal energies in order to obtain a first degree polynomial fitting to modulate any cyclotron beam energy (Figure 5.10).

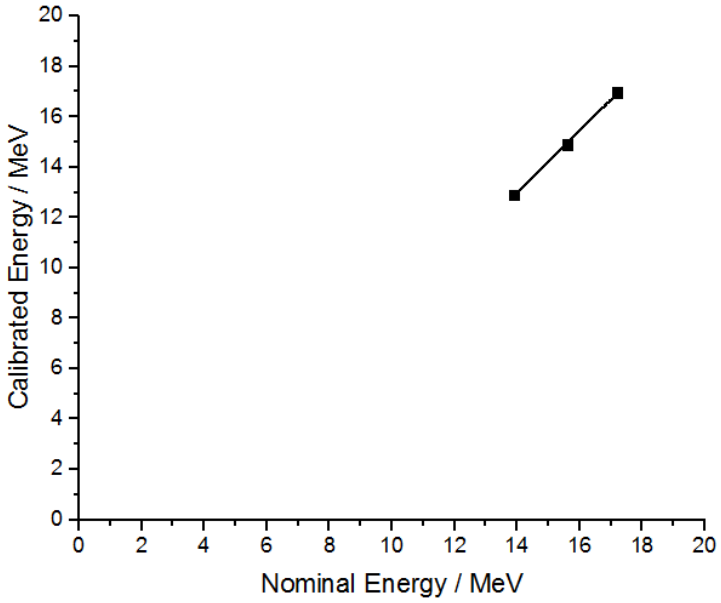

Figure 5.10 – Graphical representation of the relation between nominal energies and calibrated energies.

Linear regression of these data points resulted in the extraction of the first degree polynomial

$$E_{calib} = -4.21 + 1.23 E_{nom}\,, \qquad \textbf{Eq.5.3}$$

where E_{nom} is the nominal/tabulated energy based on SRIM calculations of beam energy degradation on the stacked foil, and E_{calib} is the calibrated beam energy on each foil.

In fact, this independent method for measuring cyclotron beam energy is simple to use and has the ability to easily verify the cyclotron beam energy with an accuracy of few tenths of MeV, providing an accurate determination of proton energies in the 13-17 MeV range without the use of complex analysis methods and avoiding all the concerns related to the HPGe system efficiency calibrations. Even so, its application on this experiment had a certain limitation related with the reduced number of calibration points included in the model (only three, due the thickness

of degraders used) and to the extrapolation of a linear calibration model to the full cyclotron energy range (explained in Figure 5.10).

To test the robustness of this independent method, and considering that copper monitor foils included in the design of the stacked foil used for this experience allow to study more than one nuclear reaction, other methods of beam energy calibration based on the conventional stacked foil technique were applied. The same irradiation for preliminary beam energy calibration was used, but switching the analysis to the absolute cross-section values for proton induced nuclear reactions on copper foils. To follow the methodology suggested by J. H. Kim, et al. [115] and M. U. Khandaker, et al. [116], and considering the energy range under evaluation, the available monitor reactions and the suitability of the HPGe detector's calibration, it were selected the reactions $^{nat}Cu(p,x)^{63}Zn$ and $^{nat}Cu(p,x)^{65}Zn$ as the preferred ones.

Target thicknesses needed for calculations were obtained using Eq.5.2 and are represented in Table 5.7.

Table 5.7 – Properties of targets used in the copper stacked foil.

Target	Density (g/cm^3)	Foil thickness (cm)	Atomic weight (g)	Relative abundance	Target thickness ($x10^{20}$ nuclei per cm^2)
^{63}Cu	8.93	0.01	62.9296	0.6917	5.91
^{65}Cu	8.93	0.01	64.9278	0.3083	2,55

Cross-section values for the two proton-induced nuclear reactions cited were calculated using Eq.5.1, being converted from square centimeters to the more typical unit of mbarn (Table 5.8).

Table 5.8 – Experimental cross-section values for the nuclear reactions $^{63}Cu(p,n)^{63}Zn$ and $^{65}Cu(p,n)^{65}Zn$.

Product	Nominal energy (MeV)	Cross-section ($x10^2$ mbarn)
^{63}Zn	17.2	2.6
^{63}Zn	15.6	5.0
^{63}Zn	13.9	5.9
^{63}Zn	12.0	6.7
^{63}Zn	9.8	4.5
^{63}Zn	7.4	0.9
^{65}Zn	17.2	3.3
^{65}Zn	15.6	10.8
^{65}Zn	13.9	13.1
^{65}Zn	12.0	10.4
^{65}Zn	9.8	2.8
^{65}Zn	7.4	0

Cross-section values determined experimentally were compared with tabulated values, for each nuclear reaction under study.

The obtained cross-section values for the reaction $^{nat}Cu(p,x)^{63}Zn$ were plotted against tabulated data of the EXFOR database [77]. In this context one should point that data presented in EXFOR database for this specific nuclear reaction is the result of the conjugation of 13 experimental papers (from a total of 27 that were analyzed and considered for inclusion). Figure 5.11 shows the above mentioned comparison of the measured (experimental) and the tabulated data.

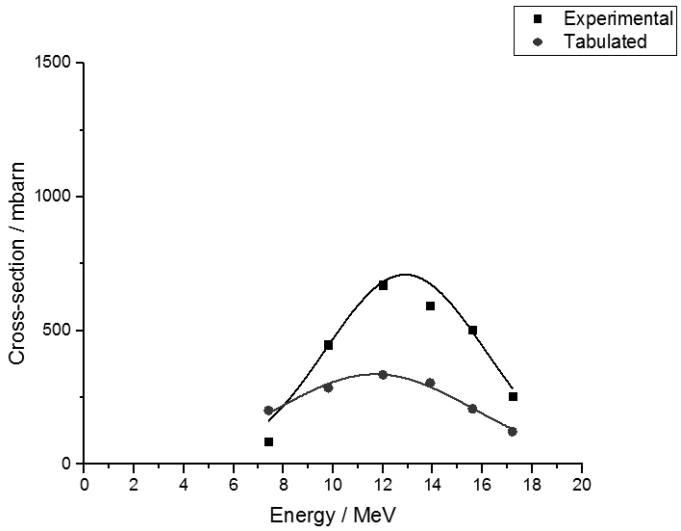

Figure 5.11 – Experimental and tabulated excitation function for the $^{nat}Cu(p,x)^{63}Zn$ reaction.

The very same procedure was repeated for the nuclear reaction $^{nat}Cu(p,x)^{65}Zn$. In this case, data present in EXFOR database for this specific nuclear reaction is the result of the conjugation of 15 experimental papers (from a total of 37 that were analyzed and considered for inclusion). Figure 5.12 illustrates the obtained comparison.

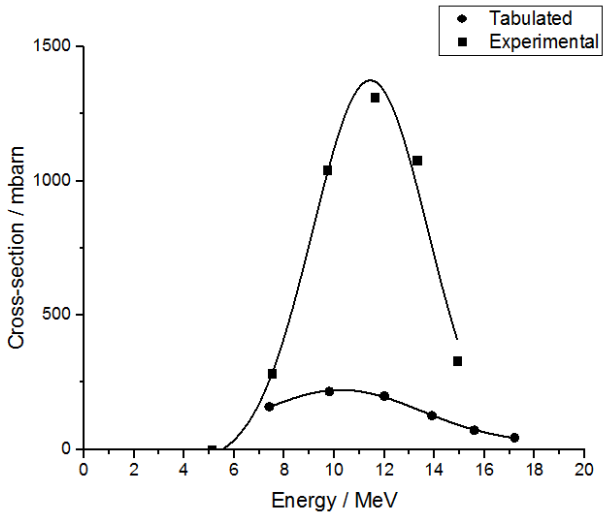

Figure 5.12 – Experimental and tabulated excitation function for the $^{nat}Cu(p,x)^{65}Zn$ reaction.

Scale errors related with the y-axis will be discussed later on an appropriate sub-chapter.

To test a different approach to achieve the goal of this preliminary experiment, it was considered that the calibrated experimental beam energy (E_{calib}) could be determined as

$$E_{calib} = c + GE_{nom}\,, \qquad \textbf{Eq.5.4}$$

where E_{nom} is the nominal/tabulated energy based on SRIM calculations of beam energy degradation on the stacked foil, *c* is a constant calibration parameter commonly named as zero and *G* is a first order calibration parameter commonly named as gain.

The calibration parameters *c* and *G* were calculated assuming the statistical nature of the radiation detection process in the HPGe detector, and using Gaussian fitting of the obtained data, either for the series of tabulated results as for the experimental results, and using the following algebraic deductions

$$c = Xc_{tab} - \left(\frac{w_{tab} Xc_{\exp}}{w_{\exp}} \right), \qquad \textbf{Eq.5.5}$$

and

$$G = \frac{w_{tab}}{w_{\exp}}, \qquad \textbf{Eq.5.6}$$

where *w* means the width of the Gaussian function used to fit the peak of each series of data, and *Xc* means the center of those Gaussian functions, while *exp* and *tab* mean experimental and tabulated data, respectively. Table 5.9 presents all the parameters obtained during the Gaussian fitting procedure.

Table 5.9 – Gaussian fitting parameters obtained using ORIGIN 2016®.

Fitting parameters	^{63}Cu(p,n)^{63}Zn		^{65}Cu(p,n)^{65}Zn	
	tab	exp	Tab	Exp
Xc	11.88	12.65	10.50	11.62
W	4.147	3.480	3.508	2.740

Given parameters of Table 5.9 and using Eq.5.4, Eq.5.5 and Eq.5.6, a new beam energy calibration model was obtained for each monitor reaction. Finally, a weighted mean was calculated having in account the relative isotope abundance on target, reaching -3.55 and 1.22 as final values for the parameters *c* and *G*, respectively. This model

of beam energy calibration allowed another attempt for the calibration of cyclotron bean energy according to the preliminary experiment undertaken (Table 5.10).

Table 5.10 – Linear cyclotron beam energy calibration results according to the Gaussian fitting of the excitation functions of the monitor reactions on copper foils.

Nominal energy	Calibrated energy
17.2	17.4
15.6	15.5
13.9	13.4
12.0	11.1
9.8	8.4
7.4	5.5

Another approach to achieve beam energy calibration was attempted, now having in account the possibility of the non-linearity of the beam energy calibration model. Here, it was considered that calibrated experimental beam energy, E_{calib}, is equal to

$$E_{calib} = c + BE_{nom} + QE_{nom}{}^{2}, \qquad \textbf{Eq.5.7}$$

where *c* is a constant point, while *B* and *Q* are first and second order calibration parameters, respectively.
Thus, the same Gaussian fitting models of the excitation functions of the two monitor nuclear reactions under study (both tabulated and experimental) were used in an integrated approach, with the inclusion of an extrapolated third fixed point (*c* equal to zero - meaning that the zero nominal energy corresponds to a calibrated zero energy). Considering $c = 0$, *B* and *Q* parameters were obtained using the following algebraic deductions:

$$B = \frac{\left({}^{63}Xc_{tab} \cdot \left(\frac{{}^{65}Xc_{\exp}}{{}^{63}Xc_{\exp}} \right) \right) - \left({}^{65}Xc_{tab} \cdot \left(\frac{{}^{63}Xc_{\exp}}{{}^{65}Xc_{\exp}} \right) \right)}{{}^{65}Xc_{\exp} - {}^{63}Xc_{\exp}}, \qquad \textbf{Eq.5.8}$$

and

$$Q = \frac{\left(\frac{{}^{65}Xc_{tab}}{{}^{65}Xc_{\exp}} \right) - \left(\frac{{}^{63}Xc_{tab}}{{}^{63}Xc_{\exp}} \right)}{{}^{65}Xc_{\exp} - {}^{63}Xc_{\exp}}, \qquad \textbf{Eq.5.9}$$

where *w* means the width of the Gaussian function used to fit the peak of each series of data, and *Xc* means the center of those Gaussian functions, *exp* and *tab* mean experimental and tabulated data, respectively, while the exponent number indicates the nuclear reaction under study, being *63* indicative of the $^{63}Cu(p,n)^{63}Zn$ and *65* of the $^{65}Cu(p,n)^{65}Zn$ nuclear reaction.

This procedure allowed the achievement of a quadratic beam energy calibration model. Obtained results are shown in Table 5.11.

Table 5.11 – Quadratic cyclotron beam energy calibration results according to the Gaussian fitting of the excitation functions of the monitor reactions on copper foils.

Nominal energy	Calibrated energy
17.2	18.9
15.6	16.2
13.9	13.7
12.0	11.0
9.8	8.2
7.4	5.6

These two cross-section dependent procedures allowed the calibration of the beam energy in this preliminary experiment, while demonstrated the ability to implement mathematical solutions for the appropriate fitting of this kind of results and allowed the development of a robust and rigorous solution for the calibration of the beam energy based on excitation functions of monitor nuclear reactions. An overall comparison of these models together with the independent model of beam energy calibration is presented in Figure 5.13.

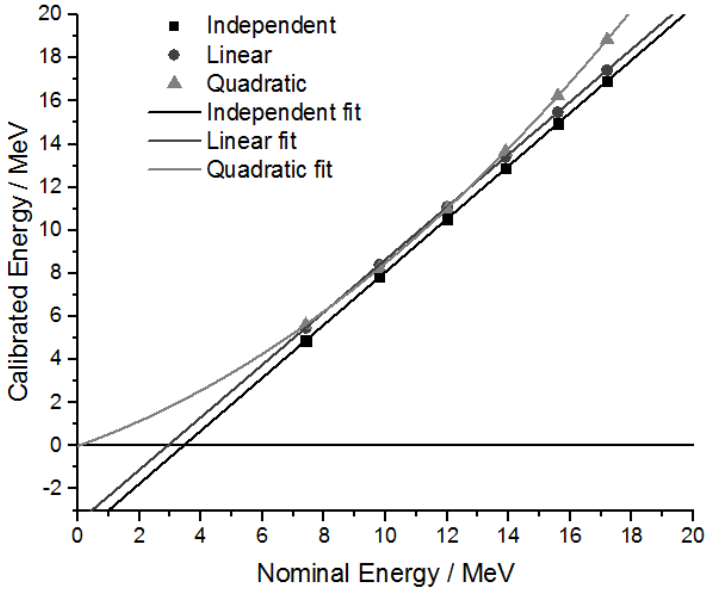

Figure 5.13 - Beam energy calibration curves obtained using the independent, the linear and the quadratic model.

Analysing the obtained calibration curves it is possible to state that the three models here described are very well correlated, giving more strength and robustness to any conclusion extracted from this data. First order polynomials (independent and linear model) can be considered overlapped in what regards to low beam energies. The quadratic model exhibits some discrepancies in the extension of the extreme energy values considered. This quadratic model accounts for any possibility of non-uniform extraction of beam from the cyclotron ports, while the other two models assume a linear functioning of the device. As a matter of fact, and even considering that efficiency calibration of the HPGe detector used for quantification was undertaken, the independent model allows a simpler understanding of this calibration. This model appears to provide results that are well correlated with the other models and with the SRIM simulated energy degradation: It also confirms the expectations of the device functioning, with a special emphasis to a maximum beam energy extracted from the cyclotron port of 17.5±0.2 MeV, already experimentally studied at the cyclotron of ICNAS [118, 119]. For these reasons, the independent method was applied to the analysis of the experimental results that will be further described here in this Thesis.

Beam energy calculation suffers from the influence of several uncertainties. Despite the typical statistical fluctuations in different experiments, the total uncertainty directly involved in the beam energy calculation in this calibration is given by uncertainties associated with the two fitting parameters used (the zero and the gain). Having in account the first order polynomial described in Eq.5.3, the zero and the gain values used together with their uncertainties were - 4.21±0.49 and 1.23±0.03, respectively.

5.3.3 Cross-section determination: correction factors

During the analysis of the preliminary experiment for beam energy calibration it was possible to verify that the absolute values of cross-sections determined for the monitor foils do not strictly correspond to the well accepted tabulated values for these nuclear reactions, seeming to indicate a scale factor on the cross-section value determined. It is known that cross-section values suffer also from the influence of several uncertainties, including beam intensity uncertainties, uncertainty in the target thickness indication, and spectroscopy quantifications uncertainty. While beam intensity uncertainties and target thickness uncertainty will be used as the basis for the total uncertainty involved in the cross-section determination, some spectroscopy-related sources of error could be accounted and corrected.

Departing from the knowledge about sources of error in the efficiency calibration of an HPGe detector for spectroscopy, and considering the specific protocol of calibration implemented before these experiments, one should correct calculated activities with a correction factor that accounts for the unsuitability of the ^{152}Eu used for efficiency calibration (very low activity) and for the mismatch in the sample configuration for calibration and for experimental quantifications (point-like versus “thin” foil configuration, different densities and possible inaccuracy of sample positioning - discussion of these topics already presented in sub-chapter 4.4).

Comparing the maximum experimental cross-section value for each monitor reaction with the corresponding tabulated value, it was identified a calibration correction factor, *F*, that is dependent on the relative isotopic abundance on target and is equal to

$$F = 0.69\,\theta\,. \qquad \textbf{Eq.5.10}$$

This proportionality constant express the correction of technical factors related with the geometry of the acquisition of data, and θ is the isotopic abundance of the target isotope for each specific nuclear reaction in the foil. All these considerations depart from the notion that the procedures implemented in the HPGe spectroscopy for the beam energy calibration irradiation and for the main experiences were strictly the same (eg.: sample dimensions, geometry of detection, self-absorption…), being the unique difference related with the material involved (copper *vs* scandium).

Given this approach, normalized cross-section values were calculated for the $^{nat}Cu(p,x)^{63}Zn$ nuclear reaction considering θ as the product between the target purity (Copper foil with 99.999% purity) and the ^{63}Cu isotopic abundance (69%), leading to a final value of the abundance of 68.99% and an *F* value of 0.48.

The same rationale was applied for the $^{nat}Cu(p,x)^{65}Zn$ nuclear reaction considering θ as the product between the target purity (Copper foil with 99.999% purity) and the ^{65}Cu isotopic abundance (31%), leading to a final value of abundance of 30.99% and an *F* value of 0.21.

Finally, for the main experiment that will be further presented, Scandium-45 target purity of 99.5% was considered to achieve an *F* value of 0.69 that must correct all the activities of ^{45}Ti determined via HPGe spectroscopy.

5.3.4 Qualitative study of $^{45}Sc(p,n)^{45}Ti$ energy threshold

This preliminary step of study of the $^{45}Sc(p,n)^{45}Ti$ nuclear reaction was conducted and lead to the qualitative validation of the theoretical value of the energy threshold of this reaction, considering that significant activity was produced at a beam energy nominal value of 5.0 MeV (above the theoretical threshold), without any measurable activity on the 2.5 MeV irradiated foil (below the theoretical threshold).

5.3.5 Determination of the excitation function for the $^{45}Sc(p,n)^{45}Ti$ nuclear reaction

Activities of ^{45}Ti induced on ^{45}Sc foils were quantified using HPGe gamma-ray spectroscopy and corrected with the above mentioned factor *F*, and are shown in Table 5.12.

Table 5.12 - Activities of ^{45}Ti produced on the stacked foils used for the experimental determination of the excitation function of the ^{45}Sc(p,n)^{45}Ti nuclear reaction, quantified using the HPGe detector and corrected with factor *F*.

Foil	Activity of ^{45}Ti (Bq) Experiment 1	Activity of ^{45}Ti (Bq) Experiment 2
Sc-1	-	-
Sc-2	-	-
Sc-3	$2.2x10^{6}$	-
Sc-4	$2.9x10^{6}$	$6.2x10^{6}$
Sc-5	$6.1x10^{6}$	$1.2x10^{7}$
Sc-6	$4.8x10^{6}$	$9.0x10^{6}$
Sc-7	$2.0x10^{6}$	$9.0x10^{5}$
Sc-8	$1.5x10^{5}$	$3.5x10^{4}$
Sc-9	$2.8x10^{4}$	$4.4x10^{3}$
Sc-10	-	-
Sc-11	-	-

Activities of ^{63}Zn and ^{65}Zn induced on copper monitor foils were also determined in order to validate the beam energy calibration model (Table 5.13).

Table 5.13 - Activities of ^{62}Zn, ^{63}Zn and ^{65}Zn produced on the monitor foils inserted in the stacked foil, quantified using the HPGe detector and corrected with factor *F*.

Foil	Activity of ^{65}Zn (Bq)	Activity of ^{65}Zn (Bq)	Activity of ^{63}Zn (Bq)	Activity of ^{63}Zn (Bq)
	Experiment 1	Experiment 2	Experiment 1	Experiment 2
Cu-1	$4.6x10^{2}$	$7.1x10^{2}$	$2.4x10^{7}$	$5.4x10^{7}$
Cu-2	$8.1x10^{2}$	$2.0x10^{3}$	$2.7x10^{7}$	$6.4x10^{7}$
Cu-3	$5.6x10^{2}$	$1.2x10^{3}$	$1.7x10^{7}$	$3.3x10^{7}$

These copper monitor foils were studied to validate the independent beam energy calibration model adopted in this Thesis and to determine mean beam energy on each foil. The energy axis calibration using the tabulated and the experimental excitation functions for the monitor nuclear reactions is shown in Figure 5.14.

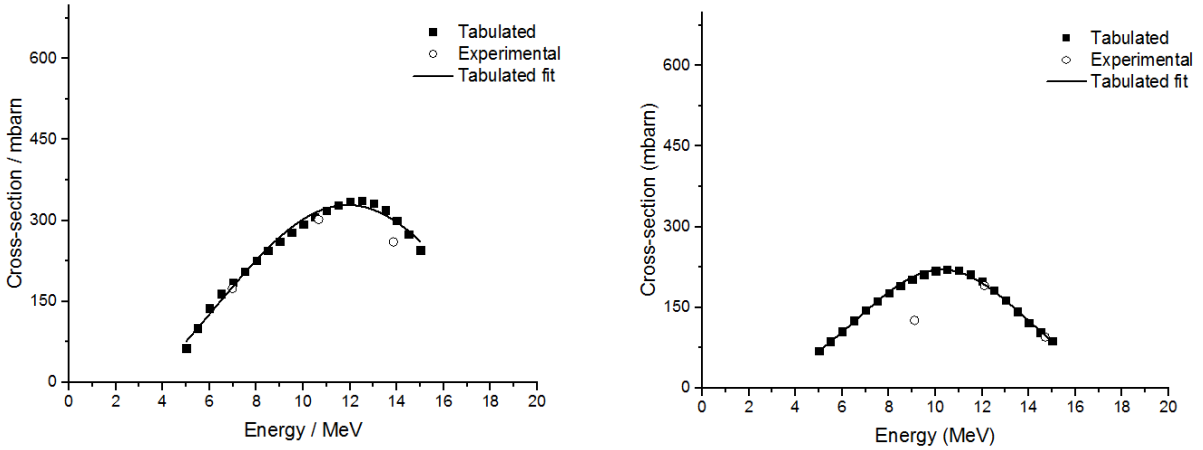

Figure 5.14 – Tabulated and experimental excitation functions for the $^{nat}Cu(p,x)^{63}Zn$ (left) and $^{nat}Cu(p,x)^{65}Zn$ (right) nuclear reactions. Experimental data is based on copper monitor foils irradiated during the main experiments for the study of the $^{45}Sc(p,n)^{45}Ti$ nuclear reaction.

As it was expected and briefly discussed in the previous sub-chapters (mainly when considering the test performed using the linear model based on the Gaussian mathematical fitting of the excitation functions), these two monitor nuclear reactions present slightly different adjustment profiles. When considered both reactions, a weighted mean model should be determined. However, in fact, the independent solution applied only takes in account $^{nat}Cu(p,x)^{63}Zn$ nuclear reaction, and it seems that the calibration is well reproduced in the main experiment data considered in Figure 5.13. Fitting of $^{nat}Cu(p,x)^{65}Zn$ nuclear reaction excitation function data using the independent calibration model demonstrate the problems related to the modelling of the low energy range. Considering the relative importance of each monitor reaction and the suitability of the selected model to fit data of $^{nat}Cu(p,x)^{63}Zn$ in the main experiment here described, it was considered that this cyclotron beam energy calibration model could be presented as a reliable solution.

Validated the independent model of beam energy calibration, calibrated energies of the beam in each foil of the stacked foil were calculated (Table 5.14).

Table 5.14 - Cyclotron beam energy calibration results for the stacked foil constituted by Scandium foils.

Foil	Nominal energy (MeV)	Calibrated energy (MeV)	Uncertainty (MeV)
Sc-1	17.7	17.6	± 1.0
Sc-2	17.1	16.8	± 1.0
Sc-3	16.5	16.1	± 1.0
Sc-4	15.9	15.3	± 1.0
Sc-5	13.5	12.4	± 0.9

Sc-6	10.7	8.9	± 0.8
Sc-7	7.4	4.9	± 0.7
Sc-8	6.2	3.4	± 0.7
Sc-9	4.9	1.8	± 0.6
Sc-10	3.3	-0.2	± 0.6
Sc-11	1.2	-2.7	± 0.5

Note that negative values resulting from the calibration of energy in Sc-10 and Sc-11 foils demonstrate the reduced capacity to approach an accurate solution for the low energy range. The particular situation of Sc-10 foil should be analyzed in accordance with the uncertainty value calculated (± 0.6 MeV), that include positive values in the possible range for energy on the foil. This situation is probably related with the fact that calibration is only studied in a reduced region of the energy spectrum (13-17 MeV), being linearly extrapolated to all the energy spectrum (0-18 MeV). In fact, this fact is the major intrinsic limitation of the selected method of calibration. Nevertheless, this limitation is also present in the other methodologies tested. For the purpose of this experimental study, negative values were taken as nule, being considered that the beam was totally absorbed in the previous foils.
The irradiation parameters are described in detail in Table 5.15.

Table 5.15 – Irradiation parameters implemented in the two independent experiments using stacked foil technique for the determination of the excitation function of the $^{45}Sc(p,n)^{45}Ti$ nuclear reaction.

Irradiation	Duration (s)	Mean current (uA)	Intensity (x10^{12} particles/s)
Experiment 1	100	0.6	3.75
Experiment 2	550	0.6	3.75

Properties of the irradiated targets (foils) could be seen in Table 5.16.

Table 5.16 - Properties of targets used in the scandium-copper stacked foils applied in the main experiments.

Target	Density (g/cm^3)	Foil thickness (cm)	Atomic weight (g)	Relative abundance	Target thickness (x10^{20} nuclei per cm^2)
^{63}Cu	8.93	0.01	62.9296	0.692	5.91
^{65}Cu	8.93	0.01	64.9278	0.308	2.55
^{45}Sc	2.99	0.01	44.9559	0.995	3.99

Again, Eq.5.1 was used to calculate cross-section values (Table 5.17). Note also that cross-section absolute values suffer from the influence of several uncertainties. The total uncertainty directly involved in the cross-section determination in these experiments is given by

$$\sigma_t^2 = \sigma_{beam}^2 + \sigma_{t\arg et}^2 + \sigma_{HPGe}^2 , \qquad \textbf{Eq.5.11}$$

where σ_t means total uncertainty, σ_{beam} means beam intensity uncertainties, σ_{target} means the uncertainty in the target thickness and σ_{HPGe} means spectroscopy quantifications uncertainty.

The uncertainty on beam intensity measurement was obtained by the calculation of the relative error in the calculation of cross-section values for the $^{63}Cu(p,n)^{63}Zn$ nuclear reaction during the experiment, achieving a mean error of 27%.

Considering the target thickness calculation, only the foil thickness uncertainty should be accounted, being excluded uncertainties of relative isotopic abundance, density and Avogadro's number - that could be considered negligible. The value of 10% indicated by the foil's manufacturer was included in the calculation.

Finally, the spectral analysis uncertainty was estimated by the analysis software and included the uncertainty in the determination of the area under the peak, counting uncertainty and efficiency, leading to an approximate value of 10%.

Total uncertainty on cross-section determination was calculated and resulted in 30.5%.

Table 5.17 - Summarized results of experimental cross-section values for the $^{45}Sc(p,n)^{45}Ti$ nuclear reaction.

Calibrated mean beam energy (MeV)	Cross-section for $^{45}Sc(p,n)^{45}Ti$ (mbarn)	Uncertainty (mbarn)
16.1	$1.2x10^2$	$\pm$ $0.4x10^2$
15.3	$2.1x10^2$	$\pm$ $0.7x10^2$
12.4	$4.4x10^2$	$\pm$ $1.4x10^2$
8.9	$3.4x10^2$	$\pm$ $1.0x10^2$
4.9	$1.2x10^2$	$\pm$ $0.4x10^2$
3.4	$0.8x10^1$	$\pm$ $0.3x10^1$
1.8	$0.2x10^1$	$\pm$ $0.1x10^1$

Indeed, in these experiences it was not possible to correctly study beam energies of 17.6 and 16.8 MeV (Sc1 and Sc2 foils, previously mentioned) mainly due to the interference of high activities of ^{44}Sc. In this context, the usual technical approach (increment of the cooling time) to avoid this interference was not useful considering the similar

physical half-lifes involved (3.08 h and 3.93 h, for ^{45}Ti and ^{44}Sc, respectively). In other words, the increment of the cooling time to reduce dead time of the HPGe detector would lead to minimal activities of ^{45}Ti that would prevent an effective and correct quantification, disallowing the experimental determination of cross-section values for those energy points. This situation, together with the impossibility to obtain a calibration of the HPGe detector for a geometric position farthest from the detector (due to the very low activity level of the ^{152}Eu source), caused reduction of the energy points planned to be collected.

But, as a matter of fact, this made possible extraction of some relevant information: i) higher beam energies (≥ 16.8 MeV) lead to increased production of contaminants, with the bigger contribution of ^{44}Sc, but also with significant and measurable quantities of ^{44m}Sc and ^{44}Ti – Figure 5.15; ii) for those mentioned higher energies, induced activities of contaminants exceed the induced activities of ^{45}Ti; iii) this energy region is expectably characterized by the decrease of the cross-section value for the reaction ^{45}Sc(p,n)^{45}Ti, with the consequent increase of other proton-induced reactions, such as (p,2n) and (p,pn).

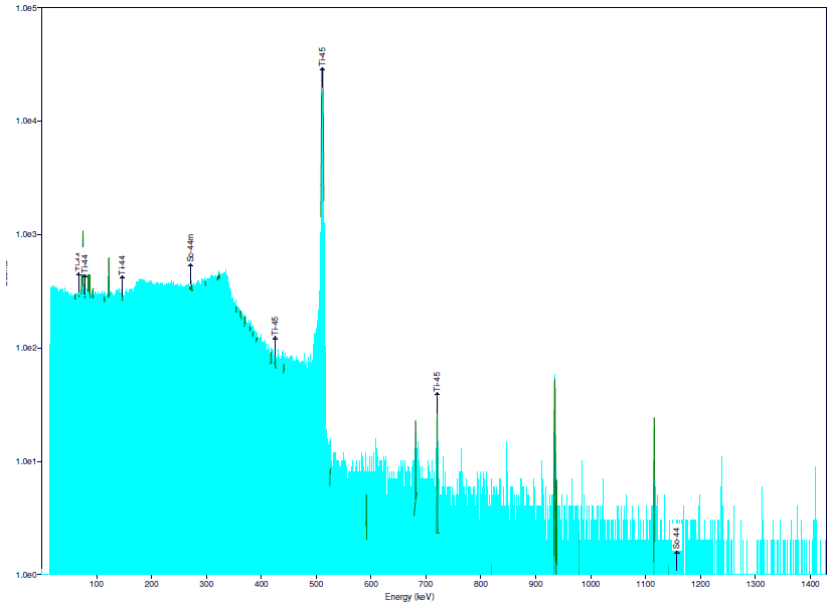

Figure 5.15 - Example of a gamma-spectrum of a Scandium foil irradiated with a mean energy higher than 17 MeV presenting production of ^{44}Ti, ^{45}Ti, ^{44}Sc and ^{44m}Sc.

As a note, the knowledge of those competitor reactions was considered before in the design of these experimental study and is now being explored by several other authors in the way to produce ^{44}Ti/^{44}Sc radionuclide generators, allowing the production of ^{44}Sc – also useful as an unconventional radionuclide for PET imaging [120, 121].

The overall experimental excitation function determined here is based on the set of cross-section values determined with appropriate mathematical fitting of the obtained curve, and is represented in Figure 5.16.

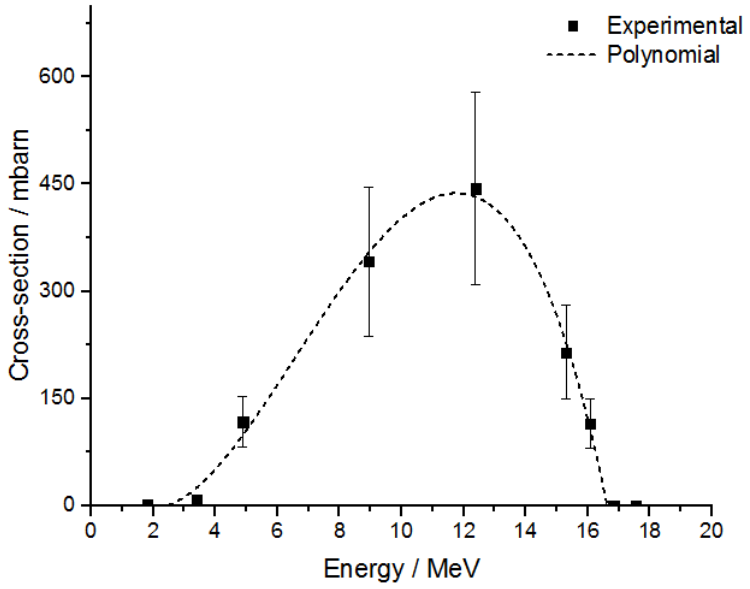

Figure 5.16 - Experimental excitation function of the $^{45}Sc(p,n)^{45}Ti$ nuclear reaction.

The mentioned mathematical fitting of nuclear data obtained in activation experiments deserves attention, and is being briefly discussed by some authors but not in a structured way. In such a context, for the purpose here considered attention was given to the procedure of fitting applied to the results obtained. Thus, to construct a recommended curve of an excitation function reliance is placed on the data fitting methods used.

The most used way to fit experimental data obtained is the application of polynomial fitting, even following several different ways to consider the uncertainties obtained in the experimental data and to fit the scattered data. In general, a polynomial would fit exactly all the constraints of the curve. However, in some cases, this exact fitting of some constraints could not represent the most accurate option. Considering this possibility, in this work it was attempted to understand the behavior of the most important excitation function under study to suggest the most efficient way to fit obtained data. Among other models that were searched, a modified Hill's function – the biphasic Hill Equation (Bi-Hill) - is suggested as the most interesting solution.

This mathematical model could efficiently reproduce processes characterized by a sigmoidal growth, with a rapid increase, followed by a saturation plateau and a rapid decrease with an high degree of symmetry with the growth phase, and its use is very common in chemistry, biology and in pharmacology [122].

The application of a polynomial fitting and a Bi-Hill fitting to the experimental data obtained was compared and is represented in Figure 5.17. The selection of the Bi-Hill model of fitting is justified by the better translation of the common behavior of an excitation function and not properly by a mathematical comparison based on the quality of adjustment (due to the reduced number of points studied to perform a fair comparison).

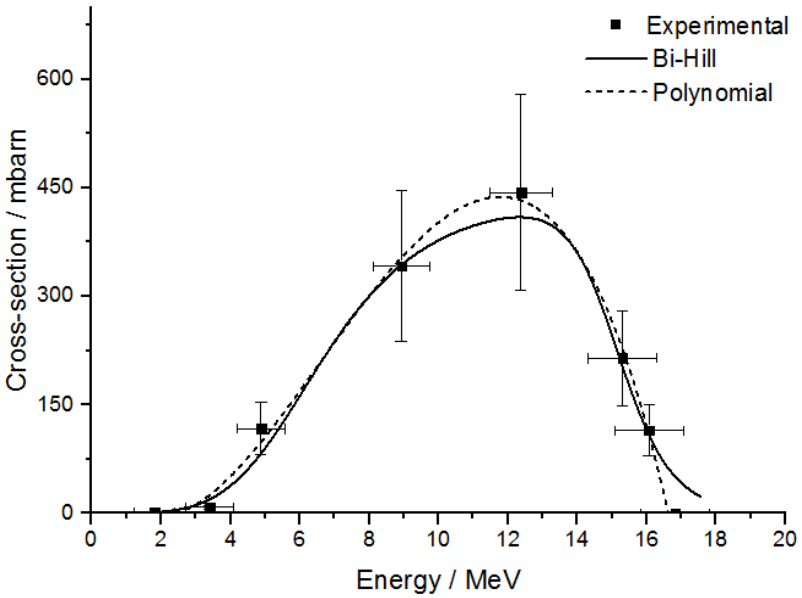

Figure 5.17 – Experimental excitation function of the $^{45}Sc(p,n)^{45}Ti$ nuclear reaction fitted with two different mathematical models.

Polynomial fitting was achieved with the fifth degree polynomial

$$y = 78.50 - 89.89x + 28.88x^2 - 2.37x^3 + 0.09x^4 - 0.002x^5, \qquad \textbf{Eq.5.12}$$

resulting in a R^2 of 0.993.

The Bi-Hill model is generally expressed as

$$y = \frac{Pm}{\left[1+\left(\frac{ka}{x}\right)Ha\right]\left[1+\left(\frac{x}{Ki}\right)Hi\right]}. \qquad \textbf{Eq.5.13}$$

In this particular situation, the excitation function of the main reaction under study was modulated by the function

$$y = \frac{443.75}{\left[1+\left(\frac{6.79}{x}\right)4.48\right]\left[1+\left(\frac{x}{15.21}\right)20.19\right]}. \qquad \textbf{Eq.5.14}$$

Among the set of values determined, the maximum cross-section value of 443.7 ± 135.3 mbarn was determined for a mean beam energy on target of 12.4 MeV.

After correct analysis and interpretation of the obtained excitation function, maximum cross-section values were identified in the energy region of 10→14 MeV, while thick target yield was obtained by the use of the integral cross-section in the region 8→16 MeV (so, including a certain margin applied to the excitation function maximum values), leading to a value of 433.64 MBq.μA^{-1}sat.

Complete overview of integral thick target yield for a saturation condition could be seen in Figure 5.18.

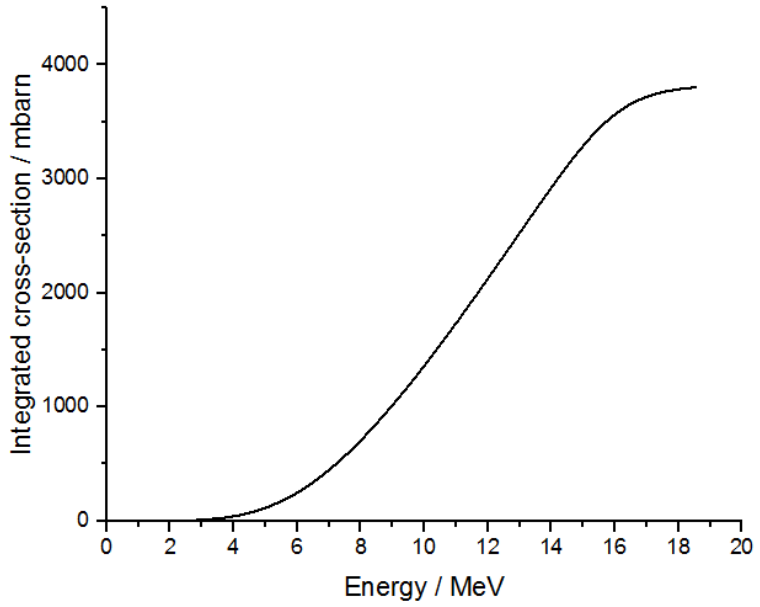

Figure 5.18 - Thick target yield of the ^{45}Sc(p,n)^{45}Ti nuclear reaction calculated for a saturation condition for proton energies between 16 and 8 MeV.

Experimental results on integrated thick target yields in the energy range of 8→16 MeV of this work are also on the same order of magnitude of some published results, as it is the case of the experimental value 420.00 MBq.μA^{-1}h^{-1} obtained after 21 production runs by Tang [110] or 422.00 MBq.μA^{-1}h^{-1} obtained after 75 production runs by Vavere, et al. [38].

Obtained results were compared with the simulated data (TALYS code) previously used to have an overview about the feasibility of this nuclear reaction as a route to obtain ^{45}Ti in low energy cyclotrons (Figure 5.19).

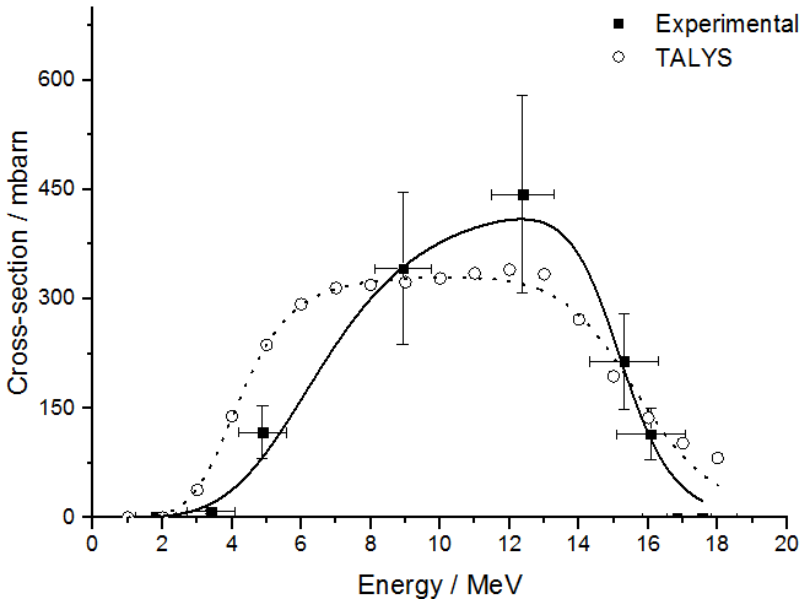

Figure 5.19 - Comparison between TALYS simulated and experimental excitation functions for the $^{45}Sc(p,n)^{45}Ti$ nuclear reaction, with respective lines indicating mathematical fitting with Bi-Hill models.

The overall tendency and behavior of the excitation function for this nuclear reaction was correctly approached by TALYS simulation, even in quantitative terms. Given the uncertainties included in this experimental determination, obtained values could be considered in the same order of magnitude of those previously calculated using this Monte Carlo simulation code, despite a small discrepancy found in the low energies region – mainly explained by the inaccurate beam energy calibration in this region.

Nevertheless the existence of a lack of complete experimental dedicated studies on the excitation function of the $^{45}Sc(p,n)^{45}Ti$ nuclear reaction in low energy cyclotrons, there are some published data on this topic, mainly from old publications, most of them concerning fundamental research on nuclear physics [123-128]. A deeper analysis of all the data found could allow the extraction of some relevant conclusions: some of the authors do not applied the stacked foil technique and only studied a limited number of (low) energy points [124, 127]; other authors focused their analysis only on induced reactions below 10 MeV [126, 128]; and only two of these six authors studied a wider range of the proton beam energies available at a low energy cyclotron [123, 125]. Even so, it was not found any published experimental study covering an energy range from the reaction threshold (~ 3 MeV) until 18 MeV – as it is the case of the work here presented. The comparison of data obtained in this work with all the other available data sets is shown in Figure 5.19. Uncertainties of the other published results were not represented for a simpler visual perception of the results.

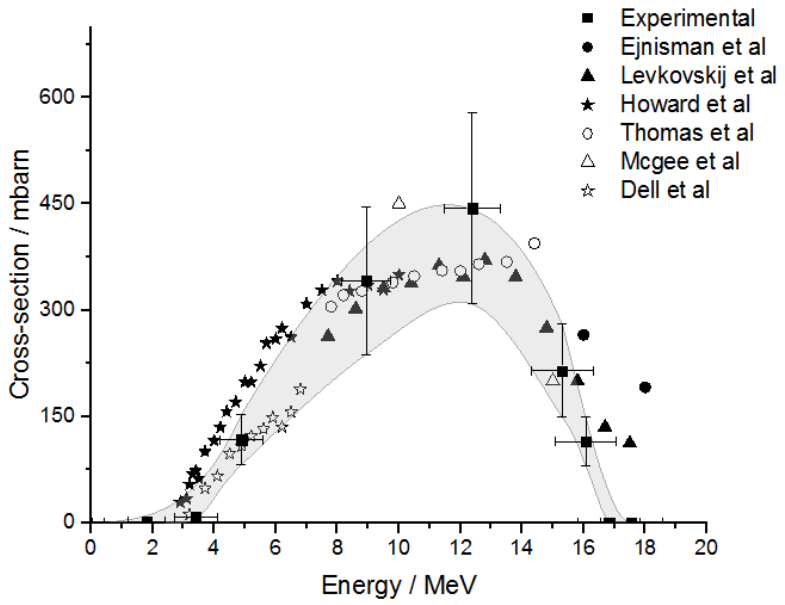

Figure 5.20 – Graphical comparison of experimental data on the excitation function of the $^{45}Sc(p,n)^{45}Ti$ nuclear reaction obtained in this work with other published results, with grey shadowed area indicating a fitted interval of experimental values considering experimental uncertainty.

Figure 5.20 illustrates a clear correspondence between this work and all the others, both in the shape as in the quantitative values obtained for the excitation function. Again, it was found a small mismatch in the low energy region, specifically in what regards to the comparison with the work published by Howard, et al. [126].

5.4 Final considerations on the excitation function of $^{45}Sc(p,n)^{45}Ti$ nuclear reaction

After the description of all the experimental assays involved in this project to achieve the goals previously stablished, including methodological aspects involved and all the results obtained, it is possible to extract some key notes as:

- ✓ The stacked foil method allows a simpler and reliable experimental study of nuclear reactions excitation functions;
- ✓ For a better interpretation of results, and to achieve the necessary compatibility of results with other experimental attempts, beam energy calibration using copper monitor foils appears to be a mandatory step;
- ✓ Calibration of beam energy is highly dependent on the mathematical approach implemented;
- ✓ HPGe efficiency calibration has a major impact on the quantitative values of activity obtained, reason why correction factors that account to any undesired effect should be calculated and used to reduce the impact of technical sources of error such as geometrical issues involved in gamma-ray spectroscopy;

- ✓ The $^{45}Sc(p,n)^{45}Ti$ nuclear reaction seems to be feasible in low energy (medical) cyclotrons, with cross-section values presenting a peak for proton beam energies in the range between 10 and 15 MeV;
- ✓ Experimental results obtained here for the excitation function of the $^{45}Sc(p,n)^{45}Ti$ nuclear reaction are comparable with other published data;
- ✓ The thick target yield for a saturation condition obtained in this experiences (433.64 $MBq.\mu A^{-1}sat$) is also in accordance with theoretical prediction and comparable to other published experimental results;
- ✓ Energies higher than 17 MeV lead to increased production of contaminants such as ^{44}Ti, ^{44}Sc and ^{44m}Sc;
- ✓ Results obtained here confirm the possibility to effectively produce ^{45}Ti using low energy cyclotrons, deserving to be incorporated and integrated in the design of an optimized production methodology for this radionuclide;

6. Potential applications of ^{45}Ti

The research project reported in this thesis was designed and developed in such a way to guarantee the conservation of most of the principles of an applied research: i) creation of fundamental knowledge with practical orientation; ii) when possible, with a market-driven approach. In such a context, there was no sense to study the production of a radionuclide without the correct exploitation of its interesting properties and, more important, its potential applications.

This Chapter provides some insights on the properties of ^{45}T and its possible future applications, including those ones already tested and a critical analysis forwarding the future to this radionuclide.

As said before, ^{45}Ti has a physical half-life of 3.09 hours, which allows its commercial distribution within a broader region than radiopharmaceuticals based on ^{18}F. In other hand, its decay is predominantly based on positron emission (85%), with maximum positron energy of 1040 keV and average energy of 439 keV, that assures the obtainment of good image quality.

Chemical properties of Ti put the nuclide in two different scenarios based on radiopharmaceuticals to be developed; i) radiolabeled nanoparticles (according to a trend to the use of nanoparticles that already exists on the field of Nuclear Medicine, and based on the interest of titanium oxide nanoparticles for clinical purposes); ii) "direct" labelling of several different ligands.

This Chapter begins with the presentation of a systematic review on the broad topic of radiolabelled nanoparticles, establishing the actual trends on the field, for the sustained technical analysis of the potential of ^{45}Ti as a radionuclide to be used in that context. To finish, it is also present a sub-chapter directed to the study of the potential applications of ^{45}Ti as a radiolabeling agent for different ligands, allowing the enumeration of the clinical fields related and the understanding of what could the future bring to the application of this radionuclide in preclinical and clinical contexts.

6.1 Nanoparticle-based radiopharmaceuticals: status *quo* and future developments

The practice of medicine seems consistently changing, with a special emphasis on the application of technological innovations, where medical imaging modalities play an important role. Between the several imaging modalities, Molecular Imaging (essentially based on Nuclear Medicine) is considered as one of the most interesting options.

On other hand, assuming that nanoparticles are being studied as drug delivery systems, its application as vectors for radionuclide-based (molecular) imaging is a powerful tool of growing interest.

6.1.1 From Nanotechnology to Nanomedicine

Nanotechnology is an interesting new concept, perfectly fitting in an era characterized by a strong pendant to innovation and high technological approaches. Several decades have passed since the first references to the

concept in a Richard Feynman's talk in 1959 [129] or the first formal designation in a Norio Taniguchi's paper in 1974 [130]. However the rationale behind it is still conserved: nanotechnology is, by definition, the scientific use that intentionally operates at the first level of organization of atoms and molecules. It promises the ability to understand, control and manipulate matter at that submicroscopic level with the use of materials processing, devices or systems with nanoscale size and shape [131, 132]. Quite often it is forgotten how much nanotechnology is involved in the modern daily life, but one should point into its importance in fields so different as the web, social media, communication, energy, food and environmental sciences or in the health field.

With a special emphasis in the very last decades, the paradigm of medicine has also been modified and after the long era of empirical medicine, where merely observational and rational basis were applied, nowadays, the evidence of the daily clinical practice demonstrates a "*science & technology-based medicine*", considered by many relevant authors as the probable starting of a new era of medicine - a medicine consistently related with (and supported by) technological approaches. Among them there is an each-day increasing number of tools targeted to the molecular level. It is believed that two past events played a major role in this change: the introduction of antibiotics and the revolution of genetics. These events could be considered as the first unequivocal demonstrations of the ability to directly interact with molecular biological processes. The practice of modern medicine is thus related with the three main branches of Nanotechnology, as defined by *Freitas* in 1999: i) Nanomaterials Technology, ii) Biotechnology, and iii) Molecular Nanotechnology [133]. Together with the application of traditional research methodologies these advances have brought us to the presently much widely used concept of Nanomedicine.

The development from the nanomedicine field involves (and relates) with advances in many techno-scientific areas, as engineering, chemistry, physics and/or biology, and is thus increasing in each day, as represented in Figure 6.1. In the design of a new nanoparticle necessary for biological/health applications a multidisciplinary approach is mandatory and a crucial factor for the success of the final product, eventually developing Nanomedicine as a whole.

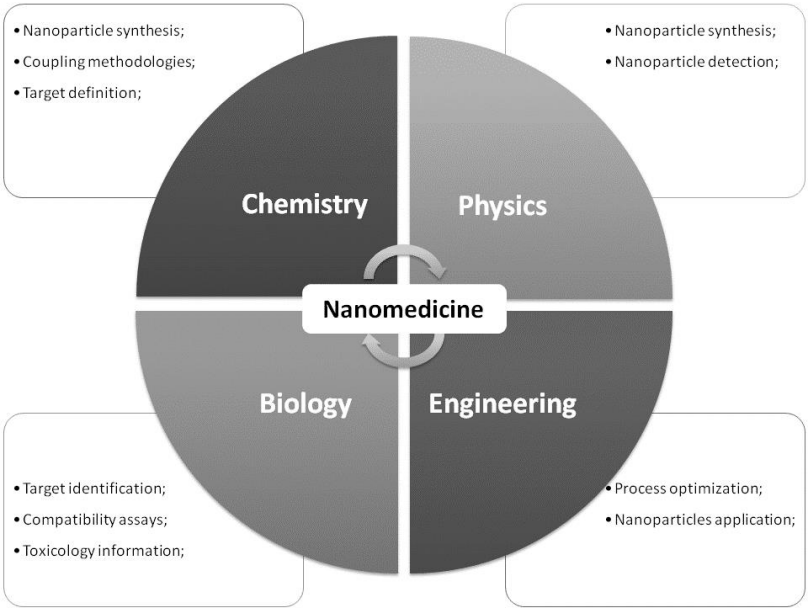

Figure 6.1 – Techno-scientific implications in nanoparticle creation and development.

Correctly define the meaning and the scope of Nanomedicine is indeed a challenge, probably with more complex issues than answers. Nevertheless it could be agreed that is becoming consensual the assumption that could be "*the field with the potential to take benefit from molecular discoveries (genomics and proteomics) and use it to increase the level of quality in medicine care*" [134]. Although this idea was later studied, developed and applied by several authors, there are evidences that Feynman was clearly aware about the potential of nanotechnology in nanomedicine applications, when considering the Nobel Prize physicist visionary talk in 1959 [129]. The reality is showing evidence of it in daily clinical practice and the results are promoting the use of this kind of technology, in a way that the future seems more and more promising [135].

The actual practical application of nanotechnologies comprises most often the use of nanofibers as biomaterials, nanoscale devices used as sensors or nanoparticles as biological mimetics [134]. On the other hand, and even considering it as an application much less recognized or implemented, the use of nanorobotics for surgical purposes is a cutting-edge research field with considerably high potential impact [136, 137].

Nanoparticles are also been widely studied as drug delivery systems, due to its key properties: i) entities with dimensions comprised in the interval 1-100nm; ii) production methodologies with fundamental control of physical and chemical attributes; and iii) ability to be combined to form larger and multi-purpose compounds [138]. This kind of application deserves careful attention due to its potential ability to solve complex problems and to create an array of new high-efficient and reliable technology-based solutions.

Targeted drug delivery systems are designed to deliver a specific drug or medication to a patient, increasing its concentration in some biological tissues relatively to others, relevantly improving its efficacy while reducing side effects [139]. Ideal properties of nanoparticles being destined for drug delivery include composition based on natural or synthetic polymer, reduced cost, non-toxic effects, particle diameter below 100nm, ability to adsorb or carry other compounds (probes or drugs), high retention rates and excellent targeted sustained releases of carried substances, among others [140]. Therefore, nanoparticles presenting the above mentioned characteristics suitable combine to be presented in an appropriate and stable chemical form for administration (parenteral, oral, topical or other considered useful for the specific application) and presenting the desired biological affinity and selective uptake/retention by target cells or tissues could be used to be targeted for almost any biological tissue transporting a specific drug. Giving this, one should also state that significant efforts are being consented to apply several different nanoconjugates to drug delivery.

Recent development of Nanomedicine takes in account the increasing need to use complementary diagnostic or therapeutic technologies, such as Nuclear Medicine methods and techniques. In turn, it raises the need of more sensitive and specific tracers for improved targeting of biological processes. This interaction between nano-based techniques and Nuclear Medicine result in potential applications that can find place in the areas of diagnostics, therapeutics or even modern concepts as theranostics and personalized medicine [141].

In this survey it is aimed to: i) introduce Nuclear Medicine and briefly clarify the role of radiopharmaceutical techniques in modern medicine; ii) systematically review the more recent literature on nanoparticle-based

radiopharmaceuticals; iii) provide a technical overview and discussion about applications of (such) radiopharmaceuticals found; and iv) evaluate future challenges and prospects of its application.
Since most of published data are mainly centered in non-technical aspects of radiolabeled nanoparticles or in a specific application, it is believed that this review can help due to its different approach, since it was conducted via a systematic work of collection, stratification and evaluation of published data, trying to simplify the access to the information.

6.1.2 Metodological aspects of the review

The systematic literature review was made using a cross-search of the keywords "*nanoparticles*" OR "*nanoconjugates*" OR "*nanocompounds*" AND "*radiopharmaceuticals*" OR "r*adionuclides*" OR "r*adiolabeled*", in articles published between 2000 and 2015 in the databases MEDLINE and CINAHL, using the search engine EBSCOhost.
Additional search in the same databases includes articles from related fields such as Nanotechnology, Nanomedicine, Molecular Imaging or Nuclear Medicine, to be included as support for results found in the systematic review.
It were found 142 articles in a first round, with 50 being immediately excluded due to the impossibility to access their full text content. All the remaining articles were pre-analyzed, following a modified version of the PICO question methodology, being classified as "experimental approaches" (45 papers), as "theoretical/review papers" (20 papers) and as "opinion letters" (4 papers), whereas the other remaining 23 articles were excluded of the overall revision work by distinct practical reasons, including language-access related aspects (*e.g.*, papers strictly available on Chinese, Japanese or German) and/or limited correlation with the main subject. The systematic analysis was then finally focused in 69 papers, that were explored specially in what regards to technical aspects involved (fields of application, imaging modalities, radionuclides, nanoparticle properties,…).

6.1.3 Nanoparticle-based radiopharmaceuticals: reviews and robust data

In the last decades a great effort has been spent to develop specific radiolabeled agents to target pathology-associated antigens/receptors/biological mechanisms. Many tools have also been developed and optimized, including the application of monoclonal antibodies (Mabs), from murine Mabs to humanized Mabs. Nevertheless, those tools could not respond to every existing need.
More recently, it has been noticed an increasing trend to develop and test approaches based on liposomes, colloids or other nanoparticle-based compositions. These compositions could be simply globally named as nanoparticles, which are used as vectors to transport and deliver radioactive agents to study specific molecular processes.

The current clinical Nuclear Medicine practice uses a very short number of nanoparticles – or nanocompounds approved as radiopharmaceuticals. It can be pointed, eventually as the most common example, the use of ^{99m}Tc-nanocolloids of albumin for lymphatic sentinel node localization [142].

Considering that the interest of a specific topic of research could most probably be measured via the direct relation with the number and frequency of publications related, this work might serve as a basis to study this tendency.

"Theoretical work" is a preliminary part of the research process but also the way to summarize several experimental findings. Table 6.1 summarizes some of the main findings related with the reviewed articles.

Table 6.1 - Analysis of 20 review papers on nanoparticle-based radiopharmaceuticals found using EBSCOhost.

Author, year [Ref]	Application(s)	Nuclear Medicine Procedures
Cai, 2008 [143]	Oncology (angiogenesis)	PET, SPECT, Radionuclide metabolic therapy
Chen, 2010 [144]	Oncology (several)	PET
Chen, 2014 [145]	Oncology (several)	PET, SPECT, Radionuclide metabolic therapy
Cutler, 2013 [146]	Oncology (several)	PET, Radionuclide metabolic therapy
de Barros, 2012 [147]	Cardiology (several) Oncology (several)	PET, SPECT, Radionuclide metabolic therapy
Ferro-Flores, 2010 [148]	Oncology (peptide receptors)	PET, SPECT
Hamoudeh, 2008 [149]	Oncology (several)	PET, SPECT, Radionuclide metabolic therapy
Hong, 2009 [150]	Oncology (several)	PET, SPECT, Radionuclide metabolic therapy
Jain, 2009 [151]	Oncology (sentinel lymph node)	SPECT
Kannan, 2012 [152]	Oncology (prostate cancer)	Radionuclide metabolic therapy
Larson, 2009 [153]	Oncology (receptors)	PET
Mitra, 2006 [154]	Oncology (several)	PET, SPECT, Radionuclide metabolic therapy
Patel, 2012 [155]	Oncology (several)	PET, SPECT
Phillips, 2009 [156]	New drug research Infection and Inflammation Oncology (several)	PET, SPECT, Radionuclide metabolic therapy
Psimadas, 2012 [157]	Oncology (receptors)	SPECT
Schottelius, 2009 [158]	Oncology (angiogenesis)	PET, SPECT
Silindir, 2012 [159]	Oncology (several)	PET, SPECT
Stockhofe, 2014 [160]	Several	PET
Torchilin, 2007 [161]	Oncology (several)	SPECT
Vanpouille-Box, 2012 [162]	Oncology (several)	Radionuclide metabolic therapy

The simple idea that it is possible to map the distribution of different nanosized compounds in humans and research animals on a whole body basis is motivating researchers to find and/or develop what it is consensually assumed as an excellent tool for developing targeted nanoparticle-based drug delivery agents [156]. In fact, several targeted radiolabeled nanocarriers have been successfully used to detect and treat tumor models. These successes had the tendency to promote further study to design of new nanocarriers based on specific biological properties of pathologies and the increment of the available knowledge led to the development of different radiolabeling strategies - a key-point to their successful application [154].

As mentioned above, radiolabeled nanoparticles should be designed to track specific biological endpoints, and review articles published are rich in the enumeration and compilation of different biomarkers already explored, for example: i) tumor vasculature retention [152]; ii) vascular endothelium growth factor (VEGF) or VEGF receptor and integrin $\alpha_V\beta_3$ expression [143, 158]; iii) somatostatin/bombesin receptors expression [146, 148]; among some others. In fact, this is another demonstration in accordance with some of the most expanding fields of Nuclear Medicine/Molecular Imaging: tumor angiogenesis evaluation [163] and somatostatin receptors expression *in vivo* measurement [164].

Actual global trends in the health field include the benefits of multimodality approaches, and imaging techniques centered in nanoparticle-based radiopharmaceuticals are not an exception. Several advantages could came from the combination of different modalities, mainly due to the complementary role of the applied modalities, whereas some problems could be pointed while attempting to design optimal procedures of combination [165]. In such a context, PET/MRI dedicated scanners are being increasingly considered as key-triggers for the development of new radiotracers and contrast agents. For example, agents that combine functional information of PET including molecular basis and functional and anatomic information, with excellent soft tissue contrast, from MRI are actually being considered as possessing an huge clinical potential and so deserve much and much more consensual interest [165-167]. On other hand, when mentioning multimodality imaging in preclinical environments, molecular imaging, with an approach essentially based on nuclear medicine methods and techniques, is indeed the most established methodology. However the most actual and better practical examples are assuming that not only Radiology conventional techniques (such as CT or MRI) but also ultrasound and optical imaging techniques (that are not yet transposed to clinical approaches) should be seriously considered and included as much as possible, in the adequate moments and levels, directly regarding the previously assumed aims [143].

Still considering analysis of data from review articles published, a simple look at Table 6.1 is illustrative of the dominance of the utilization of radiolabeled nanoparticles in the Oncology field, clearly demonstrated by the focus in 19 of 20 analyzed review papers. The most established specific utilization of radiolabeled nanocompounds is the identification of lymphatic sentinel nodes. This includes radiolabeled sulfur colloids, liposomes, quantum dots, dendrimers and magnetic nanoparticles, which are extensively studied and have been considered as possessing the appropriate characteristics for lymphatic mapping by Nuclear Medicine imaging techniques [151].

Although this dominance, other areas of application, such as Cardiology or Research & Development for drug development, have also been mentioned [147, 156].

Even considering limitations that yet need to be overcome, nanotechnology application in radiopharmacy is not only centered in diagnostic purposes. Its scope of use is extending significantly for oncologic therapy. Despite the possibility to optimize biological tracking of specific targets for therapeutic purposes, nanoparticle-based metabolic radiotherapy combines ionizing radiation and targeted nanodevices providing an unique combination of immunostimulatory properties of nanoparticles with the ability to induce immunogenic tumor cell death by ionizing radiation. This method could result in a probable improvement of patient outcome [162].

Some specific attempts are being made, at different stages of study/development, in the way to apply this concept and its advantageous ability to reduce sizes of tumor prior to surgical resection or to achieve complete ablation without surgery. An example that could be described is the use of radioactive gold nanoparticles, based on β-emitting Arabic Gum – functionalized-^{198}AuNP agent as an innovative approach in cancer therapy, using its high affinity to tumor vasculature and favorable dosimetric onsite considerations. This kind of agents could be delivery by an intratumoral injection with preclinical results indicating optimum therapeutic payloads at the tumor site without associated side effects [152].

The tremendous potential is unequivocal, even considering that dedicated research should always be performed in the future. That research should be mainly centered in topics such as radiolabeled nanoparticles targeting efficacy, robust chemistry for both radionuclide encapsulation/incorporation and targeting ligand conjugation, favorable safety profile, as well as certain specific commercial and regulatory aspects that are essentially related with market penetration (so involved with dissemination/distribution/availability issues) [150].

Indeed, all Nuclear Medicine methods and techniques are being performed via the use of radiolabeled nanoparticles, however an highlight could be given to PET procedures, covered in 15 of 20 review papers analyzed, while SPECT procedures follow directly after, being applied in 14 referred papers. Therapeutic purposes are covered in 10 papers. This rank is demonstrative that therapy is never too far from diagnostic applications, quite often just “waiting” for the right moment/opportunity to be translated into clinical applications benefiting all parts involved.

6.1.4 Nanoparticle-based radiopharmaceuticals: recent experiments and developments

While review papers show interest in a given topic and, at the same time, the existence of consistent and relevant data on the topic, experimental papers illustrate the more recent advances on a specific research topic. In this sense, Table 6.2 summarizes findings related with experimental papers found in this literature survey. Within this topic it is necessary a deeper analysis of research being performed in the field and a look for some insights into the type of experimental study, the kind of nanoparticles applied and into the radionuclide(s) used.

Table 6.2 - Analysis of 45 experimental papers found using EBSCOhost.

Author, year [Ref]	Type of study	Nanoparticle(s)	Diameter (nm)	Radionuclide(s)
Ak, 2012 [168]	*In vitro* *Ex vivo* (rats)	Folate-PEG-doxorubicin	70	^{99m}Tc
Alam, 2012 [169]	*In vitro* *In vivo* (rats)	Thymoquinone-encapsulated chitosan	150-200	^{99m}Tc
Azorín-Vega, 2015 [170]	*In vitro*	Tyr3-octreotate	17-31	^{177}Lu
Chanda, 2010 [171]	*In vivo* (mice)	Gold nanoparticles	12-18	^{198}Au
Chrastina, 2010 [172]	*In vitro* *In vivo* (mice)	Silver nanoparticles	9-16	^{125}I
Dar, 2013 [173]	*In vitro*	Rhenium sulfide	20-220	^{99m}Tc
De Groeve, 2010 [174]	*In vitro* *In vivo* (mice) *Ex vivo*	Nanobodies against dendritic cells	n.a.	^{99m}Tc
Dong, 2008 [175]	*In vivo* (rabbits)	Chromic-phosphor	30-60	^{32}P
Freund, 2012 [176]	*In vitro* *In vivo* (mice)	Iron oxide	4-12	^{59}Fe
Giri, 2011 [177]	*In vitro* *In vivo* (mice)	Hepatitis B antigen surface-absorbed PLGA	174	^{99m}Tc
Hamoudeh, 2008 [178]	*In vitro*	Holmium encapsulated in PLLA	100-1100	^{166}Ho
Helbok, 2010 [179]	*In vitro* *In vivo* (rats)	DTPA-PLP, DTPA-Chol-PLP, DTPA-MIC	20-100	^{68}Ga, ^{99m}Tc, ^{111}In, ^{177}Lu
Hosseini-Salekdeh, 2012 [180]	*In vitro* *In vivo* (mice)	Iron oxide (with folic acid)	5-10	^{67}Ga
Huang, 2011 [181]	*In vitro* *In vivo* (rats) *Ex vivo*	PEGylated nanoliposome	80	^{188}Re
Hwang, 2010 [182]	*In vitro* *In vivo* (mice)	Cobalt-ferrite within silica shell	50-70	^{67}Ga
Hwang, 2012 [183]	*In vitro* *In vivo* (mice) *Ex vivo*	Cobalt-ferrite within silica shell	50-70	^{68}Ga
Janib, 2013 [184]	*In vitro* *In vivo* (mice)	ELP nanoparticles	5-40	^{64}Cu
Kao, 2013 [185]	*In vitro*	Gold nanoparticles	n.a.	^{123}I, ^{131}I
Kitamura, 2012 [186]	*In vivo* (mice)	Phytate	n.a.	^{99m}Tc
Kim, 2012 [187]	*In vitro* *In vivo* (mice)	DEX-P	≈ 100	^{111}In
Lee, 2008 [188]	*In vitro*	Iron oxide (conjugated with RGD)	≈ 45	^{64}Cu

	In vivo (mice)			
Lee, 2012 [189]	*In vitro* *In vivo* (mice) *Ex vivo*	CdSe/ZnS quantum dots	≈ 10	^{68}Ga
Liu, 2009 [190]	*In vitro* *In vivo* (mice)	Biocampatible Iron oxide	33.5	^{125}I
Liu, 2009 [191]	*In vitro* *In vivo* (mice)	3-component streptavidin	n.a.	^{99m}Tc, ^{111}In
Liu, 2011 [192]	*In vitro* *In vivo* (mice)	DOTA-CANF, DOTA-Comb, DOTA-CANF-Comb	n.a.	^{64}Cu
Liu, 2012 [193]	*In vitro* *In vivo* (mice)	Porphysomes (porphyrin-lipid conjugates)	n.a.	^{64}Cu
Locatelli, 2012 [194]	*In vitro* *In vivo* (rats)	PEG conjugated with ceric ammonium nitrate	88-110	^{68}Ga
Luehmann, 2014 [195]	*In vitro* *In vivo* *(mice)*	D-Ala1-peptide-T-amide (PEG	n.a.	^{64}Cu
Madru, 2012 [196]	*In vitro* *In vivo* (rats)	Iron oxide (PEG coating)	≈ 13	^{99m}Tc
Majmudar, 2013 [197]	*In vitro* *In vivo* (mice)	Dextran	≈ 13	^{89}Zr
Nahrendorf, 2011 [198]	*In vivo* (mice) *Ex vivo*	Iron oxide (dextran coating)	n.a.	^{18}F
Nakamura, 2007 [199]	*In vitro* *In vivo* (mice)	Biotinylated DNA-streptavidin-carrier	n.a.	^{99m}Tc
Nikolic, 2009 [200]	*In vitro* *In vivo* (rats)	Fullerene nanocrystals	200-250	^{125}I
Oku, 2011 [201]	*In vivo* (rats)	PEG-lipossomes	100	^{18}F
Ozgur, 2012 [202]	*In vitro* *In vivo* (rats)	BSA	190-210	^{99m}Tc
Patel, 2011 [203]	*In vitro* *In vivo* (mice)	Thiolated chitosan	262-277	^{99m}Tc
Pelizzo, 2007 [204]	*In vivo* (humans)	Albumin nanocolloids	≈ 80	^{99m}Tc
Pérez-Medina, 2014	*In vitro* *In vivo* *(mice)*	PEG-lipossomes	≈ 102-108	^{89}Zr
Polyak, 2013 [205]	*In vitro* *In vivo* (rodents)	Poly-γ-glutamic-acid–folic acid conjugate conjugated with chitosan	75-200	^{99m}Tc
Rossin, 2008 [206]	*In vivo* (mice) *Ex vivo*	NPs coated with IgG (anti ICAM-1)	≈ 180	^{64}Cu
Song, 2011 [207]	*In vitro* *In vivo* (mice) *Ex vivo*	Bis-DOTA-hypericin	n.a.	^{64}Cu

Vosjan, 2012 [208]	*In vitro* *In vivo* (mice)	Nanobodies targeting HGF	n.a.	^{89}Zr
Xie, 2010 [209]	*In vitro* *In vivo* (rats)	Gold nanoshells	130	^{64}Cu
Yilmaz, 2015 [210]	*In vitro* *In vivo (rats)*	Diethylstilbestrol-glucuronide	n.a.	$^{125/131}I$
Zhu, 2013 [211]	*In vitro* *In vivo* (mice)	Glucosamide conjugated with core-cross linked polymeric micelle	≈ 25	^{111}In

Abbreviations: BSA - Bovine Serum Albumin; CANF - C-type atrial natriuretic factor; Chol-PLP - PEGylated cholesterol lipossomes; DEX-P - palmitate ester of dexamethasone; DOTA - tetraazacyclodecane-tetraacetic acid; DTPA - Diethylenetriaminepentaacetic acid; ELP - elastin-like polypeptide; HGF - hepatocyte growth factor; ICAM-1 - intercellular adhesion molecule 1; MIC - PEGylated micelles; n.a.- not available; PEG - polyethylene glycol; PLGA - poly-lactic-co-glycolitic acid; PLLA - poly-L-lactide; PLP - PEGylated liposomes; RGD - Arginylglycylaspartic acid;

A) Focus and design of experimental studies

Experimental studies found were analyzed in order to the procedure(s) cited in each paper (see Figure 6.2), type of study design (see Figure 6.3), radionuclide(s) used (see Figure 6.4) and several other nanoparticle related aspects.

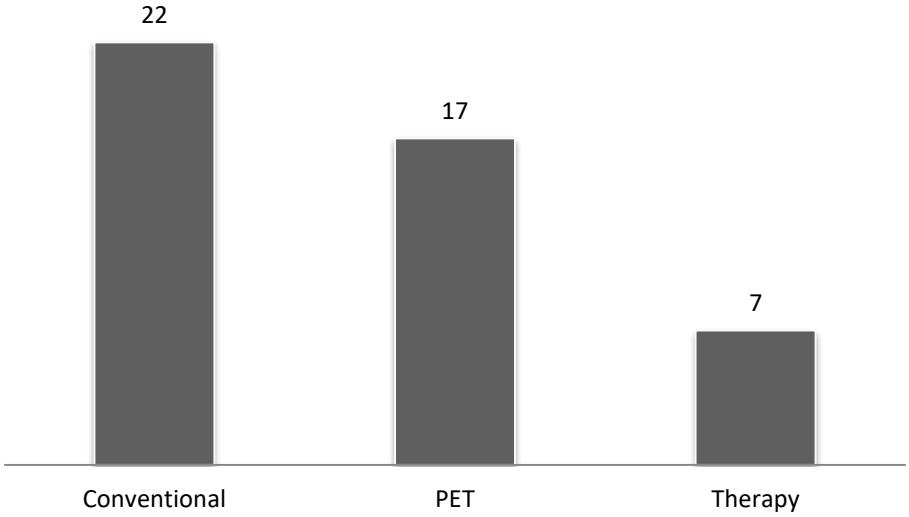

Figure 6.2 - Frequency of Nuclear Medicine procedures adopted in experimental papers analyzed.

Figure 6.2 shows the preponderance of Conventional Nuclear Medicine procedures in recently published research on this field (since used in 22 out of 45 analyzed papers), followed by the important role of procedures included in Positronic Nuclear Medicine (17 papers from the total of 45). Therapeutic procedures continue to be less explored (only 7 out of 45), however they have been referenced in a significant number of papers as future tendency, anyhow predicting a significant growth on this field in a near future.

Figure 6.3 allows to conclude that experimental papers in the field of radiolabeled nanoparticles mainly include the conjugation of *in vitro* with *in vivo* techniques, while, however, the number of clinical studies performed in humans is yet – understandably – very poor (only one paper out of 45), so easily demonstrating the huge potential for research development in what seems to be a near future.

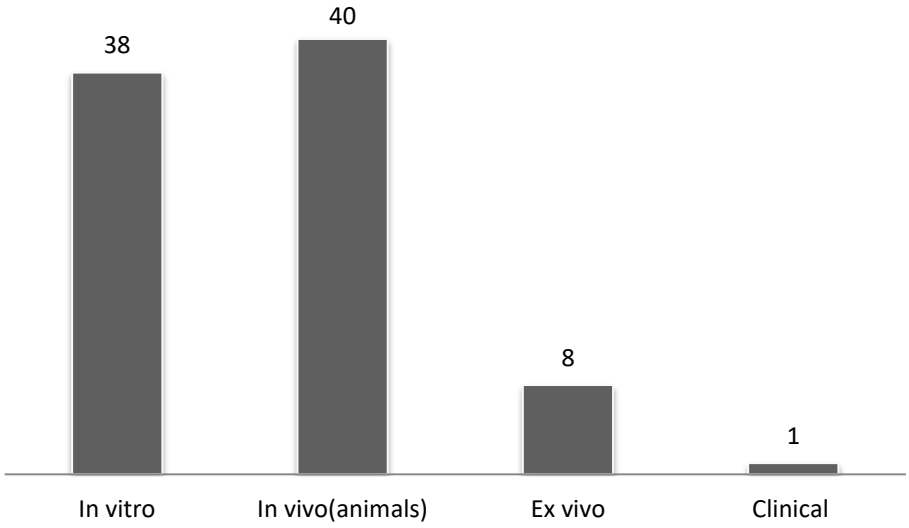

Figure 6.3 - Study design and population used in experimental papers analyzed.

When referring to *in vitro* studies, we have included and analyzed all the studies that comprise laboratory techniques involved in nanoparticle characterization, such as nuclear magnetic resonance spectroscopy, quality control of radiolabeling procedures using appropriated methods as HPLC, cellular distribution studies, with influx and efflux profiles quantification, among other specific laboratory determinations.

In vivo procedures are related with animal biodistribution studies, with preclinical imaging, normally with small animals (mice or rats), either using dedicated imaging equipment or not, while *ex vivo* studies include animal studies performed *post-mortem*, mainly involving autoradiography or activity quantification in extracted organs.

Finally, the unique clinical study was focused in the clarification of the role of nanocolloids for sentinel lymph node detection in thyroid cancer staging. The study presents a new clinical application of an already approved radiopharmaceutical. From this data it seems clear that the global stage of development of this field is yet in the preclinical phase, but can be expected growth over the next years for more complex preclinical studies, as well as through clinical trials.

B) Radionuclides used to label nanoparticles

Figure 6.4 is the graphical representation of radionuclides used in experimental studies analyzed.

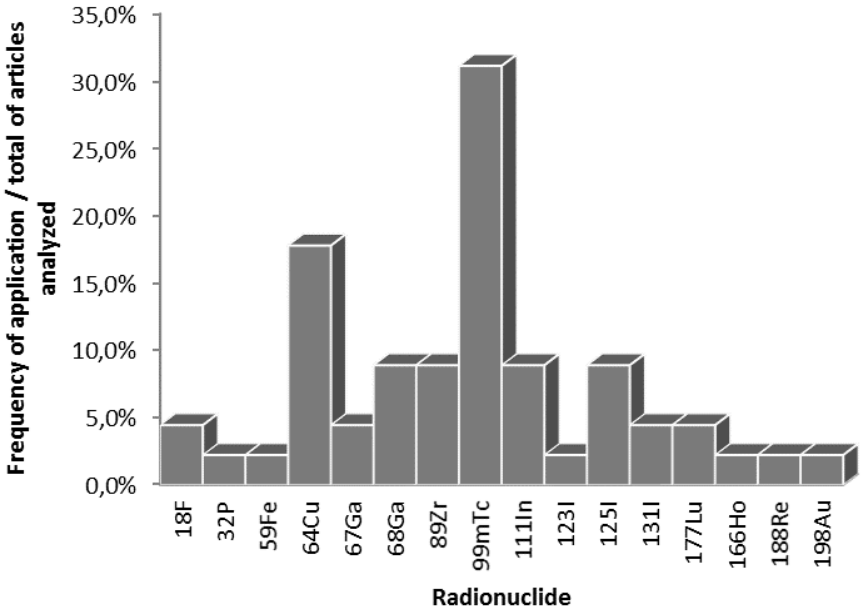

Figure 6.4 - Relative frequency of application for each radionuclide in experimental papers analyzed.

In accordance with results already presented in Figure 6.2, the above presented Figure 6.4 shows that, despite the special case of ^{99m}Tc, radionuclides used in research articles are mainly positron emitters, followed by gamma emitters used in Conventional Nuclear Medicine, and by beta minus and alpha particles for Therapy.

The dominance of use of ^{99m}Tc is unequivocal, expectably based on its availability, low cost, ideal physical properties and acquired knowledge on its inorganic chemistry, representing almost all the applications of Conventional Nuclear Medicine procedures. These characteristics allow its application for a wide range of different situations. Some examples were so simple as radiolabeling of nanocompounds for lymphatic mapping explorations [173, 186, 196, 204], also passing through tumor evaluations with different folate ligands [168, 205]. Radiochemistry using chelator systems is being adopted for ^{99m}Tc labelling procedures, and one of the most interesting advantages is that the same chelator could be used to establish connections with different radiometals (e.g.: ^{111}In or ^{68}Ga), as it was tested in a study conducted by Helbok et al [179]. This radionuclide could also bring advantages like: local availability – it is *in loco* produced with a radionuclide generator); low radiation dosimetry for the subject under evaluation (animal or patient) and the operator (researcher/technologist) involved; and while promoting ideal imaging results – favorable physical decay with high photon flux and ideal gamma energy for the most of the detector systems actually under use.

As Positronic Nuclear Medicine is the second most explored group of Nuclear Medicine procedures, it is without any surprise that positron emitters play an important role in the list of radionuclides used for labeling nanoparticles. The most significant example is ^{64}Cu, which is probably one of the positron emitters with more potential applications, because of its physicochemical properties that also allow/promises theranostics applications. The exploration of the use of microPET imaging to track protein polymer nanoparticles over several days, using ^{64}Cu radiolabeling,

revealed that there is a molecular weight dependence of the pharmacokinetic profile of labeled compounds, but confirms its suitability for theranostics applications [184]. Other potential applications have being explored as well, all of them belonging to the field of Oncology, but so intrinsically distinct as targeting lung endothelium [206], monitoring thermal therapy cell damage [207, 209] or image prostate cancer models [193].

Another generic aspect that could be presented is the fact that almost the totally of radionuclides used belong to the group of metallic radionuclides (including ^{99m}Tc, ^{64}Cu, $^{67/68}$Ga, ^{111}In, among others…), probably due to the difficulties inherent in the labeling of complex structures, such as metallic nanoparticles, with organic elements. Therefore inorganic chemistry using chelation of macromolecules appears to be the most applied strategy to label nanoparticles with these radionuclides.

In fact, nanoparticle radiolabeling is an important issue to be considered. There can be applied many different approaches depending on available resources, radionuclide desired and other technical requirements asked, *e.g.*, total and specific activity constraints, type of nanoparticle or kind of application to be implemented after radiolabeling. As a matter of fact, this issue doesn't seem well established and further studies might be implemented. However, approaches based on accelerated particles direct activation, synthesis from radioactive precursors or chemical incorporation/coupling methodologies could be mentioned [212].

The frequency of application of organic positron emitters is much reduced, considering the low rate of application of ^{18}F and the inexistence (yet) of any application using ^{11}C, ^{13}N or ^{15}O. Even considering the limitations of these organic agents, ^{18}F-radiolabeled nanoparticles were already reported for the detection of aortic aneurisms by macrophage tracking [198] or imaging of brain cancer [201].

As mentioned before, the therapeutic applications are each day more important. Different particle-emitting radionuclides such as ^{32}P, ^{166}Ho, ^{177}Lu and ^{198}Au are being studied for several different treatment applications, as examples like prostate cancer [171], lymph node metastasis [175], gliomas [181] or intratumoral radiotherapy approaches [178].

C) Other technical considerations

A careful examination of Table 6.2 gives also the opportunity to state that some published articles do not specify correctly all the physicochemical properties of radiolabeled nanoparticles developed and studied, with a significant preponderance with the absence of reference to its size. This constitutes not only a limitation on this data collection, but as well a limitation of the available data. Indeed, it is dramatic when noticing, even in articles where the measured size is specified, that there is a clear discrepancy between methods and the identification of the situation when the determination was made, *i.e.*, laboratory techniques used, determination before *versus* determination after radiolabeling, *etc*. These generates the suspicion that the values referred might not deserve the adequate level of confidence, and are not suitable, as it could be desirable for comparison between distinct studies.

Keeping in mind that some nanoparticle-related aspects were not fully described and characterized in each paper, it was tried to look for information available. Metal-based nanoparticles appear as the most used, either based on

iron oxides [176, 180, 188, 190, 196, 198], on gold [171, 185, 209] or even on silver [172]. This seems reasonable and almost predictable, since metallic nanoparticles have some characteristics that play an important role when designing their applications, such as: i) large surface-area-to-volume ratio compared to bulk materials; ii) large surface energies, increased number of kinks; and iii) a large number of low-coordination sites such as corners and edges, that consequently gives specific chemical properties and the ability to store excess electrons. This last aspect is a very useful characteristic when forming stable radiolabeled complexes is intended.

In fact, it should be emphasized that metal oxide nanoparticles can exhibit unique physical and chemical properties, some of them are shown at all bulk materials from the same origin. In this way, in order to achieve this and display mechanical and/or structural stability, special attention should be paid to some parameters that are intrinsically correlated such as size, chemical structure and surface energy. Examples of complexes that have these properties and are being named in the literature are FeO_x, TiO_2, VO_x, Al_2O_3 or MoO_x oxides. These examples could include labeled derivatives, considering possible direct labeling with radioactive precursors included in its synthesis (where special interest should be paid to ^{45}Ti radiolabeling of TiO_2 nanoparticles - already mentioned several occasions, but still without any solid approach developed in this moment).

Specifically in this context, it has been already pointed that iron oxide nanoparticles (FeO_x) are being consistently studied. Despite their interesting nanostructure characteristics (associated to the achievable proper surface architecture, size and stability), iron oxide complexes have also magnetic properties that enhance Magnetic Resonance contrast.

Small particles of iron oxide (SPIO) and ultra-small particles of iron oxide (USPIO) have recently received intensive investigations: SPIO or USPIO typically consist of two components, an iron oxide core and a hydrophilic coating, ranging from 2 to 3 nm for citrate inhibited growth SPIO, tens of nanometers for polymer-coated polycrystalline iron oxide nanoparticles through to micrometers for orally ingestible contrast agents, with their magnetic properties being the result of aligned unpaired electron spins [213]. Together, these magnetic properties and appropriate radiolabeling, gave to SPIO and USPIO nanoparticles the ability to act as dual probes for PET/MRI imaging [188, 190, 196].

Other radiolabeled nanoparticles resort to polymeric coatings with PEG (Polyethylene glycol), for example [168, 181, 194, 201].

To conclude, most of the existent literature is concentrated in the time period between 2008 and 2014. Another interesting aspect is that it was not possible to find any article published before 2006 and that the maximum publication frequency was found in 2012, with 27.5 % of all analyzed articles, representing 19 papers published at that date (Figure 6). An overall analysis, conjugated with the fact that most of the excluded articles were published between 2013 and 2015, shows a general increasing trend in the yearly frequency of publication in the field.

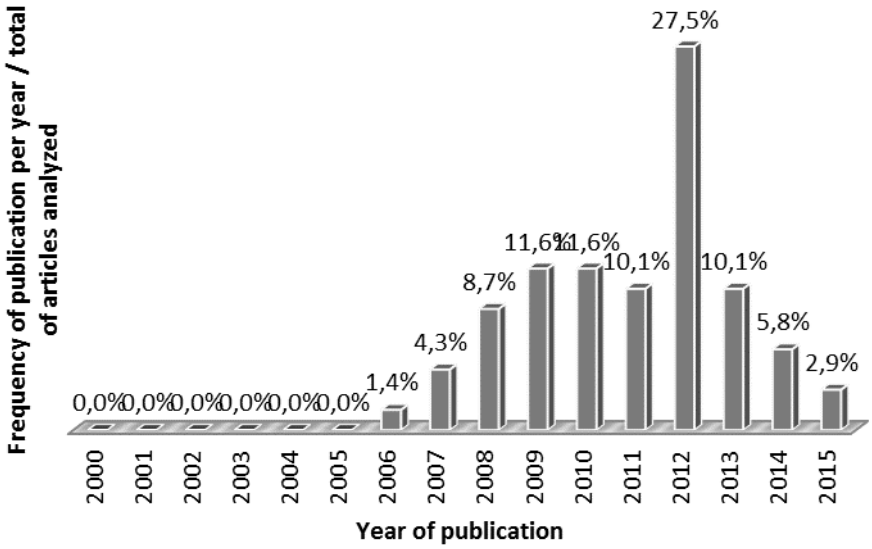

Figure 6.5 - Relative frequency of articles analyzed per year of publication.

Limitations to this paper data collection could be summarized in what relates to the search criteria, to the process of keyword designation by the authors of published data searched, compiled and analyzed.

Finally, the chosen analysis criteria, that do not followed PICO question (just because it would not fully cover the technical requirements selected for this survey) and suffered an adaptation to fit the previously stablished goals, being mainly focused on Nuclear Medicine specific technical parameters.

6.1.5 Final remarks and future perspectives

Nuclear Medicine methods and related technologies are indeed crucial tools when modern medicine, biological research, innovation and development processes are concerned. As a specific and autonomous specialty, Nuclear Medicine is benefiting, since its origin, from discoveries and inventions in all the multiple technological fields that are related. As it could be expected, nanotechnologies, and specially biologically targeted nanoparticles, might be considered as some of the most notable and yet promising achievements of modern science, with an high potential to play a key role concerning clinically personalized applications.

Actually, different groups are actively working in the production, development, characterization and implementation of biologically targeted nanoparticles. Considerable efforts are focused on its radiolabeling for direct involvement in Nuclear Medicine procedures.

It could be relevant to note that this field is actually in a clear development stage, mainly focused on the preclinical phase of evolution, with a considerable number of *in vitro* and animal *in vivo* studies under execution or already performed.

The present work summarizes some findings obtained with the review of existing literature, seeming possible to conclude the actual predominance of Oncology-tailored applications, either using Conventional Nuclear Medicine or PET, with few reports on therapeutic procedures, even considering its expectable growth in the near future. ^{99m}Tc-labeled nanocompounds dominate our findings, but several appointments were also found, concerning the use of radionuclides like ^{64}Cu, ^{68}Ga or ^{111}In.

Apart from other specific examples, radiolabeled metallic nanoparticles should be emphasized, essentially because of their interesting chemical and physical properties that include practical production processes, target affinity and ability to act as multimodality probes, with a special note and attention for the suitability of their application in PET/MR imaging.

In the near future it seems expectable that techno-scientific work on nanoparticle-based radiopharmaceuticals would be focused on topics such as nanoparticle synthesis optimization and radiolabeling procedures, but also on the continuation of preclinical studies yet under development as well as the implementation of new studies, each time more refined and directed, paving the way and creating the fundamental evidences necessary to sustain the decision for beginning the indispensable clinical studies that will always precede the wider use at clinical level, so finally directly benefiting huge populations of patients.

6.2 Nanoparticle-based radiopharmaceuticals: is there a future to $^{45}TiO_2$ nanoparticles?

Having in consideration the conclusions extracted from the systematic review on the use of radiolabeled nanoparticles presented before, it must be noted that the role this kind of approaches is gaining importance and relevance in the context of modern personalized medicine. There is no doubt about the potential interest of the study and possible utilization of radiolabeled nanoparticles in Nuclear Medicine procedures.

Even considering that there is no notice of labeling nanoparticles with ^{45}Ti, but paying attention to the fact that metallic nanoparticles and metal radionuclides, especially for PET imaging, are on the top of use in actual research studies, it seems very promising and consistent the possibility of using ^{45}Ti to radiolabel nanoparticles.

In such a context, although chelation inorganic chemistry allows the coupling of a radionuclide to a desired nanoparticle made of other chemical elements, the first direction to try should be the direct use of ^{45}Ti to radiolabel titanium nanoparticles. To support the applicability of this idea it will be introduced the enumeration of the properties and possible applications of titanium nanoparticles that will be then followed by the proposal of the challenge to radiolabel these nanoparticles.

Actually, the need to develop modern tools to fight against cancer or viral infections, based on the several limitations appointed to conventional methods in use, is directing scientists to the study of the use of interesting chemical and biological properties of titanium. Thus, nano-sized titanium dioxide represents a promising research subject for various modern fields of science and technology that focus studies on the use of TiO_2 nanoparticles aimed at curing cancer and viral or genetic diseases [214].

A problem that could arise and prevent the use of a given nanoparticle (with or without appropriate radiolabeling) is its reliable production methodology. In what directly refers to titanium nanoparticles, recent studies demonstrated that the problem of synthesizing stable forms of titanium dioxide nanoparticle is being successfully solved [214, 215]. Thus, titanium nanoparticles production and stabilization are being studied in a proper manner that in the future a given biological application that could be designed and studied will not be prevented by the production methodology.

On the other hand, the delivery of nanoparticles to human cells, an aspect that is also named as biodistribution, is also fundamental. A clinical application of these nanoparticles forces to avoid any induced chemical or biological transformation on the non-pathological cells. In this particular case, recent data suggest that TiO_2 nanoparticles have the ability to enter eukaryotic cells and stay retained in the cell, even considering that the specific mechanism of diffusion is not yet totally understood [216]. Then, when inside certain groups of cells, UV-stimulated titanium nanoparticles have shown antitumor activity, namely the capacity to inhibit proliferation cell lines, inhibit platelet's aggregation and stops at a certain level the expression of 2,3-lipoxygenase reaction, while they did not provided any toxic effect when applied to a normal fibroblast cell line ("healthy" cell lines) [217]. Deeper investigations on the molecular mechanisms involved in titanium nanoparticles antitumor activity indicate that these nanoparticles enhance reactive oxygen species generation, activate caspase-3 and induce oxidative stress, leading to DNA double strand breaks, as well as chromatin condensation, nuclear fragmentation and apoptosis [218]. In the same context, recent data is also suggesting that functionalized TiO_2 nanoparticles can be surface-engineered for targeted cancer therapy as direct photo-sensitizing agents to be delivered to eliminate cancer cells [219]. Finally, and still on the context of cancer treatment, these nanoparticles had also been applied as drug delivery systems for drugs such as doxorubicin and paclitaxel [219-221].

The modern trend of the use of radiolabeled nanoparticles results of the review previously presented, and it supports the potential to radiolabel ^{45}Ti-nanoparticles (read nanoparticles as titanium dioxide nanoparticles, but include also other possible chemical forms). In short, titanium (di)oxide nanoparticles are being studied for cancer therapy enhancement by its direct antitumor activity, as an adjuvant phototherapeutic agent and as a drug delivery system. A study conducted by Smith, et al. [222] point into some evidence of the titanium nanoparticles role as a CT imaging contrast.

According to all evidences already tested and conjugated with the theoretical and prospective vision here presented, the radiolabeling of these nanoparticle agents could constitute a tool to provide *in vitro* biodistribution studies (using radionuclide *in vitro* studies), allowing also the *in vivo* monitoring of its biological distribution and pharmacokinetics, using PET imaging or even contrast-enhanced hybrid PET/CT imaging. Thus, one could suggest titanium nanoparticles as a potential powerful theranostic agent for the validation of research studies already under development and aimed to improve the efficacy of clinical diagnosis and therapy mainly in oncological field.

6.3 ^{45}Ti-labeled compounds for use in PET imaging

This last sub-chapter includes an overview on the possible compounds that could be labeled with ^{45}Ti for use on preclinical or clinical PET imaging.

The first known mention of a potential application of ^{45}Ti belongs to a Japanese team of scientists in 1981 and was published by the *Cyclotron and Radionuclide Center* (CYRIC), from the Tokohu University [109]. At that time, the group evaluated simultaneously the production, target chemistry (extraction and purification of ^{45}Ti), radiochemistry (labeling) and animal experiments. The main conclusion was centered on the potential of ^{45}Ti-compounds to become "*as a new series of the positron emitting radiopharmaceutical*", even considering some problems related with the stability of $^{45}TiCl_4$ [109]. Examples of ^{45}Ti-phytate and ^{45}Ti-DTPA images are shown in Figure 6.6.

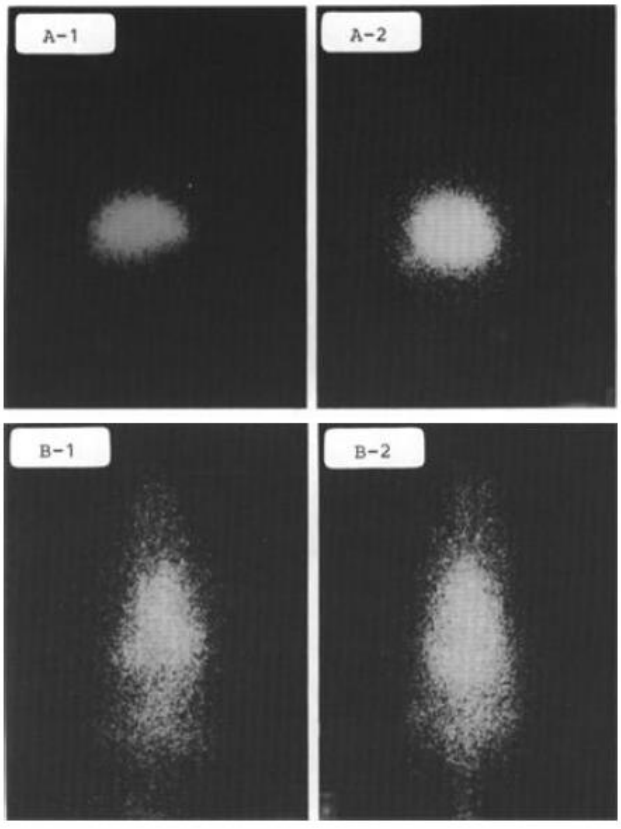

Figure 6.6 – Whole body images of ^{45}Ti-phytate (A) and ^{45}Ti-DTPA (B) acquired 10 mins (A1 and B1) and 60 mins (A2 and B2) after injection in rats.

Source: K. Ishiwata, T. Ido, M. Monma, M. Murakami, H. Fukuda, K. Yamada, S. Endo, H. Yoshioka, T. Sato, and T. Matsuzawa, "Preparation and Medical Application of ^{45}Ti," *CYRIC Annual Report,* 1981.

Some years later, the same group reported the potential of some ^{45}Ti-labeled compounds publishing an article indicating $^{45}TiOCl_2$ or ^{45}TiO-phytate as potential colloid agents for the imaging of the reticuloendothelial system. They also appointed ^{45}Ti-DTPA, ^{45}Ti-citrate and ^{45}Ti-HSA (human serum albumin) as possible agents for estimating blood volume and indicators of the breakdown of the blood-brain barrier [223].

Considering the beginning of the study on the pathway of the titanium-based anticancer drugs (such as budotitane) incorporation, ^{45}Ti-budotitane was prepared and incorporated into liposomes to provide optimal tumor targeting [224]. In the continuation of this work, it was not found any biodistribution or imaging study using this compound.

After a gap on the study of ^{45}Ti-labeled compounds, Vavere, et al. [38] studied the potential of this radionuclide as a candidate for PET imaging. Despite other considerations reported about the cyclotron production and purification of ^{45}Ti (already discussed on this Thesis), the work reported a clear spatial resolution observed down to a rod diameter of 1.25 mm using a Derenzo phantom, comparable to the resolution obtained with ^{18}F, only with a slight degradation due to the higher energy, and consequently range, of ^{45}Ti positrons (see Figure 6.7) [38].

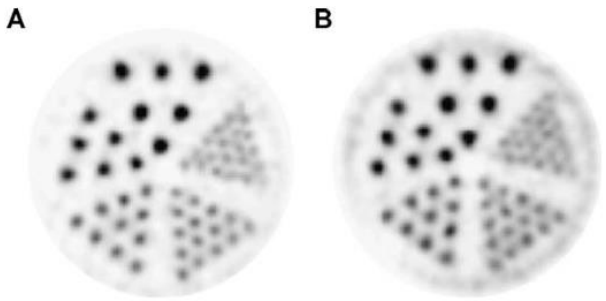

Figure 6.7 – Comparison of image quality of ^{18}F (A) and ^{45}Ti (B) using a Derenzo phantom.

Source: A. L. Vavere, R. Laforest, and M. J. Welch, "Production, processing and small animal PET imaging of titanium-45," *Nucl Med. Biol,* vol. 32,

Another study of Vavere and Welch [225] produced ^{45}Ti and used small animal imaging with ^{45}Ti-transferrin in the way to provide new insights about the mechanism of action of a new class of cytostatic agents based on titanium complexes. In this study, it was performed direct labeling of apotransferrin *in situ* with ^{45}Ti and biodistribution studies. MicroPET images provide evidences on the increased uptake of ^{45}Ti-transferrin in tumors, with retention up to 24 hours, demonstrating that titanium radiopharmaceuticals could be explored as a new tool for *in vivo* imaging of tumors [38]. This data also supports the role of ^{45}Ti-labeled compounds in theranostics and personalized medicine, having in account the ability to select patients for a specific type of treatment.

Price, et al. [226] published a work pointing in this direction, reporting that they studied the use of ^{45}Ti-transferrin but encountered some problems regarding the purification of the radionuclide to be used in the radiolabeling process. It was reported a loss of 53% of the ^{45}Ti activity to the waste fractions during the separation process. However, this seems to be a problem with this particular experiment because, appart from the ones already cited, other authors have achieved in the past good radiochemical yields in the labeling of proteins such as transferrin or Df-antibody [227].

Considering the success that is being achieved in the reappearance of titanium-based drugs to treat cancer, due to the development of several chemical steps needed to stabilize this new titanium-based antineoplastics, in which the ligand salan plays a major role, it is being observed a significant investment in the development of this new

class of drugs [228, 229]. However, it is also known that this phase of drug development represents a highly complex, inefficient and costly process that takes huge amounts of time and money. In this context, Nuclear Imaging can play a determinant role in improving the efficiency of the selection of candidate drugs that should either be abandoned or moved forward into clinical trials [230]. Therefore, conjugating the need for information about drug biodistribution and pharmacokinetics, and the added value of Nuclear Medicine in the drug development process, emerges another idea presented in this work: the case of titanium-based drugs investigation could be enhanced by the use of ^{45}Ti-labeling of the compounds of interest. And, in fact, this conceptual idea is not totally original because recent data already published shows the use of ^{45}Ti-salan compounds as translational tools to help the passage from fundamental research to clinical application of these drugs (example in Figure 6.8) [231].

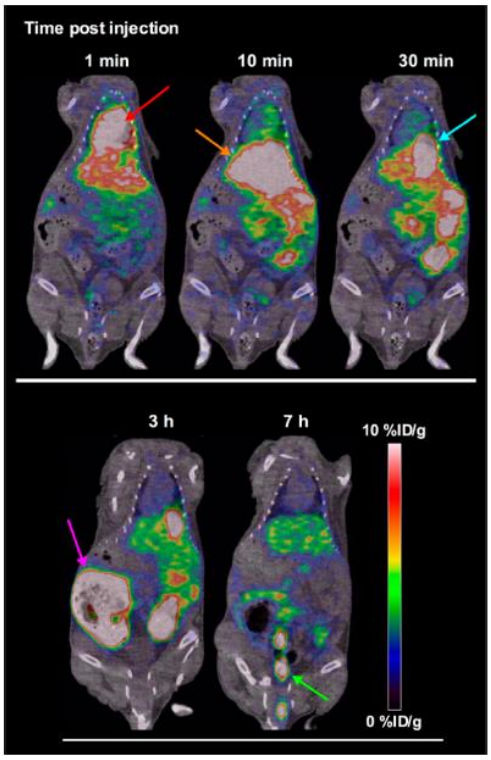

Figure 6.8 – Example of acquired PET/CT images of a ^{45}Ti-compound in mice.

Source: G. W. Severin, C. H. Nielsen, A. I. Jensen, J. Fonslet, A. Kjær, and F. Zhuravlev, "Bringing Radiotracing to Titanium-Based Antineoplastics: Solid Phase Radiosynthesis, PET and ex Vivo Evaluation of Antitumor Agent [45Ti](salan)Ti(dipic)," *Journal of Medicinal Chemistry,* vol. 58, pp. 7591-7595, 2015.

The concept can be taken further, and hypothesize that ^{45}Ti-compounds could be used as diagnostic imaging agents of the same cancers that could be hereafter treated with titanium-based drugs. Again suggesting the role of ^{45}Ti in theranostics and personalized medicine.

As a final note, the literature review made about this topic found only one non-oncological application of ^{45}Ti-cations for the investigation of cerebral neurodegeneration [232].

6.4 Final considerations on potential applications of ^{45}Ti

After the description of data found on all the applications of ^{45}Ti already tested for PET imaging purposes, among other hypothesis here presented that were not yet experimentally tested, it is possible to extract some key notes as:

- ✓ ^{45}Ti could provide good PET image quality;
- ✓ Applications of ^{45}Ti-compounds already tested are closely related to studies on a new class of anticancer drugs based on titanium complexes;
- ✓ ^{45}Ti-ligands could add significant preclinical and clinical data for the ongoing investigations for drug approval;
- ✓ ^{45}Ti-ligands seem to have the ability to be studied as potential theranostic agents for personalized medicine;
- ✓ The same methodologies applied to the improvement of titanium-based drugs stability and chemistry should be used to develop stable and useful ^{45}Ti-radiopharmaceuticals;
- ✓ Considering the applicability of titanium dioxide nanoparticles in cancer, ^{45}Ti could be used to radiolabel these nanoparticles, either for its validation as candidate drugs and for its use as *in vivo* diagnostic tools;

7. Final remarks

7.1 Research summary and general discussion

The research work here presented was focused on the fundamental study, development and optimization of the production process of ^{45}Ti in low energy cyclotrons. The first task of the doctoral research project was the identification of the appropriate nuclear reactions allowing useful routes for ^{45}Ti production. Then it was all the planning needed to perform the controlled nuclear activation experiment and the analysis of the results. To conclude it, the thesis provides some theoretical insights about possible applications of this radionuclide on PET imaging for biomedical applications.

In **Chapter 1** it were introduced some basic ideas and fundamental concepts in the scientific fields involved on this doctoral project, mainly in Radiation Physics and its application in medical scenarios such as Medical Imaging. This chapter reviews radionuclides used in PET, demonstrating that although the variety of radionuclides already known, routine clinical applications of PET continue to be based on only a few radionuclides (^{11}C, ^{13}N, ^{15}O, ^{18}F, ^{68}Ga). However, it has been evidenced that this trend is changing, and that in the near future new solutions could come to play and take a role in clinical PET studies. This later point is the starting premise of this project - the need of new radionuclides with different properties to PET field. The identification of those radionuclides is not enough, there is also a need to study and develop optimized production processes.

An overview on the actual state of the worldwide production of radionuclides was presented in **Chapter 2**, with an emphasis on the description of the scientific knowledge needed to understand the associated processes, namely nuclear reaction physics and principles underlying one of the major methods of radionuclide production – cyclotrons. In fact, cyclotrons provide the ability to induce nuclear reactions using protons as projectiles. Although nothing new and or innovative was presented in this section, the idea was to stablish the fundamental knowledge of nuclear physics through its application for industrial purposes such as commercial radionuclide production. Together with Chapter 1, it constitutes what could be called the theoretical introduction of the thesis.

As demonstrated before, the execution of nuclear activation studies deserve special attention and a careful integration of all the available information already collected. Given this, Monte Carlo simulation methods are presented as a very interesting way to perform preliminary studies about nuclear reactions and to plan an activation study – as it could be seen in **Chapter 3**. This chapter includes some theory about this simulation methods, but also its practical application on the problem here considered. The results of the calculation were totally integrated in the design of experimental studies performed in the project, and carefully described on the thesis.

Before running the activation experiments emerged the need to understand properly how to monitor and collect the data using gamma spectroscopy. **Chapter 4** is the reflex of its importance, reason why it deserved a special description. For a better characterization and a deeper understanding of the technique, some preliminary experimental studies were performed with calibrated radionuclide sources as demonstration of the general ability

of the technique, and also to have quantitative information about the physical phenomena such as radioactive decay and radiation interaction with matter.

Chapter 5 should be seen as the principal section of the work. It presents the experimental results obtained in the activation studies performed. Here it is shown that the production of ^{45}Ti in low energy cyclotrons is possible and viable, achieving the major aim of this doctoral program. Among other preliminary hypothesis, ^{45}Sc(p,n)^{45}Ti nuclear reaction was selected due its potential and interest. Experimental results demonstrated its feasibility in low energy cyclotrons, with maximum cross-section values determined in the range between 10 and 14 MeV proton beam energies. Significant interference with concurrent reactions was found for energies higher than 16.8 MeV, where concomitant production of ^{44}Ti, ^{44m}Sc and ^{44}Sc occurs. For the development of a routine production process, there is still the need to develop a prototype of target. And the next steps imply the development of ideas already briefly studied. It was already performed a theoretical review of the available methodologies for the deposition of ^{45}Sc on the substrate of the target (planned to be in aluminum), resulting in the selection of electrodeposition as the methodology of choice and to be experimentally studied. A simpler design of the target could include the deposition of around 642 μm of pure ^{45}Sc for a complete beam energy degradation from 15 to 10 MeV (based on personal SRIM calculations). However, some modifications in the irradiation protocol could result in the positioning of the target with some tilt (*e.g.*, 3˚ to 6˚) and the consequent modification on the target thickness. Other possibility to be tested is the inclusion of a standardized thin foil of pure ^{45}Sc as the target supported on a massive aluminum holder. These hypothesis would be evaluated considering different requisites, namely: technical easiness, overall costs and quality of the obtained target.

Chapter 6 illustrates potential applications of ^{45}Ti, including some already proposed and briefly studied by other groups (preclinical imaging with ^{45}Ti-transferrin to study Titanium-based chemotherapy agents, and preclinical imaging with ^{45}Ti-salan compounds). A systematic review about nanoparticle-based radiopharmaceuticals was presented in a dedicated section (6.1) in the way to provide basis for the innovative proposal about the use of $^{45}TiO_2$ nanoparticles (6.2). The sub-chapter 6.3 includes an overview on the possible compounds that could be labeled with ^{45}Ti for use on PET imaging.

As a concluding remark it is also possible to evaluate some limitations that partially compromised the overall quality of the research project. Naturally, some of them belong to practical and operational issues that could be solved or avoided in the future, and some others are intrinsic limitations based on the physical phenomena under study.

Thus, as major points of limitations it should be mentioned:

- Incomplete development of the *Gamma Spectra Analyzer* and inability to prove its usefulness with a practical demonstration on this specific context;
- Reduced number of experimental activation studies, due to limited material resources available;
- High level of uncertainties involved in the obtained results, due to the calibration and operation of the HPGe detector and also to some intrinsic physical properties of ^{45}Ti (0.154% relative abundance of the main photopeak);

- Inability to obtain activation information for the maximum proton beam energy (18 MeV), due to saturation of HPGe detector and to the intrinsic properties of the radionuclides involved (similar half-lives, high-level of activation via concurrent nuclear reactions,…);
- Lack of incorporation of the results obtained in the nuclear activation studies in the design of a prototype of target to be used and tested for ^{45}Ti production;

7.2 Conclusion and future perspectives

Over the last decades, significant efforts have been made in the fundamental study, test, development and optimization of radionuclide production processes. Such achievements have benefited the field of Medical Imaging, and particularly, radionuclide imaging using Nuclear Medicine methods and techniques.

Among the different branches of Nuclear Medicine, Positron Emission Tomography (PET) field presents some advantages that could be used in accordance with the most actual paradigms of Medicine, in such a way that personalized medical care could be conducted to patients in a truly modern approach.

Thus, the thesis focused on the exploration of a possible candidate to be used in PET imaging – ^{45}Ti – emphasizing the importance of the radionuclide availability issue as a crucial step for the future development of its real applications. Thus, appropriate routes for production of ^{45}Ti in low energy cyclotrons have been studied and evaluated.

Simulation codes allow the user to obtain a generic perspective of the excitation functions of selected reactions under study, extracting relevant information and supporting the planning of a stacked foil experiment to prevent technical errors. Specifically in this project, TALYS code allowed a generic overview of excitation functions for the most relevant nuclear reactions, while SRIM code allowed the study of beam energy degradation, and the SSSM sub-routine was used for the optimized simulation of the implantation of a realistic beam into the target.

In the other hand, and considering experimental techniques applied, gamma-ray spectroscopy based on an HPGe detector allowed the characterization of complex radioactive samples such as activated foils from a stacked foil experiment. Results obtained using HPGe-based gamma-ray spectroscopy also allowed the understanding of the impact of the efficiency calibration procedure. The importance of some technical sources of error was analyzed and correction factors to account for attenuation and geometric issues were determined and applied.

The experimental results of the stacked foil method experiment allowed a simpler and reliable experimental study of nuclear reaction excitation functions. Beam energy procedure was deeply analyzed and three different methods were compared. The independent method based on the differential ratio of ^{63}Zn activity induced on copper monitor foils revealed to be useful and provide acceptable results. However, all the methods tested demonstrate some problems in the calibration of low energies, emphasizing the need to improve technical protocols for cyclotron beam energy calibration.

Obtained results demonstrated that ^{45}Sc(p,n)^{45}Ti nuclear reaction is feasible in low energy (medical) cyclotrons and that cross-section values present a peak for proton beam energies in the range between 10 and 15 MeV.

Experimental results now obtained are comparable with other published data. Thick target yield for a saturation condition was experimentally determined as 433.64 MBq.μA^{-1}sat, confirming that ^{45}Ti could be effectively produced for medical applications using low energy cyclotrons. In the systematization of a routine production process, energies higher than 17 MeV should be avoided due to the increased production of contaminants such as ^{44}Ti, ^{44}Sc and ^{44m}Sc.

In the near future, it is aimed to develop a prototype for a target based on ^{45}Sc and to incorporate these findings in order to have a fully standardized process of target irradiation, before starting the studies for extraction and purification issues.

Considering the results already obtained, and in an overall conclusion, it is possible to state that there is the possibility to effectively obtain significant quantities of ^{45}Ti allowing its possible commercial/industrial production, distribution and use. This new radionuclide presents the comparative advantage to enhance the range of distribution and use relatively to the production center. Furthermore ^{45}Ti could then provide good PET images and be used for labeling different compounds already tested or to be incorporated in the development of nanoparticle-based radiopharmaceuticals.

8. References

[1] R. Acharya, R. Wasserman, J. Stevens, and C. Hinojosa, "Biomedical imaging modalities: a tutorial," *Comput Med Imaging Graph,* vol. 19, pp. 3-25, Jan-Feb 1995.

[2] L. Fass, "Imaging and cancer: a review," *Mol Oncol,* vol. 2, pp. 115-52, Aug 2008.

[3] S. R. Cherry, "Multimodality in vivo imaging systems: twice the power or double the trouble?," *Annu Rev Biomed Eng,* vol. 8, pp. 35-62, 2006.

[4] H. Zaidi and B. H. Hasegawa, "Overview of Nuclear Medical Imaging: Physics and Instrumentation," in *Quantitative Analysis in Nuclear Medicine Imaging*, H. Zaidi, Ed., ed: Springer, 2006, pp. 1-35.

[5] World Health Organization, "Technical Report Series no 492," ed. Geneva: World Health Organization, 1972, pp. 34-50.

[6] U. Haberkorn and M. Eisenhut, "Molecular imaging and therapy -- a programme based on the development of new biomolecules," *Eur J Nucl Med Mol Imaging,* vol. 32, pp. 1354-9, Dec 2005.

[7] Society of Nuclear Medicine. (14/07/2015). *Important Moments in the History of Nuclear Medicine*. Available: http://interactive.snm.org/index.cfm?PageID=1107

[8] D. Delbeke and G. M. Segall, "Status of and trends in nuclear medicine in the United States," *J Nucl Med,* vol. 52 Suppl 2, pp. 24S-8S, Dec 2011.

[9] Dose Data Med 2. (2014, 15-07-2015). *Dose Datamed 2 Project: Study on European Population Doses From Medical Exposure*. Available: http://ddmed.eu/_media/news:ddm2_project_report_population_dose_estimation_final_draft_for_web_page_28_jan_2013.pdf

[10] R. A. de Kemp, F. H. Epstein, C. Catana, B. M. Tsui, and E. L. Ritman, "Small-animal molecular imaging methods," *J Nucl Med,* vol. 51 Suppl 1, pp. 18S-32S, May 1 2010.

[11] R. A. Frank, B. Langstrom, G. Antoni, M. C. Montalto, E. D. Agdeppa, M. Mendizabal, I. A. Wilson, and J.-L. Vanderheyden, "The imaging continuum: bench to biomarkers to diagnostics," *Journal of Labelled Compounds and Radiopharmaceuticals,* vol. 50, pp. 746-769, 2007.

[12] S. M. Moriguchi, K. t. H. Koga, P. H. A. Togni, and M. J. d. Santos, "Clinical Applications of Nuclear Medicine," in *Medical Imaging in Clinical Practice*, O. F. Erondu, Ed., ed: InTech, 2013.

[13] L. E. Williams, "Anniversary paper: Nuclear medicine: Fifty years and still counting," *Medical Physics,* vol. 35, pp. 3020-3029, Jul 2008.

[14] M. H. Seymour, "Quantum ChromoDynamics," presented at the 5th CERN-Latin-American School of High-Energy Physics, Recinto Quirama, Colombia, 2010.

[15] M. Naghdi, "Nucleon-Nucleon Interaction: A Typical/Concise Review," *Phys. Part. Nucl.,* vol. 5, 2014.

[16] R. Machleidt, "Origin and properties of strong inter-nucleon interactions," presented at the International Conference on Nuclear Theory in the Supercomputing Era, Iowa, 2013.

[17] R. Machleidt, "The nucleon-nucleon interaction," *J. Phys. G: Nucl. Part. Phys,* vol. 27, 2001.

[18] B. R. Martin, *Nuclear and Particle Physics*: John Wiley and Sons, Ltd, 2006.

[19] J.-L. Basdevant, J. Rich, and M. Spiro, *Fundamentals in Nuclear Physics: From Nuclear Structure to Cosmology*: Springer, 2005.

[20] Contemporary Physics Education Project, *Nuclear Science - A Guide to Nuclear Science Wall Chart*, Third ed.: Science Kit, 2003.

[21] C. Levin, "Basic Physics of Radionuclide Imaging," in *Emission Tomography: The Fundamentals of PET and SPECT*, M. N. Wernick and J. N. Aarsvold, Eds., ed: Elsevier, 2004.

[22] S. R. Cherry, J. A. Sorensen, and M. E. Phelps, *Physics in Nuclear Medicine*, Fourth ed.: Saunders, 2012.

[23] S. S. M. Wong, *Introductory Nuclear Physics*, Second Edition ed.: Wiley-VCH, 2004.

[24] G. Rajasekaran, "Fermi and the theory of weak interactions," *Resonance,* vol. 19, pp. 18-44, 2014.

[25] C. D. Anderson, "The positive electron," *Physical Review,* vol. 43, pp. 491-494, Mar 1933.

[26] M. Charlton and J. W. Humberston, *Positron Physics*: Cambridge University Press, 2001.

[27] M. D. Harpen, "Positronium: Review of symmetry, conserved quantities and decay for the radiological physicist," *Med Phys,* vol. 31, pp. 57-61, 2004.

[28] G. B. Saha, "Cyclotron and Production of PET Radionuclides," in *Basics of PET Imaging: Physics, Chemistry and Regulations*, G. B. Saha, Ed., ed: Springer, 2005.

[29] G. B. Saha, "Cyclotron and Production of PET Radionuclides," in *Basics of PET Imaging: Physics, Chemistry and Regulations*, G. B. Saha, Ed., ed: Springer, 2005, pp. 99-110.

[30] Entidade Reguladora da Saúde, "Acesso, concorrência e qualidade na realização de exames de Tomografia por Emissão de Positrões (PETSCAN)," Porto2013.

[31] A. R. Jalilian, "The Application of Unconventional PET Tracers in Nuclear Medicine," *Iran J Nucl Med,* vol. 17, pp. 1-11, 2009.

[32] M. J. Welch, R. Laforest, and J. S. Lewis, "Production of Non-Standard PET Radionuclides and Application of Radiopharmaceuticals Labeled with these Nuclides," in *PET Chemistry: The Driving Force in Molecular Imaging Series*, P. A. Schubiger, L. Lehmann, and M. Friebe, Eds., ed: Springer, 2007.

[33] A. P. Selwyn, R. M. Allan, A. L'Abbate, P. Horlock, P. Camici, J. Clark, H. A. O'Brien, and P. M. Grant, "Relation between regional myocardial uptake of rubidium-82 and perfusion: Absolute reduction of cation uptake in ischemia," *American Journal of Cardiology,* vol. 50, pp. 112-121, 1982.

[34] AAA. (2016, 12-06-2016). *Advanced Accelerator Applications Announces FDA Approval of NETSPOT™ (Somakit-TATE), a Kit for the Preparation of Gallium Ga 68 Dotatate for Neuroendocrine Tumor Detection – NETSPOT™ will*

be the new name for Somakit-TATE, a PET (Positron Emission Tomography) Diagnostic. Available: http://www.adacap.com/flash-news/2016/06/advanced-accelerator-applications-announces-fda-approval-of-netspottm-somakit-tate-a-kit-for-the-preparation-of-gallium-ga-68-dotatate-for-neuroendocrine-tumor-detection-2/

[35] World Nuclear Association. (2015, 18/08/2015). *Radioisotopes in Medicine*. Available: http://www.world-nuclear.org/info/Non-Power-Nuclear-Applications/Radioisotopes/Radioisotopes-in-Medicine/

[36] D. Meierfrankenfeld, A. Bury, and M. Thoennessen, "Discovery of scandium, titanium, mercury, and einsteinium isotopes," *Atomic Data and Nuclear Data Tables,* 2011.

[37] M. Sadeghi, M. Enferadi, and H. Nadi, "^{45}Ti, a Candidate for Positron Emission Tomography: Study of the Cyclotron Production," *Radiochemistry,* vol. 53, pp. 411-414, 2011.

[38] A. L. Vavere, R. Laforest, and M. J. Welch, "Production, processing and small animal PET imaging of titanium-45," *Nucl Med Biol,* vol. 32, pp. 117-22, Feb 2005.

[39] S. Rafique, M. Idrees, A. Nasim, H. Akbar, and A. Athar, "Transition metal complexes as potential therapeutic agents," *Biotechnology and Molecular Biology Reviews,* vol. 5, pp. 38-45, 2010.

[40] S. Bhaskar, F. Tian, T. Stoeger, W. Kreyling, J. M. d. l. Fuente, V. Grazú, P. Borm, G. Estrada, V. Ntziachristos, and D. Razansky, "Multifunctional Nanocarriers for diagnostics, drug delivery and targeted treatment across blood-brain barrier: perspectives on tracking and neuroimaging," *Particle and Fibre Toxicology,* vol. 7, 2010.

[41] R. W. Cheyne, T. A. D. Smith, L. Trembleau, and A. C. Mclaughlin, "Synthesis and characterisation of biologically compatible TiO2 nanoparticles," *Nanoscale Research Letters,* vol. 6, Jun 14 2011.

[42] M. De, P. S. Ghosh, and V. M. Rotello, "Applications of Nanoparticles in Biology," *Advanced Materials,* vol. 20, pp. 4225-4241, Nov 18 2008.

[43] H. O. Lundqvist, "Radionuclide Production," in *Nuclear Medicine Physics: A Handbook for Teachers and Students*, D. L. Bailey, J. L. Humm, A. Todd-Pokropek, and A. v. Aswegen, Eds., ed Vienna: International Atomic Energy Agency, 2014, pp. 117-148.

[44] B. Hutton, "The contribution of Medical Physics to Nuclear Medicine: looking back - a physicist's perspective," *EJNMMI Physics,* vol. 1, pp. 1-7, 2014.

[45] E. O. Lawrence, "Artificial Radioactivity," *Ohio Journal of Science,* vol. 35, pp. 388-405, 1935.

[46] G. B. Saha, *Production of Radionuclides*, Sixth Edition ed.: Springer, 2010.

[47] International Atomic Energy Agency, "IAEA Tec Doc 1340 - Manual for reactor produced radioisotopes," ed. Vienna: IAEA, 2003.

[48] International Atomic Energy Agency, "Directory of Cyclotrons used for Radionuclide Production in Member States - 2006 Update," ed. Vienna: IAEA, 2006.

[49] C. A. Bertulani, "Nuclear Reactions," in *Wiley Encyclopedia of Physics* ed Berlin: Wiley-VCH, 2010.

[50] W. N. Cottingham and D. A. Greenwood, *An Introduction to Nuclear Physics*, Second ed. Cambridge: Cambridge University Press, 2004.

[51] D. Griffiths, "Elementary Particle Dynamis," in *Introduction to Elementary Particles*, Second ed: WILEY-VCH, 2008, pp. 59-88.

[52] G. Choppin, J. Rydberg, and J. O. Liljenzin, "Mechanisms and Models of Nuclear Reactions," in *Radiochemistry and Nuclear Chemistry: Theory and Applications*, Second ed: Butterworth-Heinemann Ltd, 1995, pp. 366-387.

[53] N. K. Glendenning, *Direct Nuclear Reactions*. Singapure: World Scientific Publishing, 2004.

[54] K. S. Krane, *Introductory Nuclear Physics*: John Wiley and Sons, 1988.

[55] J. K. Shultis and R. E. Faw, *Fundamentals of Nuclear Science and Engineering*. New York: Marcel Dekker, Inc., 2002.

[56] E. B. Podgorsak, *Radiation Physics for Medical Physicists*: Springer, 2006.

[57] R. A. Serway, C. J. Moses, and C. A. Moyer, *Modern Physics*, Third Edition ed.: Thomson Learning, 2005.

[58] W. D. Loveland, D. J. Morrisey, and G. T. Seaborg, *Modern Nuclear Chemistry*: John Wiley & Sons, 2006.

[59] S. M. Qaim, "Nuclear data for medical applications: an overview," *Radiochim. Acta,* vol. 89, pp. 189-196, 2001.

[60] International Atomic Energy Agency, "Technical Report Series No465 - Cyclotron Produced Radionuclides: Principles and Practice," ed. Vienna: IAEA, 2008, pp. 59-72.

[61] American Institute of Physics. (24/08/2015). *The first cyclotrons*. Available: www.aip.org/history/lawrence/first.htm

[62] E. O. Lawrence, "The Production of High Speed Protons Without the use of High Voltages," *Rhys. Rev.,* vol. 38, 1931.

[63] E. O. Lawrence and M. S. Livingston, "The Production of High Speed Light Ions Without The Use of High Voltages," *Physical Review,* vol. 40, 1932.

[64] Nobel Media. (27/08/2015). *The Nobel Prize in Physics 1939*. Available: http://www.nobelprize.org/nobel_prizes/physics/laureates/1939/

[65] E. O. Lawrence, "The Evolution of the Cyclotron," in *Nobel Lectures*, ed Amsterdam: Elsevier Publishing Company, 1965.

[66] Mayer-Boricke, "Applications of Cyclotrons in Nuclear Physics," in *7th International Conference on Cyclotrons and their Applications*, Zurich, Switzerland, 1975.

[67] S. M. Qaim, "Use of cyclotrons in medicine," *Radiation Physics and Chemistry,* vol. 71, pp. 917-926, 2004.

[68] P. Schmor, "Review of Cyclotrons for the Production of Radioactive Isotopes for Medical and Industrial Applications," *Reviews of Accelerator Science and Technology,* vol. 4, pp. 103-116, 2011.

[69] D. L. Friesel and T. A. Antaya, "Medical cyclotrons," *Reviews of Accelerator Science and Technology,* vol. 2, pp. 133-156, 2009.

[70] E. Baron, "World trends in cyclotron developments for nuclear physics and applications," *Nukleonika,* vol. 48, pp. S3-S11, 2003.

[71] A. Das and T. Ferbel, *Introduction to Nuclear and Particle Physics*, 2nd ed. Singapore: World Scientific Publishing Co, 2003.

[72] S. M. Qaim, "Nuclear data relevant to the production and application of diagnostic radionuclides," *Radiochim. Acta,* vol. 89, pp. 223-232, 2001.

[73] A. I. Papash and Y. G. Alenitskii, "Commercial Cyclotrons. Part I: Commercial Cyclotrons in the Energy Range 10–30 MeV for Isotope Production," *Physics of Particles and Nuclei,* vol. 39, pp. 597-631, 2008.

[74] V. Bui, Y. Sheh, R. Finn, L. Francesconi, S. Cai, D. Schlyerb, and B. Wieland, "Electroplated targets for production of unique PET radionuclides," *Nuclear Instruments and Methods in Physics Research A,* vol. 366, pp. 415-417, 1995.

[75] A. Hevner, S. T. March, J. Park, and S. Ram, "Design Science in Information Systems Research," *MIS Quarterly,* vol. 28, pp. 75-105, 2004.

[76] T. Ruth, "Radionuclide Production for the Biosciences," *IEEE,* pp. 67-69, 1996.

[77] International Atomic Energy Agency. (29/08/2015). *EXFOR*. Available: http://www-nds.iaea.org/medical/.

[78] International Atomic Energy Agency, "IAEA Tec Doc 1211 - Charged particle cross-section database for medical radioisotope production: diagnostic radioisotopes and monitor reactions," ed. Vienna: IAEA, 2001.

[79] A. F. Bielajew, *Fundamentals of Monte Carlo method for neutral and charged particle transport*. Michigan, USA: The University of Michigan, 2001.

[80] G. Comte de Buffon, "Essai d'arithmetique morale," *Supplement a l'Histoire Naturelle,* vol. 4, 1777.

[81] M. H. Kalos and P. A. Whitlock, *Monte Carlo methods* vol. Volume I: Basics. New York: John Wiley and Sons, 1986.

[82] International Atomic Energy Agency, "Technical Report Series No 273 - Handbook on Nuclear Activation Data," ed. Vienna: IAEA, 1987.

[83] A. J. Koning and D. Rochman. (2011, 01-09-2015). *TALYS-based Evaluated Nuclear Data Library*. Available: ftp://ftp.nrg.eu/pub/www/talys/tendl2011/tendl2011.html

[84] J. F. Ziegler, J. P. Biersack, and M. D. Ziegler, *The Stopping and Range of Ions in Matter*. USA: Lulu Press Co., 2008.

[85] J. F. Ziegler, J. P. Biersack, and U. Littmark, *The Stopping and Range of Ions in Solids*. New York: Pergamon, 1985.

[86] M. Pavlovic and I. Strasik, "Supporting routines for the SRIM code," *Nuclear Instruments and Methods in Physics Research B,* vol. 257, pp. 601-604, 2007.

[87] Ion Beam Applications. (01/09/2015). *Cyclone 18/9 product description*. Available: http://www.iba-radiopharmasolutions.com/products-cyclo/cyclone-18-9

[88] C. Tamburella, T. J. Giles, G. J. Beyer, and D. Soloviev, "Beam Diagnostics for an 18 MeV Medical Cyclotron," in *10th Workshop on Targetry and Target Chemistry*, Madison, USA, 2004.

[89] L. Picardi, P. Panichelli, G. Prete, F. Romano, and G. Valentini, "Accelerating a cyclotron 18 MeV proton beam by a scdtl LINAC," in *PAC09*, Vancouver, Canada, 2009.

[90] M. Pavlovič and I. Strasik, "Beam transport with scattering using SRIM supporting software routines codes," in *EPAC08*, Genoa, Italy, 2008, pp. 1767-1769.

[91] D. Gandarias-Cruz and K. Okamoto, "Status on the compilation of nuclear data for medical radioisotopes produced by accelerators," ed. Vienna: IAEA, 1988, p. 16.

[92] N.U.H. Syed, A.C. Larsen, A. Bürger, M. Guttormsen, S. Harissopulos, M. Kmiecik, T. Konstantinopoulos, M. Krticka, A. Lagoyannis, T. Lönnroth, K.Mazurek, M. Norby, H. T. Nyhus, G. Perdikakis, S. Siem, and A. Spyrou, "Extraction of thermal and electromagnetic properties in 45Ti," *Physical Review C,* vol. 80, 2009.

[93] G. Battistoni, "Mechanisms of the Interactions Between Radiation and Matter," in *Radiation Physics for Nuclear Medicine*, M. C. Cantone and C. Hoeschen, Eds., ed: Springer, 2011.

[94] I. Strašík and M. Pavlovič, "Improvements to the SRIM simulations," *Radiation Effects and Defects in Solids: Incorporating Plasma Science and Plasma Technology,* vol. 164, pp. 470-476, 2009.

[95] J. E. Turner, *Atoms, Radiation, and Radiation Protection*: Wiley-VCH, 2007.

[96] G. F. Knoll, *Radiation Detection and Measurement*: John Wiley & Sons, 2000.

[97] R. D. Evans, *The Atomic Nucleus*: McGraw-Hill, 1965.

[98] N. Tsoulfanidis, *Measurement and Detection of Radiation*, Second Edition ed.: Taylor & Francis, 1995.

[99] G. Gilmore and J. Hemingway, *Practical Gamma-Ray Spectrometry*. New York: John Wiley & Sons, 1995.

[100] J. L. Parker, "Instrumentation for Gamma-Ray Spectroscopy," in *Passive Nondestructive Assay of Nuclear Materials*, D. Reilly, N. Ensslh, H. Smith, and S. Kreiner, Eds., ed Los Alamos: United States Nuclear Regulatory Commision, 1991.

[101] I. Rittersdorf, *Gamma Ray Spectroscopy*. Michigan: University of Michigan, 2007.

[102] International Atomic Energy Agency, "IAEA Tec Doc 1049 - Software for nuclear spectrometry," ed. Vienna: IAEA, 1998.

[103] P. Costa and M. Duarte Naia, "Espectroscopia Gama: Código de análise e simulação," presented at the Física 2012, Aveiro, 2012.

[104] M. Saizu and M. Calin, "Basic aspects concerning the validation of the measuring method using a new spectrometric gamma system with HPGe detector," *Rom. Journ. Phys,* vol. 56, pp. 1108-1115, 2011.

[105] A. Luca, B. Neacsu, A. Antohe, and M. Sahagia, "Calibration of the high and low resolution gamma-ray spectrometers," *Romanian Reports in Physics,* vol. 64, pp. 968-976, 2012.

[106] R. Njinga and S. Jonah, "Calibration of the High Purity Germanium Gamma-Ray Spectrometer in CERT, ABU Zaria, Nigeria," *Modern Instrumentation,* vol. 4, pp. 11-17, 2015.

[107] S. Harb, K. Din, and A. Abbady, "Study of Efficiency Calibrations of HPGe Detectors for Radioactivity Measurements of Environmental Samples," in *3rd Environmental Physics Conference*, Aswan, Egypt, 2008, pp. 207-218.

[108] M. Lépy, A. Pearce, and O. Sima, "Uncertainties in gamma-ray spectrometry," *Metrologia,* vol. 52, pp. S123-S145, 2015.

[109] K. Ishiwata, T. Ido, M. Monma, M. Murakami, H. Fukuda, K. Yamada, S. Endo, H. Yoshioka, T. Sato, and T. Matsuzawa, "Preparation and Medical Application of ^{45}Ti," *CYRIC Annual Report,* 1981.

[110] L. Tang, "Radionuclide production and yields at Washington University School of Medicine," *Q J Nucl Med Mol Imaging,* vol. 52, pp. 121-133, 2008.

[111] Y. Fazaeli, M. Aboudzadeh, K. Aardaneh, T. Kakavand, F. Bayat, and K. Yousefi, "A new approach to targetry and cyclotron production of ^{45}Ti by proton irradiation of ^{45}Sc," *Nuclear Technology & Radiation Protection,* vol. 29, pp. 28-33, 2014.

[112] C. Vandecasteele, "Activation analysis: Present status in relation to other analytical techniques," *Microchimica Acta,* vol. 104, pp. 379-389, 1991.

[113] Ion Beam Applications. (07/09/2015). *Cyclone®18/9 - Moving ahead, delivering more.* Available: http://www.iba-cyclotron-solutions.com

[114] K. Gagnon, "Cyclotron Production of Technetium-99m," PhD in Medical Physics, Faculty of Graduate Studies and Research, University of Alberta, Edmonton, Alberta 2012.

[115] J. H. Kim, H. Park, S. Kim, J. S. Lee, and K. S. Chun, "Proton Beam Energy Measurement with the Stacked Cu Foil Technique for Medical Radioisotope Production," *Journal of the Korean Physical Society,* vol. 48, pp. 755-758, 2006.

[116] M. U. Khandaker, G. Kim, K. Kim, H. B. A. Kassim, and B. Nikouravan, "Investigations of proton beam energy of the MC-50 cyclotron at KIRAMS," *International Journal of the Physical Sciences,* vol. 6, pp. 3168-3174, 2011.

[117] K. Gagnon, M. Jensen, H. Thisgaard, J. Publicover, S. Lapi, S.A. McQuarrie, and T. J. Ruth, "A new and simple calibration-independent method for measuring the beam energy of a cyclotron," *Appl. Radiat. Isot.,* vol. 69, pp. 247–253, 2011.

[118] S. Ghithan, "Development of a PET Cyclotron based irradiation setup for proton radiobiology," PhD in Physics Engineering, Department of Physics, University of Coimbra, Coimbra, 2014.

[119] M. Cunha, "Radiobiology with proton cyclotron beams: a viability study," Masters in Biomedical Engineering, Department of Physics, University of Coimbra, Coimbra, 2010.

[120] D. Filosofov, N. Loktionova, and F. Rösch, "A ^{44}Ti/^{44}Sc radionuclide generator for potential application of ^{44}Sc-based PET-radiopharmaceuticals," *Radiochim. Acta,* vol. 98, pp. 149-156, 2010.

[121] Hernandez R, Valdovinos HF, Yang Y, Chakravarty R, Hong H, Barnhart TE, and C. W, "^{44}Sc: an attractive isotope for peptide-based PET imaging.," *Mol Pharm,* vol. 11, pp. 2954-2961, 2014.

[122] S. Frank, "Input-output relations in biological systems: measurement, information and the Hill equation," *Biology Direct,* vol. 8, 2013.

[123] Richard G. Thomas Jr. and W. Bartolini, "Excitation functions for (p, n) and (p, 2n) interactions in Sc, Cr, Mo, Cd and W between 8 and 14 MeV," *Nuclear Physics A,* vol. 106, pp. 323-336, 1967.

[124] R. Ejnisman, I. D. Goldman, P. R. Pascholati, M. T. da Cruz, R. M. Oliveira, E. B. Norman, I. I. Zlimen, F. E. Wietfeldt, R. M. Larimer, Y. D. Chan, K. T. Lesko, and A. García, "Cross sections for 45Sc(p,2n)44Ti and related reactions.," *Physical Review C - Nucl Phys,* vol. 54, pp. 2047-2050, 1996.

[125] V. N. Levkovskij, "Activation cross section nuclides of average masses (A = 40 – 100) by protons and alpha particles with average energies (E = 10 – 50 MeV)," *Inter Vesi, Moscow,* 1991.

[126] A. J. Howard, H. B. Jensen, M. Rios, W. A. Fowler, and B. A. Zimmerman, "Measurement and Theoretical Analysis of Some Reaction Rates of Interest in Silicon Burning," *Astrophysical Journal,* vol. 188, pp. 131-140, 1974.

[127] T. McGee, C. L. Rao, G. B. Saha, and L. Yaffe, "Nuclear interactions of ^{45}Sc and ^{68}Zn with protons of medium energy," *Nuclear Physics A,* vol. 150, pp. 11-29, 1970.

[128] George F. Dell, W.D. Ploughe, and H. J. Hausman, "Total reaction cross sections in the mass range 45 to 65," *Nuclear Physics,* vol. 64, pp. 513-523, 1965.

[129] R. P. Feynman, "There's a plenty of room at the bottom," *Journal of Microelectromechanical Systems,* vol. 1, pp. 60-66, 1992.

[130] N. Taniguchi, "On the Basic Concept of "Nano-Technology"," *Proceedings of the International Conference on Production Engineering,* 1974.

[131] M. C. Roco, "National Nanotechnology Initiative - Past, Present, Future," in *Handbook of Nanoscience, Engineering, and Technology*, W. A. G. Iii, D. W. Brenner, S. E. Lyshevski, and G. J. Iafrate, Eds., Second Edition ed: Taylor and Francis, 2007.

[132] D. Bhattacharyya, S. Singh, N. Satnalika, A. Khandelwal, and S. Jeon, "Nanotechnology, Big things from a Tiny World: a Review " *International Journal of u- and e- Service, Science and Technology* vol. 2, 2009.

[133] R. A. Freitas, Jr., *Nanomedicine: Basic Capabilities* vol. I: Landes Bioscience, 1999.

[134] S. M. Moghimi, A. C. Hunter, and J. C. Murray, "Nanomedicine: Current status and future prospects," *The FASEB Journal,* vol. 19, pp. 311-330, 2005.

[135] R. A. Freitas, Jr., "What is nanomedicine?," *Nanomedicine: Nanotechnology, Biology and Medicine,* vol. 1, pp. 2-9, Mar 2005.

[136] R. A. Freitas, Jr., "Nanotechnology, nanomedicine and nanosurgery," *Int J Surg,* vol. 3, pp. 243-6, 2005.

[137] R. A. Freitas, Jr., "Current status of Nanomedicine and Medical Nanorobotics," *Journal of Computational and Theoretical Nanoscience,* vol. 2, pp. 1-25, 2005.

[138] J. Safari and Z. Zarnegar, "Advanced drug delivery systems: Nanotechnology of health design - A review," *Journal of Saudi Chemical Society,* vol. 18, pp. 85-99, 2014.

[139] G. Manish and S. Vimukta, "Targeted drug delivery system: A review," *Research Journal of Chemical Sciences,* vol. 1, pp. 135-138, 2011.

[140] R. Bagul, V. Mahajan, and A. Dhake, "New approaches in nanoparticulate drug delivery system - A review," *International Journal of Current Pharmaceutical Research,* vol. 4, pp. 29-38, 2012.

[141] M. Assadi, K. Afrasiabi, I. Nabipour, and M. Seyedabadi, "Nanotechnology and nuclear medicine; research and preclinical applications," *Hellenic Journal of Nuclear Medicine,* vol. 14, 2011.

[142] I. Zolle, *Preparation and Quality Control in Nuclear Medicine*: Springer, 2007.

[143] W. Cai and X. Chen, "Multimodality Molecular Imaging of Tumor Angiogenesis," *J Nucl Med,* vol. 49, pp. 113S-128S, 2008.

[144] K. Chen and P. S. Conti, "Target-specific delivery of peptide-based probes for PET imaging," *Advanced Drug Delivery Reviews,* vol. 62, pp. 1005-1022, 2010.

[145] F. Chen, E. Ehlerding, and W. Cai, "Theranostic Nanoparticles," *Journal of Nuclear Medicine,* vol. 55, pp. 1919-1922, 2014.

[146] C. S. Cutler, N. Chanda, R. Shukla, N. Sisay, M. Cantorias, A. Zambre, M. McLaughlin, J. Kelsey, A. Upenandran, D. Robertson, S. Deutscher, R. Kannan, and K. Katti, "Nanoparticles and Phage Display Selected Peptides for Imaging and Therapy of Cancer," in *Theranostics, Gallium-68, and Other Radionuclides*, R. P. Baum and F. Rösch, Eds., ed: Springer, 2013, pp. 133-147.

[147] A. L. B. d. Barros, A. Tsourkas, B. Saboury, V. N. Cardoso, and A. Alavi, "Emerging role of radiolabeled nanoparticles as an effective diagnostic technique," *EJNMMI Research,* vol. 2, 2012.

[148] G. Ferro-Flores, F. d. M. Ramírez, L. Meléndez-Alafort, and C. L. Santos-Cuevas, "Peptides for In Vivo Target-Specific Cancer Imaging " *Mini-Reviews in Medicinal Chemistry,* vol. 10, pp. 87-97, 2010.

[149] M. Hamoudeh, M. A. Kamleh, R. Diab, and H. Fessi, "Radionuclides delivery systems for nuclear imaging and radiotherapy of cancer," *Advanced Drug Delivery Reviews,* vol. 60, pp. 1329-1346, 2008.

[150] H. Hong, Y. Zhang, J. Sun, and W. Ca, "Molecular imaging and therapy of cancer with radiolabeled nanoparticles," *Nano Today,* vol. 4, pp. 399-413, 2009.

[151] R. Jain, P. Dandekar, and V. Patravale, "Diagnostic nanocarriers for sentinel lymph node imaging," *Journal of Controlled Release,* vol. 138, pp. 90-102, 2009.

[152] R. Kannan, A. Zambre, N. Chanda, R. Kulkarni, R. Shukla, K. Katti, A. Upendran, C. Cutler, E. Boote, and K. V. Katti, "Functionalized radioactive gold nanoparticles in tumor therapy," *WIREs Nanomed Nanobiotechnol,* vol. 4, pp. 42-51, 2012.

[153] S. M. Larson, "Cancer Drug Development with the Help of Radiopharmaceuticals: Academic Experience " *Current Pharmaceutical Design,* vol. 15, pp. 950-956, 2009.

[154] A. Mitra, A. Nan, B. R. Line, and H. Ghandehar, "Nanocarriers for Nuclear Imaging and Radiotherapy of Cancer," *Current Pharmaceutical Design,* vol. 12, pp. 4729-4749, 2006.

[155] V. Patel, R. V. L. Papineni, S. Gupta, R. Stoyanova, and M. M. Ahmed, "A Realistic Utilization of Nanotechnology in Molecular Imaging and Targeted Radiotherapy of Solid Tumors," *Radiation Research,* vol. 177, pp. 483-495, 2012.

[156] W. T. Phillips, B. A. Goins, and A. Bao, "Radioactive liposomes," *Wiley Interdiscipl. Rev. Nanomed. Nanobiotechnol.,* vol. 1, pp. 69-83, 2009.

[157] D. Psimadas, P. Georgoulias, V. Valotassiou, and G. Loudos, "Molecular Nanomedicine Towards Cancer: 111In-Labeled Nanoparticles," *Journal of Pharmaceutical Sciences,* vol. 101, pp. 2271-2280, 2012.

[158] M. Schottelius, B. Laufer, H. Kessler, and H. R. Wester, "Ligands for Mapping alpha-v-beta-3 -Integrin Expression in Vivo," *Accounts of Chemical Research,* vol. 42, pp. 969-980, 2009.

[159] M. Silindir, S. Erdogan, A. Y. Özer, and S. Maia, "Liposomes and their applications in molecular imaging," *Journal of Drug Targeting,* vol. 20, pp. 401-415, 2012.

[160] K. Stockhofe, J. M. Postema, H. Schieferstein, and T. L. Ross, "Radiolabeling of Nanoparticles and Polymers for PET Imaging," *Pharmaceuticals,* vol. 7, pp. 392-418, 2014.

[161] V. P. Torchilin, "Targeted Pharmaceutical Nanocarriers for Cancer Therapy and Imaging," *The AAPS Journal,* vol. 9, pp. E128-E147, 2007.

[162] C. Vanpouille-Box and F. Hindré, "Nanovectorized radiotherapy: a new strategy to induce anti-tumor immunity," *Frontiers in Oncology,* vol. 2, 2012.

[163] X.-d. Hu, L.-g. Xing, and J.-m. Yu, "Nuclear medical molecular imaging of tumor angiogenesis: current status and future prospects," *Chinese Medical Journal,* vol. 126, pp. 2741-2746, 2013.

[164] H. R. Maecke and J. C. Reubi, "Somatostatin Receptors as Targets for Nuclear Medicine Imaging and Radionuclide Treatment," *Journal of Nuclear Medicine,* vol. 52, pp. 841-844, 2011.

[165] O. C. Boerman and W. Oyen, "Multimodality Probes: Amphibian Cars for Molecular Imaging," *Journal of Nuclear Medicine,* vol. 49, pp. 1213-1214, 2008.

[166] A. W. Sauter, H. F. Wehrl, A. Kolb, M. S. Judenhofer, and B. J. Pichler, "Combined PET/MRI: one step further in multimodality imaging," *Trends Mol Med,* vol. 16, pp. 508-15, Nov 2010.

[167] F. Nensa, K. Beiderwellen, P. Heusch, and A. Wetter, "Clinical applications of PET/MRI: current status and future perspectives," *Diagn Interv Radiol,* vol. 20, pp. 438-47, Sep-Oct 2014.

[168] G. Ak, F. Y. Lambrecht, and S. H. Sanlier, " Radiolabeling of folate targeted multifunctional conjugate with Technetium-99m and biodistribution studies in rats," *Journal of Drug Targeting,* vol. 20, pp. 509-514, 2012.

[169] S. Alam, Z. I. Khan, G. Mustafa, M. Kumar, F. Islam, A. Bhatnagar, and F. J. Ahmad, "Development and evaluation of thymoquinone-encapsulated chitosan nanoparticles for nose-to-brain targeting: a pharmacoscintigraphic study," *International Journal of Nanomedicine,* vol. 7, pp. 5705-5718, 2012.

[170] E. P. Azorín-Vega, O. D. Zambrano-Ramírez, E. L. Rojas-Calderón, B. E. Ocampo-García, and G. Ferro-Flores, "Tumoral fibrosis effect on the radiation absorbed dose of ^{177}Lu–Tyr^{3}-octreotateand, ^{177}Lu–Tyr^{3}-octreotate conjugated to gold nanoparticles," *Applied Radiation and Isotopes,* vol. 100, pp. 96-100, 2015.

[171] N. Chanda, P. Kan, L. D. Watkinson, R. Shukla, A. Zambre, T. L. Carmack, H. Engelbrecht, J. R. Lever, K. Katti, G. M. Fent, S. W. Casteel, C. J. Smith, W. H. Miller, S. Jurisson, E. Boote, J. D. Robertson, C. Cutler, M. Dobrovolskaia, R. Kannan, and K. V. Katti, "Radioactive gold nanoparticles in cancer therapy: therapeutic efficacy studies of GA-198AuNP nanoconstruct in prostate tumor – bearing mice," *Nanomedicine: Nanotechnology, Biology, and Medicine,* vol. 6, pp. 201-209, 2010.

[172] A. Chrastina and J. e. Schnitzer, "Iodine-125 radiolabeling of silver nanoparticles for in vivo SPeCT imaging," *International Journal of Nanomedicine,* vol. 5, pp. 653-659, 2010.

[173] U.-K. Dar, I. U. Khan, M. Javed, M. Ali, S. W. Hyder, S. Murad, and J. Anwar, "In house development of 99mTc-Rhenium sulfíde colloidal nanoparticles for sentinel lymph node detection," *Pak. J. Pharm. Sei.,* vol. 26, pp. 367-373, 2013.

[174] K. D. Groeve, N. Deschacht, C. D. Koninck, V. Caveliers, T. Lahoutte, N. Devoogdt, S. Muyldermans, P. D. Baetselier, and G. Raes, "Nanobodies as Tools for In Vivo Imaging of Specific Immune Cell Types," *Journal of Nuclear Medicine,* vol. 51, pp. 782-789, 2010.

[175] S. Dong, G. Huang, P. Liu, Y. Ma, W. Yan, L. Wan, and C. Zhu, "Efficacy and safety of 32P-nanocolloid for treatment of distant lymph node metastasis in VX2 tumor-bearing rabbits," *Ann Nucl Med,* vol. 22, pp. 849-858, 2008.

[176] B. Freund, U. I. Tromsdorf, O. T. Bruns, M. Heine, A. Giemsa, Alexander Bartelt, S. C. Salmen, N. Raabe, J. Heeren, H. Ittrich, R. Reimer, H. Hohenberg, U. Schumacher, H. Weller, and P. Nielsen, "A Simple and Widely Applicable Method to 59Fe-Radiolabel Monodisperse Superparamagnetic Iron Oxide Nanoparticles for In Vivo Quantification Studies," *ACS Nano,* vol. 6, pp. 7318-7325, 2012.

[177] N. Giri, P. Tomar, V. S. Karwasara, R. S. Pandey, and V. K. Dixit, "Targeted novel surface-modified nanoparticles for interferon delivery for the treatment of hepatitis B," *Acta Biochim Biophys Sin,* vol. 43, pp. 877-883, 2011.

[178] M. Hamoudeh, H. Fessi, H. Salim, and D. Barbos, "Holmium-Loaded PLLA Nanoparticles for Intratumoral Radiotherapy Via the TMT Technique: Preparation, Characterization, and Stability Evaluation after Neutron Irradiation," *Drug Development and Industrial Pharmacy,* vol. 34, pp. 796-806, 2008.

[179] A. Helbok, C. Decristoforo, G. Dobrozemsky, C. Rangger, E. Diederen, B. Stark, R. Prassl, and E. v. Guggenberg, "Radiolabeling of lipid-based nanoparticles for diagnostics and therapeutic applications: a comparison using different radiometals," *Journal of Liposome Research,* vol. 20, pp. 219-227, 2010.

[180] S. L. Hosseini-Salekdeh, A. R. Jalilian, H. Yousefnia, K. Shafaii, M. Pouladian, and M. Mahmoudi, "Evaluation of radiogallium-labeled, folate-embedded superparamagnetic nanoparticles in fibrosarcoma-bearing mice," *Journal of Cancer Research and Therapeutics,* vol. 8, pp. 204-208, 2012.

[181] F.-Y. J. Huang, T.-W. Lee, C.-H. K. Kao, C.-H. Chang, X. Zhang, W.-Y. Lee, W.-J. Chen, S.-C. Wang, and J.-M. Lo, "Imaging, Autoradiography, and Biodistribution of 188 Re-Labeled PEGylated Nanoliposome in Orthotopic Glioma Bearing Rat Model," *Cancer Biotherapy and Radiopharmaceuticals,* vol. 26, pp. 717-725, 2011.

[182] D. W. Hwang, H. Y. Ko, J. H. Lee, H. Kang, S. H. Ryu, I. C. Song, D. S. Lee, and S. Kim, "A Nucleolin-Targeted Multimodal Nanoparticle Imaging Probe for Tracking Cancer Cells Using an Aptamer," *J Nucl Med,* vol. 51, pp. 98-105, 2010.

[183] D. W. Hwang, D. S. Lee, and S. Kim, "Gene Expression Profiles for Genotoxic Effects of Silica-Free and Silica-Coated Cobalt Ferrite Nanoparticles," *Journal of Nuclear Medicine,* vol. 53, pp. 106-112, 2012.

[184] S. M. Janib, S. Liu, R. Park, M. K. Pastuszka, P. Shi, A. S. Moses, M. M. Orosco, Y. A. Lin, H. Cui, P. S. Conti, Z. Li, and J. A. MacKay, "Kinetic quantification of protein polymer nanoparticles using non-invasive imaging," *Integr. Biol.,* vol. 5, pp. 183-194, 2013.

[185] H.-W. Kao, Y.-Y. Lin, C.-C. Chen, K.-H. Chi, D.-C. Tien, C.-C. Hsia, M.-H. Lin, and H.-E. Wang, "Evaluation of EGFR-targeted radioimmuno-gold-nanoparticles as a theranostic agent in a tumor animal model," *Bioorganic & Medicinal Chemistry Letters,* vol. 23, pp. 3180-3185, 2013.

[186] N. Kitamura, S. Kosuda, K. Araki, M. Tomifuji, D. Mizokami, A. Shiotani, H. Shinmoto, H. Fuji, and K. Ichihara, "Comparison of animal studies between interstitial magnetic resonance lymphography and radiocolloid SPECT/CT lymphoscintigraphy in the head and neck region," *Ann Nucl Med,* vol. 26, pp. 281-285, 2012.

[187] J.-K. Kim, H. Yuan, J. Nie, Y.-T. Yang, M. Leggas, P. M. Potter, J. Rinehart, M. Jay, and X. Lu, "High Payload Dual Therapeutic-Imaging Nanocarriers for Triggered Tumor Delivery," *Small,* vol. 8, pp. 2895-2903, 2012.

[188] H.-Y. Lee, Z. Li, K. Chen, A. R. Hsu, C. Xu, J. Xie, S. Sun, and X. Chen, "PET/MRI Dual-Modality Tumor Imaging Using Arginine-Glycine-Aspartic (RGD)–Conjugated Radiolabeled Iron Oxide Nanoparticles," *J Nucl Med,* vol. 49, pp. 1371-1379, 2008.

[189] Y. K. Lee, J. M. Jeong, L. Hoigebazar, B. Y. Yang, Y.-S. Lee, B. Chul, H. Youn, D. SooLee, J.-K. Chung, and M. ChulLee, "Nanoparticles Modified by Encapsulation of Ligands with a Long Alkyl Chain to Affect Multispecific and Multimodal Imaging," *Journal of Nuclear Medicine,* vol. 53, pp. 1462-1470, 2012.

[190] S. Liu, B. Jia, R. Qiao, Z. Yang, Z. Yu, Z. Liu, K. Liu, J. Shi, H. Ouyang, F. Wang, and M. Gao, "A Novel Type of Dual-Modality Molecular Probe for MR and Nuclear Imaging of Tumor: Preparation, Characterization and in Vivo Application," *Molecular Pharmaceutics,* vol. 6, pp. 1074-1082, 2009.

[191] X. Liu, Y. Wang, K. Nakamura, S. Kawauchi, A. Akalin, D. Cheng, L. Chen, M. Rusckowski, and D. J. Hnatowich, "Auger Radiation–Induced, Antisense-Mediated Cytotoxicity of Tumor Cells Using a 3-Component Streptavidin-Delivery Nanoparticle with 111In," *J Nucl Med,* vol. 50, pp. 582-590, 2009.

[192] Y. Liu, E. D. Pressly, D. R. Abendschein, C. J. Hawker, G. E. Woodard, P. K. Woodard, and M. J. Welch, "Targeting Angiogenesis Using a C-Type Atrial Natriuretic Factor–Conjugated Nanoprobe and PET," *Journal of Nuclear Medicine,* vol. 52, pp. 1956-1963, 2011.

[193] T. W. Liu, T. D. MacDonald, J. Shi, B. C. Wilson, and G. Zheng, "Intrinsically Copper-64-Labeled Organic Nanoparticles as Radiotracers," *Angew. Chem. Int. Ed.,* vol. 51, pp. 13128-13131, 2012.

[194] E. Locatelli, L. Gil, L. L. Israel, L. Passoni, M. Naddaka, A. Pucci, T. Reese, V. Gomez-Vallejo, P. Milani, M. Matteoli, J. Llop, J. P. Lellouche, and M. C. Franchini, "Biocompatible nanocomposite for PET/MRI hybrid imaging," *International Journal of Nanomedicine,* vol. 7, pp. 6021-6033, 2012.

[195] H. P. Luehmann, E. D. Pressly, L. Detering, C. Wang, R. Pierce, P. K. Woodard, R. J. Gropler, C. J. Hawker, and Y. Liu, "PET/CT Imaging of Chemokine Receptor CCR5 in Vascular Injury Model Using Targeted Nanoparticle," *J Nucl Med,* vol. 55, pp. 629-634, 2014.

[196] R. Madru, P. Kjellman, F. Olsson, K. Wingardh, C. Ingvar, F. Stahlberg, J. Olsrud, J. Latt, S. Fredriksson, L. Knutsson, and S.-E. Strand, "99m Tc-Labeled Superparamagnetic Iron Oxide Nanoparticles for Multimodality SPECT/MRI of Sentinel Lymph Nodes," *J Nucl Med,* vol. 53, pp. 459-463, 2012.

[197] M. D. Majmudar, J. Yoo, E. J. Keliher, J. J. Truelove, Y. Iwamoto, B. Sena, P. Dutta, A. Borodovsky, K. Fitzgerald, M. F. D. Carli, P. Libby, D. G. Anderson, F. K. Swirski, R. Weissleder, and M. Nahrendorf, "Polymeric Nanoparticle PET/MR Imaging Allows Macrophage Detection in Atherosclerotic Plaques," *Circ Res,* vol. 112, pp. 755-761, 2013.

[198] M. Nahrendorf, E. Keliher, B. Marinelli, F. Leuschner, C. S. Robbins, R. E. Gerszten, M. J. Pittet, F. K. Swirski, and R. Weissleder, "Detection of Macrophages in Aortic Aneurysms by Nanoparticle Positron Emission Tomography Computed Tomography," *Arterioscler Thromb Vasc Biol.,* vol. 31, pp. 750-757, 2011.

[199] K. Nakamura, Y. Wang, X. Liu, A. Kubo, and D. J. Hnatowich, "Cell Culture and Xenograft-Bearing Animal Studies of Radiolabeled Antisense DNA–Carrier Nanoparticles with Streptavidin as a Linker," *J Nucl Med,* vol. 48, pp. 1845-1852, 2007.

[200] N. Nikolic, S. Vranjes-Đuric, D. Jankovic, D. Đokic, M. Mirkovic, N. Bibic, and V. Trajkovic, "Preparation and biodistribution of radiolabeled fullerene C60 nanocrystals," *Nanotechnology,* vol. 20, 2009.

[201] N. Oku, M. Yamashita, Y. Katayama, T. Urakami, K. Hatanaka, K. Shimizu, T. Asai, H. Tsukada, S. Akai, and H. Kanazawa, "PET imaging of brain cancer with positron emitter-labeled liposomes," *International Journal of Pharmaceutics,* vol. 403, pp. 170-177, 2011.

[202] A. Ozgur, F. Y. Lambrecht, K. Ocakoglu, C. Gunduz, and M. Yucebas, "Synthesis and biological evaluation of radiolabeled photosensitizer linked bovine serum albumin nanoparticles as a tumor imaging agent," *International Journal of Pharmaceutics,* vol. 422, pp. 472-478, 2012.

[203] D. Patel, S. Naik, and A. Misra, "Improved Transnasal Transport and Brain Uptake of Tizanidine HCl-Loaded Thiolated Chitosan Nanoparticles for Alleviation of Pain," *Journal of Pharmaceutical Sciences,* vol. 101, pp. 690-706, 2011.

[204] M. R. Pelizzo, D. Rubello, I. M. Boschin, A. Piotto, C. Paggetta, A. Toniato, G. L. D. Salvo, A. Giulian, G. Mariani, and D. Casara, "Contribution of SLN investigation with 99mTc-nanocolloid in clinical staging of thyroid cancer: technical feasibility," *Eur J Nucl Med Mol Imaging,* vol. 34, pp. 934-938, 2007.

[205] A. Polyák, I. Hajdu, M. Bodnár, G. Trencsényic, Z. Pöstényi, V. Haász, G. Jánoki, G. A. Jánoki, L. Balogh, and J. Borbély, "99mTc-labelled nanosystem as tumour imaging agent for SPECT and SPECT/CT modalities," *International Journal of Pharmaceutics,* vol. 449, pp. 10-17, 2013.

[206] R. Rossin, S. Muro, M. J. Welch, V. R. Muzykantov, and D. P. Schuster, "In Vivo Imaging of 64 Cu-Labeled Polymer Nanoparticles Targeted to the Lung Endothelium," *J Nucl Med,* vol. 49, pp. 103-111, 2008.

[207] S. Song, C. Xiong, M. Zhou, W. Lu, Q. Huang, G. Ku, J. Zhao, L. G. Flores, Y. Ni, and C. Li, "Small-Animal PET of Tumor Damage Induced by Photothermal Ablation with 64 Cu-Bis-DOTA-Hypericin," *J Nucl Med,* vol. 52, pp. 792-799, 2011.

[208] M. J. W. D. Vosjan, J. Vercammen, J. A. Kolkman, M. S.-v. Walsum, H. Revets, and G. A. M. S. v. Dongen, "Nanobodies Targeting the Hepatocyte Growth Factor: Potential New Drugs for Molecular Cancer Therapy," *Mol Cancer Ther,* vol. 11, pp. 1017-1025, 2012.

[209] H. Xie, Z. J. Wang, A. Bao, B. Goins, and W. T. Phillips, "In vivo PET imaging and biodistribution of radiolabeled gold nanoshells in rats with tumor xenografts," *International Journal of Pharmaceutics,* vol. 395, pp. 324-330, 2010.

[210] T. Yilmaz, P. Unak, F. Z. B. Muftuler, E. I. Medine, C. Ichedef, and A. Y. Kilcar, "Magnetic nanoparticle-conjugated and radioiodinated-DESG: in vitro and in vivo efficiency investigation," *J Radioanal Nucl Chem,* vol. 303, pp. 63-69, 2015.

[211] H. Zhu, J. Zhao, X. Lin, Y. Hong, C. Li, and Z. Yang, "Design, Synthesis and Evaluation of Dual-Modality Glyco-Nanoparticles for Tumor Imaging," *Molecules,* vol. 18, pp. 6425-6438, 2013.

[212] N. Gibson, U. Holzwarth, K. Abbas, F. Simonelli, J. Kozempel, I. Cydzik, G. Cotogno, A. Bulgheroni, D. Gilliland, J. Ponti, F. Franchini, P. Marmorato, H. Stamm, W. Kreyling, A. Wenk, M. Semmler-Behnke, S. Buono, L. Maciocco, and N. Burgio, "Radiolabelling of engineered nanoparticles for in vitro and in vivo tracing applications using cyclotron accelerators," *Arch Toxicol,* vol. 85, pp. 751-773, 2011.

[213] D. L. J. Thored, A. K. Chen, J. Czupryna, and A. Tsourkas, "Superparamagnetic Iron Oxide Nanoparticle Probes for Molecular Imaging," *Annals of Biomedical Engineering,* vol. 34, pp. 23-38, 2006.

[214] Z. R. Ismagilov, L. T. Tsykoza, N. V. Shikina, V. F. Zarytova, V. V. Zinoviev, and S. N. Zagrebelnyi, "Synthesis and stabilization of nano-sized titanium dioxide," *Russian Chemical Reviews,* vol. 78, 2009.

[215] M. Mehta, Y. Sung, V. Raman, and R. O. Fox, "Multiscale Modeling of TiO2 Nanoparticle Production in Flame Reactors: Effect of Chemical Mechanism," *Ind. Eng. Chem. Res.,* vol. 49, pp. 10663-10673, 2010.

[216] V. F. Zarytova, V. V. Zinov'ev, Z. R. Ismagilov, A. S. Levina, M. N. Repkova, N. V. Shikina, A. A. Evdokimov, E. F. Belanov, S. M. Balakhnin, O. A. Serova, S. I. Baiborodin, E. G. Malygin, and S. N. Zagrebel'nyi, "An Examination of the Ability of Titanium Dioxide Nanoparticles and Its Conjugates with Oligonucleotides to Penetrate into Eucariotis Cells," *Nanotechnologies in Russia,* vol. 4, pp. 732-735, 2009.

[217] E. Stefanou, A. Evangelou, and P. Falaras, "Effects of UV-irradiated titania nanoparticles on cell proliferation, cancer metastasis and promotion," *Catalysis Today,* vol. 151, pp. 58-63, 2010.

[218] K. S. El-Said, E. M. Ali, K. Kanehira, and A. Taniguchi, "Molecular mechanism of DNA damage induced by titanium dioxide nanoparticles in toll-like receptor 3 or 4 expressing human hepatocarcinoma cell lines," *Journal of Nanobiotechnology,* vol. 12, 2014.

[219] M. P. Vinardell and M. Mitjans, "Antitumor Activities of Metal Oxide Nanoparticles," *Nanomaterials,* vol. 5, pp. 1004-1021, 2015.

[220] R. Mund, N. Panda, S. Nimesh, and A. Biswas, "Novel titanium oxide nanoparticles for effective delivery of paclitaxel to human breast cancer cells," *Journal of Nanoparticle Research,* vol. 16, 2014.

[221] Y. Chen, Y. Wan, Y. Wang, H. Zhang, and Z. Jiao, "Anticancer efficacy enhancement and attenuation of side effects of doxorubicin with titanium dioxide nanoparticles," *International Journal of Nanomedicine,* vol. 6, pp. 2321-2326, 2011.

[222] L. Smith, Z. Kuncic, K. K. Ostrikov, and S. Kumar, "Nanoparticles in Cancer Imaging and Therapy," *Journal of Nanomaterials,* vol. 2012, 2012.

[223] K. Ishiwata, T. Ido, M. Monma, M. Murakami, H. Fukuda, M. Kameyama, K. Yamada, S. Endo, H. Yoshioka, T. Sato, and T. Matsuzawa, "Potential radiopharmaceuticals labeled with titanium-45," *International Journal of Radiation Applications and Instrumentation. Part A. Applied Radiation and Isotopes,* vol. 42, pp. 707-712, 1991.

[224] R. N. Waterhouse, F. Mattner, L. Najdovski, T. L. Collier, and J. Fallon, "Synthesis and Characterisation of [^{111}In]-Liposome Encapsulated [45Ti]-Budotitane," in *Eleventh International Symposium on Radiopharmaceutical Chemistry*, Vancouver, Canada, 1995.

[225] A. L. Vavere and M. J. Welch, "Preparation, biodistribution, and small animal PET of ^{45}Ti-transferrin," *J Nucl Med,* vol. 46, pp. 683-90, Apr 2005.

[226] R. I. Price, R. W. Sheil, R. K. Scharli, S. Chan, P. Gibbons, C. Jeffery, and L. Morandeau, "Titanium-45 as a Candidate for PET Imaging: Production, Processing & Applications," in *15th International Workshop on Targetry and Target Chemistry*, Prague, Czech Republic, 2015.

[227] J. Siikanen, H. Hong, H. Valdovinos, R. Hernandez, Y. Zhang, T. Barnhart, W. Cai, and R. Nickles, "Production, separation and labeling of ^{45}Ti," in *SNMMI Annual Meeting*, Vancouver, Canada, 2013.

[228] E. Y. Tshuva and J. A. Ashenhurst, "Cytotoxic Titanium(IV) Complexes: Renaissance," *European Journal of Inorganic Chemistry,* vol. 2009, pp. 2203-2218, 2009.

[229] T. A. Immel, U. Groth, and T. Huhn, "Cytotoxic Titanium Salan Complexes: Surprising Interaction of Salan and Alkoxy Ligands " *Chemistry: an European Journal,* vol. 16, pp. 2775-2789, 2010.

[230] L. Cunha, K. Szigeti, D. Mathé, and L. F. Metello, "The role of molecular imaging in modern drug development," *Drug Discovery Today,* vol. 19, pp. 936-948, 2014.

[231] G. W. Severin, C. H. Nielsen, A. I. Jensen, J. Fonslet, A. Kjær, and F. Zhuravlev, "Bringing Radiotracing to Titanium-Based Antineoplastics: Solid Phase Radiosynthesis, PET and ex Vivo Evaluation of Antitumor Agent [45Ti](salan)Ti(dipic)," *Journal of Medicinal Chemistry,* vol. 58, pp. 7591-7595, 2015.

[232] D. Salber, J. Manuvelpillai, I. Spahn, S. Klein, F. Uhlenbruck, C. Palm, A. Matusch, S. Becker, K. J. Langen, and H. H. Coenen, "45Ti-cations as potential PET-tracers for cerebral neurodegeneration," in *International Symposium on TECHNETIUM and OTHER RADIOMETALS in CHEMISTRY and MEDICINE*, Bressanone, Italy, 2010.